CNWRA 93-024

EVALUATION OF ROCK JOINT MODELS AND COMPUTER CODE UDEC AGAINST EXPERIMENTAL RESULTS

Prepared for

Nuclear Regulatory Commission

Contract NRC-02-88-005

Prepared by

Center for Nuclear Waste Regulatory Analyses
San Antonio, Texas

December 1993

CNWRA 93-024

EVALUATION OF ROCK JOINT MODELS AND COMPUTER CODE UDEC AGAINST EXPERIMENTAL RESULTS

Prepared for

Nuclear Regulatory Commission

Contract NRC-02-88-005

Prepared by

Center for Nuclear Waste Regulatory Analyses
San Antonio, Texas

December 1993

CNWRA 93-024

EVALUATION OF ROCK JOINT MODELS AND COMPUTER CODE UDEC AGAINST EXPERIMENTAL RESULTS

Prepared for

Nuclear Regulatory Commission
Contract NRC-02-88-005

Prepared by

Sui-Min Hsiung
Amitava Ghosh
Asadul H. Chowdhury
Mikko P. Ahola

Center for Nuclear Waste Regulatory Analyses
San Antonio, Texas

DECEMBER 1993

PREVIOUS REPORTS IN SERIES

Number	Name	Date Issued
CNWRA 90-004	Qualification Studies on the Distinct Element Code UDEC Against Some Benchmark Analytical Problems	January 1990
CNWRA 90-005	Development of a Rock Joint Dynamic Shear Test Apparatus	January 1990
CNWRA 90-006	Qualification Studies on the Finite Element Code HONDO II Against Some Benchmark Analytical Problems	February 1990
NUREG/CR-5440	Critical Assessment of Seismic and Geomechanics Literature Related to a High-Level Nuclear Waste Underground Repository	June 1991
CNWRA 92-005	Thermo-Hydro-Mechanical Coupled Modeling: Multiple Fracture Model, BMT2 Coupled Stress — Flow Model, TC1 DECOVALEX — PHASE I	April 1992
CNWRA 92-012	Field Site Investigation: Effect of Mine Seismicity on a Jointed Rock Mass	December 1992
CNWRA 93-002	Thermo-Hydro-Mechanical Coupled Modeling: Near Field Repository Model, BMT3 DECOVALEX — PHASE II	August 1993
CNWRA 93-013	Laboratory Characterization of Rock Joints	September 1993

ABSTRACT

The Mohr-Coulomb, Barton-Bandis, and Continuously-Yielding rock joint models and their numerical implementation in the UDEC code were evaluated for their ability to simulate joint behavior under cyclic pseudostatic and dynamic loading conditions. Some deficiencies of these joint models and their implementation in UDEC were identified. These deficiencies include that the rock joint models under evaluation may not be able to sufficiently predict the joint shear and dilation behavior during reverse joint shearing. Both joint forward and reverse shearing are important phenomena of a rock joint behavior. Reverse shearing can result from earthquakes, thermal load, or both - all of which are expected to be experienced during the life of a high-level waste repository. These deficiencies could result in an overestimation of the stability of emplacement drifts and emplacement boreholes and prediction of incorrect near-field flow pattern (including preferential pathways for water and gas).

CONTENTS

FIGURES

FIGURES

FIGURES

FIGURES

TABLES

ACKNOWLEDGMENTS

The authors thank Dr. Graham G.W. Mustoe of the Colorado School of Mines and Dr. Wesley C. Patrick of the Center for Nuclear Waste Regulatory Analyses (CNWRA) for their technical reviews of this document. The authors also express their appreciation to Mr. Majid Mahrafza for his assistance in processing UDEC data. The authors are also thankful to Ms. Rebecca A. Sanchez for typing and formatting of the report, and to Southwest Research Institute Publications Services, who provided a full range of editorial services in the preparation of the final document.

This report was prepared to document work performed by the CNWRA for the U.S. Nuclear Regulatory Commission (NRC) under Contract No. NRC-02-88-005. The activities reported here were performed on behalf of the NRC Office of Nuclear Regulatory Research, Division of Regulatory Applications. This report is an independent product of the CNWRA and does not necessarily reflect the views or regulatory position of the NRC.

EXECUTIVE SUMMARY

A state-of-the-art literature review revealed that repetitive ground motions due to seismic activities may impact both the short- and long-term performance of a repository. The fundamental failure mechanism for an excavation subjected to repetitive seismic loading is through accumulation of shear displacements along joints. Specific seismic implications to repository design and performance may include cumulative effects of repetitive seismic loads on (i) emplacement borehole/drift stability; (ii) underground opening stability; and (iii) creation of preferential water pathways to connect the emplacement area with perched water zones, neighboring steep hydraulic gradient zones, or the condensation area above the emplacement area. These cumulative effects cannot be analyzed by extrapolation of response data from a single earthquake or nuclear test. New techniques need to be established for simulation of a rock mass subjected to repetitive seismic waves. The Seismic Rock Mechanics Research Project is a study of repository response due to repetitive dynamic loadings. As part of this research project, a program of qualification study for the assessment of rock joint models and the associated computer codes has been undertaken at the Center for Nuclear Waste Regulatory Analyses (CNWRA). The goal of the program is to evaluate the ability of existing rock joint models and the associated computer codes to represent dynamic or cyclic joint behavior.

There are two phases in this program. In the first phase of qualification study, a few commercially available computer codes were selected and evaluated using four well-established benchmark problems involving a rock joint that have closed-form solutions or suitable approximations to closed-form solutions. These commercially available codes included the distinct element codes UDEC and 3DEC, the discrete element code DECICE, and the finite element codes HONDO II and SPECTROM—331. The first phase of study was intended to confirm that a code can reproduce the rock joint response of these benchmark problems. Codes with an acceptable performance would be candidates for the second phase of the qualification study, in which the dynamic response of well-designed and executed laboratory experiments on single-joint rock specimens would be analyzed. This first-phase study showed that only the UDEC and 3DEC (which is, in general, a 3D version of UDEC) were able to reproduce the response of all four benchmark problems. The UDEC code was selected for the second-phase study. The objective of the second phase of qualification study is to determine whether the existing rock joint models and the associated computer codes can simulate the laboratory experimental behavior of single-joint rock specimens when subjected to cyclic pseudostatic and dynamic loads. This report presents the results of the second phase of qualification study of UDEC.

Three commonly used empirical representations for rock joint behavior were examined in their primary form to assess their ability for joint behavior prediction. These models were the Mohr-Coulomb, Barton-Bandis, and Continuously-Yielding models. The numerical implementation for each of these three models in the UDEC code was evaluated by modeling five cyclic pseudostatic tests, one harmonic test, and one earthquake test on Apache Leap tuff joints.

Careful examination of the Mohr-Coulomb, Barton-Bandis, and Continuously-Yielding rock joint models has revealed that all three models have adopted essentially the same principle in determining the joint shear strength during reverse shearing. This principle asserts the same joint behaviors under both forward and reverse shearing conditions. With this principle, the same shear strength criterion is applicable to both conditions. The Mohr-Coulomb joint model is the simplest of the three evaluated in this report. This model further assumes that no joint wear will occur under either forward or reverse shearing conditions. Consequently, based on this model, the shear strengths are the same for shearing in both directions. For

the other two models, however, joint wear is explicitly considered in the shear strength criteria, and the joint friction behavior is considered to be governed by two friction properties; one is the fundamental friction property or the residual friction property, and the other one is the friction property representing joint roughness. The fundamental or residual friction properties for these two models are similar, in concept, to the friction property in the Mohr-Coulomb joint model. These residual friction properties represent essentially the rock joint surfaces without roughness, a condition indicating that the joint will not wear. The roughness property is a function of joint shear displacement. The extent of wear increases with joint shear displacement. To preserve the necessary continuity in joint wear in case of changing direction of shear, both the Barton-Bandis and Continuously-Yielding joint models assert that the remaining friction property at the end of the forward shearing process should control the joint response in the reverse shearing process. In other words, the shear strength at the end of the forward shearing is considered to be the peak shear strength at the beginning of the reverse shearing. The implementations of these three models in the UDEC code primarily follow this principle. As a result, neither these models nor their implemented versions in the UDEC code can simulate satisfactorily the joint shear experimental behavior during reverse shearing in which the shear strength is different from that at the end of the forward shearing. As observed from the laboratory cyclic pseudostatic and dynamic (harmonic and earthquake) test results, this difference could be large depending upon joint profiles.

All three models assume an increasing nature of joint dilation, that is, the dilation will never decrease no matter along which direction the joint is being sheared. This assumption is not consistent with the joint dilation behavior found in the laboratory. Laboratory results showed that a joint tends to recover from the forward shearing dilation during reverse shearing with a certain amount of hysteresis between the dilation and dilation recovery curves. The dilation recovery can be complete. The Barton-Bandis and Continuously-Yielding joint models link joint dilation due to shearing directly with the roughness properties. Since a joint continues to wear during the process of shearing, the dilation angle used to calculate joint dilation continues to decrease. This implies, therefore, that a joint will eventually stop dilating when it is completely worn. The Mohr-Coulomb joint model calculates dilation based on a constant dilation angle. Dilation starts when shear strength is reached and stops when a critical shear displacement is reached.

The joint dilation in the Barton-Bandis and Mohr-Coulomb joint models have not been implemented properly in the UDEC code. A dilation versus shear displacement curve, predicted by the Barton-Bandis model, reaches a constant value after a small shear displacement. This constant value is significantly smaller than the peak dilation observed in laboratory experiments. Mohr-Coulomb model as implemented in the UDEC code predicts complete recovery of joint dilation only if the critical shear displacement is not reached. However, if the critical shear displacement is exceeded during forward shearing, dilation remains constant during the remaining period of forward shearing and the entire period of reverse shearing.

All three rock joint models have deficiencies in the prediction of joint shear and dilation behavior during reverse shearing. It should be emphasized that both joint forward and reverse shearing are important phenomena of a rock joint. Reverse shearing can result from earthquakes, thermal load, or both - all of which are expected to be experienced during the life of a high-level waste (HLW) repository. Using these three models in their present form could result in (i) an overestimation of the stability of emplacement drifts and emplacement boreholes, and (ii) prediction of an incorrect pattern of near-field flow (including preferential pathways for water and gas).

In addition to the deficiencies of the rock joint models in the UDEC code, the study results identified a minor problem with the UDEC in the logic used for joint shear stress calculation at contact points. Incorrect results on joint shear stress at a contact point may be obtained if the assigned joint length for the shear stress calculation continues to decrease due to joint shear displacement. This problem could be remedied by careful design of the UDEC model to maintain a constant joint length.

1 INTRODUCTION

1.1 BACKGROUND

In 1987, the United States Congress designated Yucca Mountain, in southern Nevada, as the only site to be characterized to determine its suitability for building a repository for high-level nuclear waste (HLW). The proposed repository horizon is about 300 m beneath Yucca Mountain, in a densely welded prominently vertically and subvertically jointed tuff. The unit was chosen as the proposed repository horizon because of its thickness, lateral continuity, dense welding, and its location in the unsaturated zone about 200 to 400 m above the water table.

An important phenomenon that could affect the preclosure and postclosure performance of a repository is repeated ground motion due to seismic activities (Kana et al., 1991; Nuclear Waste Technical Review Board, 1992). The fundamental failure mechanism for an excavation in a jointed rock mass subjected to repetitive seismic loading is the accumulation of shear displacements at joints. Specific seismic implications for repository design and performance may include cumulative effects of repetitive seismic loads on (i) emplacement borehole/drift stability; (ii) underground opening stability; and (iii) creation of preferential water pathways to connect the emplacement area with perched water zones, neighboring steep hydraulic gradient zones, or the condensation area above the emplacement area.

The cumulative effects of these repetitive seismic loadings cannot be analyzed by extrapolation of response data from a single earthquake or nuclear test. New techniques need to be established to simulate rock mass that has been subjected to repetitive seismic waves. The technique should (i) determine the significance of the geomechanical responses due to repetitive seismic events, (ii) establish reliable data sets that permit a better understanding of important parameters controlling the joint dynamic behavior and that reflect the relation between geomechanical responses and repetitive seismic events in a properly characterized rock mass, and (iii) determine if currently available rock joint models adequately describe the dynamic behavior of rock joints.

The exploratory Seismic Rock Mechanics Research Project, conducted by the Center for Nuclear Waste Regulatory Analyses (CNWRA), is studying repository response due to repetitive dynamic loadings. This research project has the dual focus of (i) understanding the key parameters affecting repository performance under repeated seismic loadings, and (ii) evaluating current capabilities for calculating such effects. A primary goal of this research project is to develop methodologies to evaluate, validate, and reduce uncertainties in the prediction models. These models eventually will be used to assess the effects of possible earthquakes as well as ground shock events on the short- and long-term performances of a proposed underground repository at Yucca Mountain. The U.S. Nuclear Regulatory Commission (NRC) staff and its contractors anticipate using the results of this study during the process of License Application review to determine the adequacy of the U.S. Department of Energy (DOE) repository design relevant to seismic activities.

As part of this research project, a program of qualification study for the assessment of rock joint models and the associated computer codes has been undertaken at the CNWRA. The current rock joint models were developed based primarily on data taken under unidirectional pseudostatic loading conditions. Thus, the ability of the models to predict joint performance under cyclic pseudostatic and dynamic loading conditions has not been tested. The goal of the program is to evaluate the ability of existing rock joint models and the associated computer codes to represent dynamic or cyclic joint

behavior. There are two phases in this program. In the first phase of qualification study, a few commercially available computer codes were selected and evaluated for the response of four well-established benchmark problems involving a rock joint that have closed-form solutions or suitable approximations to closed-form solutions. These commercially available codes included the distinct element codes UDEC (Brady et al., 1990) and 3DEC (Hsiung and Chowdhury, 1991; 1993), the discrete element code DECICE (Hsiung et al., 1993a), and the finite element codes HONDO II (Brandshaug et al., 1990) and SPECTROM—331 (Hsiung and Chowdhury, 1993). The first phase of study was intended to confirm that a code can reproduce the rock joint response of these benchmark problems. Codes with an acceptable performance would be candidates for the second phase of the qualification study, in which the dynamic response of well-designed and executed laboratory experiments on single-joint rock specimens would be analyzed. The first phase study showed that only the UDEC and 3DEC (which is, in general, a 3D version of UDEC) were able to reproduce the response of all four benchmark problems. The UDEC code was selected for the second phase study. The objective of the second phase of qualification study is to evaluate the existing rock joint models and the associated computer code against experimental results (Hsiung et al., 1993b). This report presents the results of the second phase of qualification study of UDEC.

1.2 PURPOSE AND SCOPE

The purpose of the second phase of qualification study is to evaluate the ability of the existing rock joint models and the associated computer codes to simulate the behavior of joints when subjected to cyclic pseudostatic and dynamic loads by comparing the simulated results with those obtained from the laboratory experiments on single-jointed rock specimens collected from the Apache Leap site near Superior, Arizona.

The activities associated with this second phase study included assessing: (i) the Mohr-Coulomb, Barton-Bandis, and Continuously-Yielding rock joint models, and (ii) the implementation of these rock joint models in the UDEC computer code by comparing the simulated results with those from laboratory cyclic pseudostatic and dynamic experiments. Five cyclic pseudostatic tests, one harmonic test, and one earthquake test on dry single-joint specimens were simulated using UDEC. Each test was simulated using Mohr-Coulomb, Barton-Bandis, and Continuously-Yielding rock joint models.

2 LABORATORY DIRECT SHEAR EXPERIMENTS

The performance of an underground excavation in meeting its designated purpose is determined by the stresses and displacements which develop around the excavation under the loads arising from the prevailing field conditions. These conditions include rock mass strength, deformability, initial *in situ* stresses, groundwater pressure distribution, thermal stress field, and dynamic loading. Consequently, analysis of the performance of rock excavations (emplacement drifts and emplacement boreholes in the context of HLW disposal) requires prior definition of the strength, stiffness, and stability parameters for the rock mass where those excavations are located.

Normally, in analyzing the behavior of underground structures in hard rocks which contain discontinuities, such as faults, joints, shear zones, and beddings, the shear behavior of these discontinuities will determine the rock mass deformation and the stability of the underground structures under various loading conditions. Conditions for slip on major pervasive features such as joints and faults or for the sliding of individual blocks from the boundaries of excavations are governed by the shear strengths that can be developed by the discontinuities concerned.

The conditions for joint behavior to be considered explicitly in assessing the performance of jointed rock mass around a repository include:

- joints under pseudostatic loading conditions
- joints under dynamic loading conditions, and
- joints under repetitive episodes of dynamic loading arising from a series of earthquakes or a series of underground nuclear explosions

Commonly used empirical representations of jointed rock behavior reside in the Mohr-Coulomb, Barton-Bandis, and Continuously-Yielding models. These models were developed based primarily on the data taken under unidirectional pseudostatic loading conditions. The ability of these models to predict joint performance under the cyclic pseudostatic loading conditions as well as the second and third conditions listed above has not been tested. Further, only limited data under cyclic pseudostatic and dynamic loading conditions are currently available for the purpose of validation of these rock joint models. Consequently, joint behavior under cyclic pseudostatic and dynamic loading is not well understood. To address these issues, a laboratory experimental program for the characterization of rock joints, as a part of the activities for the ongoing Seismic Rock Mechanics Research Project, had been undertaken at the CNWRA. In this program, a series of direct shear tests under both cyclic pseudostatic and dynamic loading conditions was conducted on Apache Leap tuff joints in order to obtain a better understanding of the dynamic joint shear behavior and to generate a complete data set that can be used for validation of the rock joint models. In the following subsections, a summary of the results of these cyclic pseudostatic and dynamic direct shear tests needed for the evaluation of the three rock joint models is discussed. A detailed discussion on these test results is given by Hsiung et al. (1993b).

2.1 DIRECT SHEAR SPECIMENS

The rock joint specimens used for the cyclic pseudostatic and dynamic direct shear tests were collected from the Apache Leap site near Superior, Arizona. The rock type at the Apache Leap site is a vitrified and densely welded tuff that is moderately and heavily jointed. The large diameter core drilling technique was used for sample collection. The rock joint specimens were prepared from the cores

collected to a predetermined size such that the rock block on one side of the joint had dimensions of $305 \times 203 \times 102$ mm and the rock block on the other side of the joint had dimensions of $203 \times 203 \times 102$ mm. The joint surfaces on both rock blocks were matched when the rock block with smaller size (top block) was seated at the center of the larger size rock block (bottom block). A detailed discussion on the experimental setup is given by Hsiung et al. (1993b).

2.2 JOINT CYCLIC PSEUDOSTATIC RESPONSE

During a cyclic pseudostatic direct shear test, the top block was sheared a distance of 50.8 mm in one direction followed by a reversal of shearing back to the original starting position under a predetermined constant normal stress and at a constant velocity of about 4.2×10^{-2} mm/sec. The same process could be repeated on the same joint specimen under a different normal stress level. To aid the discussion, the term "forward shearing" is used throughout this report to indicate that the top rock block moves away from its original position while the term "reverse shearing" denotes the top rock block moves toward its original position, regardless of the absolute direction of movement.

Figure 2-1 shows the shear stress response for test no. 17 (Hsiung et al., 1993b) under various normal stress levels. The test sequence followed an ascending order with respect to the normal stress. The curve with the 1-MPa normal stress (the first cycle of shearing) illustrates the shear behavior of an originally undamaged (fresh) joint and shows a distinct peak shear strength at the early stage of the shear cycle. The shear strength of the joint gradually reduces to a residual value at greater shear displacements. No distinct peak shear strength was observed for other cycles of shearing. Figure 2-1 also indicates a gradual increase in shear strength during reverse shearing when the top block was approaching its original position. The potential cause of this behavior has been explained by Hsiung et al. (1993b) and will not be repeated in this report. Another feature that can be observed in this figure is that the shear strength during the reverse shearing is smaller than the shear strength during the forward shearing.

The relation between normal displacement (dilation) and shear displacement for test no. 17 is given in Figure 2-2. This figure indicates that joint dilations at various levels of normal stresses increase during forward shearing. For reverse shearing, there is some degree of hysteresis with the joint dilation decreasing towards zero from below the dilation curve of forward shearing. In general, for repeated shear cycles, the amount of joint dilation decreased with increasing normal stress.

2.3 JOINT DYNAMIC RESPONSE

Figures 2-3 and 2-4 show the characteristic plot of the joint shear stress versus joint shear displacement under harmonic and earthquake loading conditions, respectively. The harmonic load for Figure 2-3 was generated from a prescribed shear displacement drive input in a sinusoidal wave form. The frequency and amplitude of the harmonic input motion were 1.4 Hz and 12.7 mm, respectively. The earthquake input motion used in Figure 2-4 is shown in Figure 2-5 with a maximum displacement amplitude of 25.4 mm and a dominant frequency of about 0.5 Hz. This displacement input signal was developed based on the acceleration response signal recorded from the Guerrero accelerograph array for the earthquake of September 19, 1985, in Mexico. The development of this displacement input has been discussed by Hsiung et al. (1993b). All figures include the test results of the first three cycles and Figure 2-3 also includes the result of the 40th cycle.

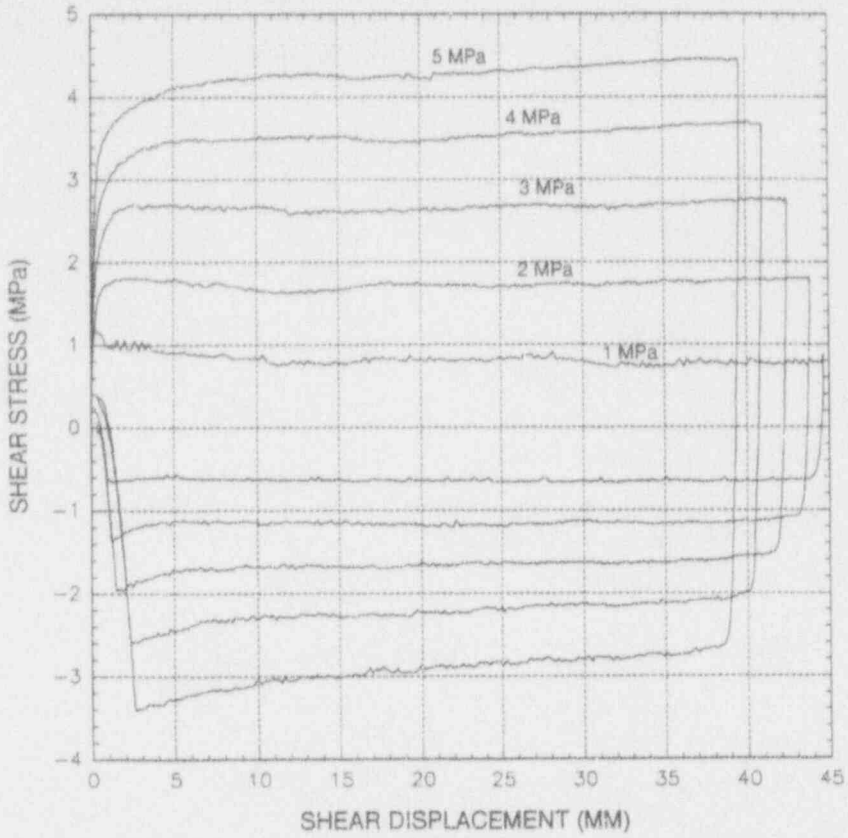

Figure 2-1. Shear stress response of test no. 17 specimen under pseudostatic cyclic loading condition as a function of normal stress

For Figures 2-3 and 2-4, the experiment started with the shearing of the top rock block from its original position (represented as the zero shear displacement in the figures) toward one end of the bottom rock block until a predetermined maximum value of shear displacement (based on the input displacement time history) was reached. The corresponding shear stress versus shear displacement characteristic curve with this portion of shearing is shown in the first quadrant of the figures (i.e., clockwise progression around the figure). After the maximum shear displacement in the first quadrant was reached, the top rock block began to move backward and eventually past its original position. The corresponding shear stress versus shear displacement characteristic curves are presented in the fourth and third quadrants of the figures, respectively. After the maximum shear displacement in the third quadrant was reached, the top rock block moved again back to its original position to complete a cycle of shear motion, and the associated shear stress versus shear displacement characteristic curve is presented in the second quadrant of the figures. This process was repeated for a number of cycles. As shown in the figures, the shear stress is assigned to be positive when the shearing is along one direction and becomes negative when the shearing follows the opposite direction. Consequently, the sign for the shear stress denotes the direction of the shear instead of the magnitude of the shear stress.

A peak joint shear strength was observed for the first cycle of both harmonic and earthquake tests if the jointed specimens used for the tests were never shear tested before or did not show signs of past shearing before specimen collection. This observation is consistent with the joint pseudostatic

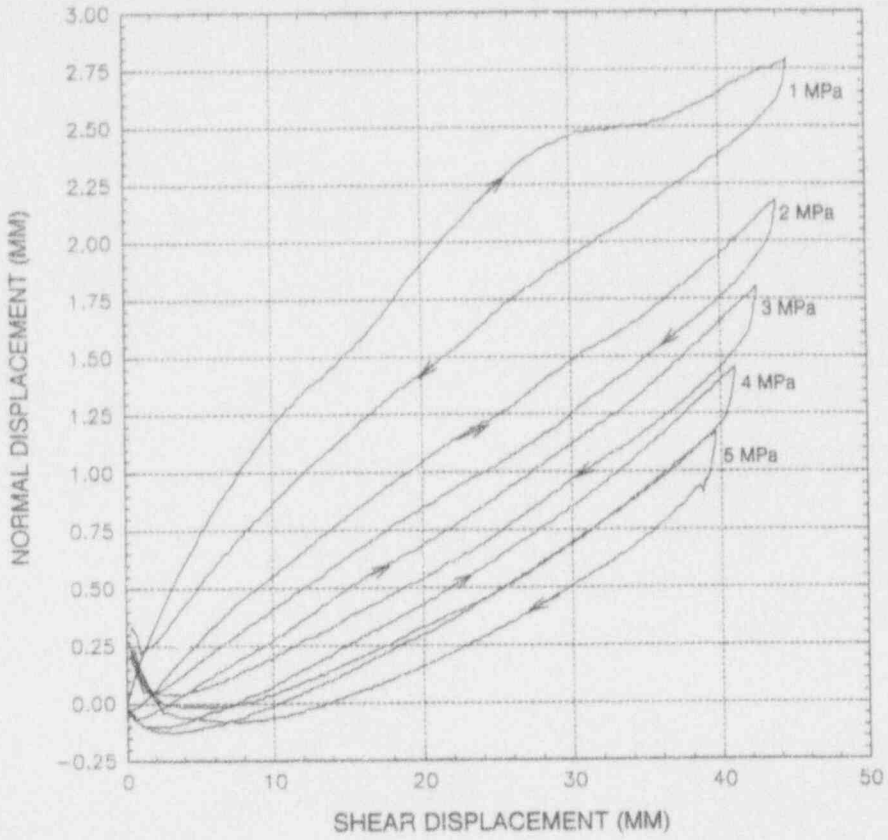

Figure 2-2. Joint dilation curves for test no. 17 specimen under pseudostatic cyclic loading condition as a function of normal stress

behavior. The phenomenon of wear of the joint is also clearly shown in the figures as the shear stress (joint shear strength) decreases with the number of cycles.

As observed for the cyclic pseudostatic tests (Figure 2-1), one distinct feature of the shear stress versus shear displacement characteristic curve in Figures 2-3 and 2-4 is the nature of the smaller shear strength upon reverse shearing as compared to that of forward shearing (the first quadrant versus the fourth quadrant, the third quadrant versus the second quadrant). The equivalent input frequency for the cyclic pseudostatic test as shown in Figure 2-1 is about 2.1×10^{-4} Hz. The same behavior was also reported by other researchers (Jing et al., 1992; Wibowo et al., 1992; Huang et al., 1993) for rock joint replicas under cyclic pseudostatic loads.

It can also be observed in Figures 2-3 and 2-4 that the shear stress curves are zigzag instead of being smooth during the course of forward and reverse shearing. These variations can be better characterized as stick-slip (chatter) behavior. This chatter behavior may be related to the waviness of the joint surface and rock fragments broken from the joint surface (asperities), state of normal stress, frequency of the loading cycles (velocity of shear displacement), and the variation of strength of the asperities or rock fragments. During a shear test, when the shear stress is equal to the joint shear strength, joint slip begins. This joint slip will continue until asperities are encountered that tend to resist joint slip, that is, increase the joint shear resistance (strength). In such a situation, the joint stops slipping.

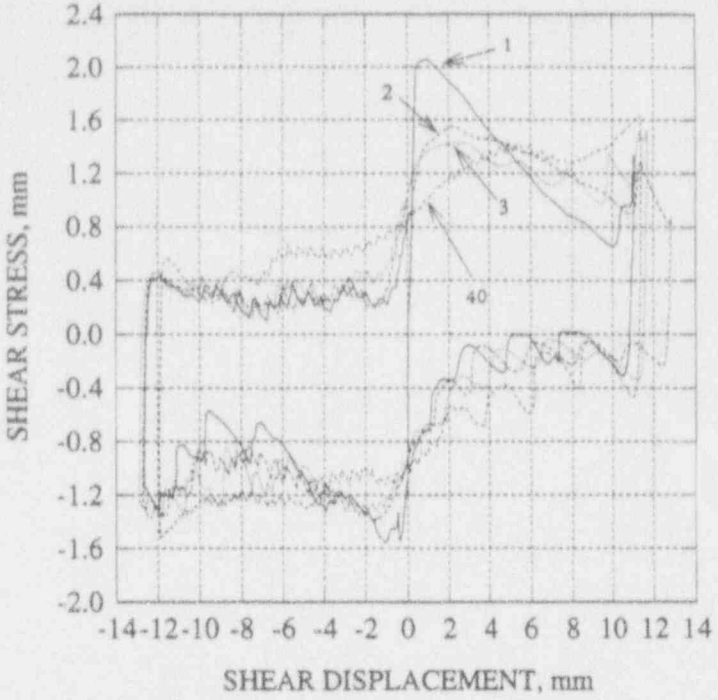

Figure 2-3. Shear stress versus shear displacement curve of a joint under a harmonic load with 1.4-Hz input frequency and 12.7-mm input displacement amplitude (load cycle numbers are indicated in the figure)

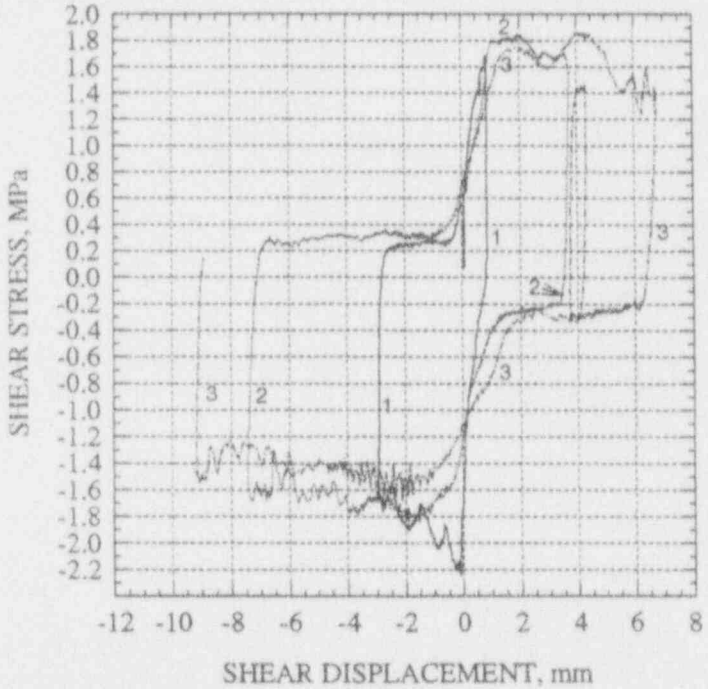

Figure 2-4. Shear stress versus shear displacement curve of a joint under an earthquake load with a maximum input displacement amplitude of 25.4 mm (load cycle numbers are indicated in the figure)

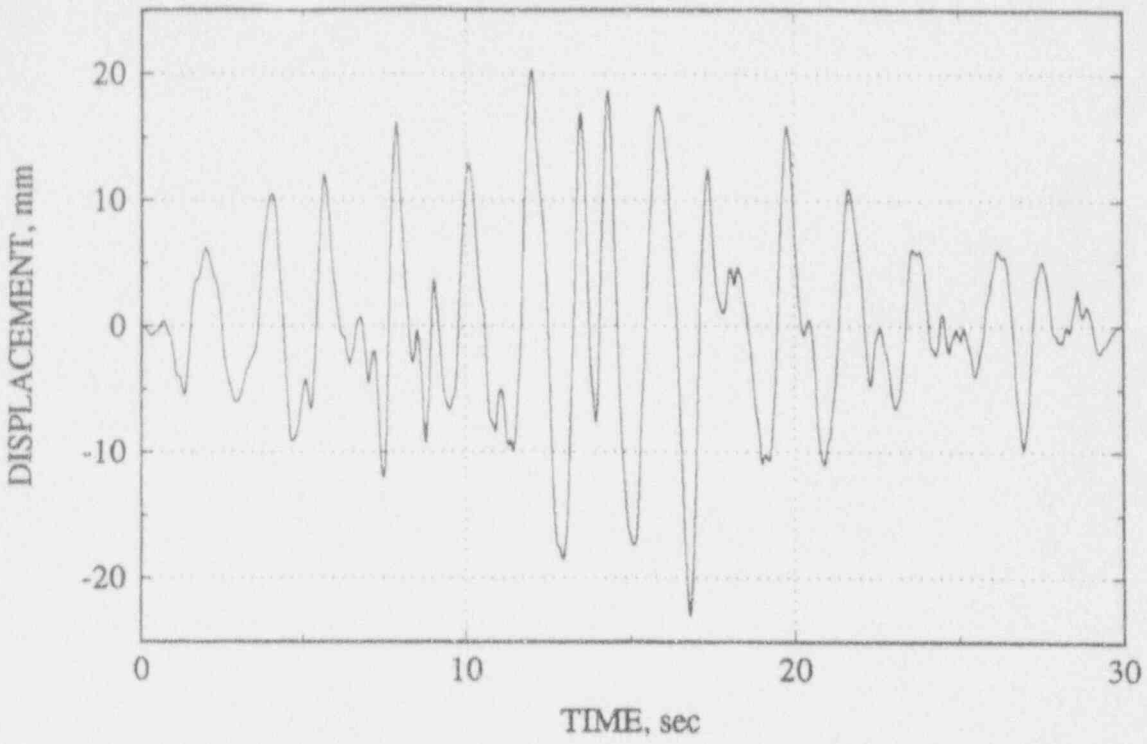

Figure 2-5. Input earthquake displacement time history

The termination of a joint slip is the "stick" component of the phenomenon. The joint slip will not resume until the applied shear stress is increased to a level that overcomes this additional amount of joint shear resistance.

If the rock fragments between the joint surfaces are strong, additional shear stress is needed in order for the top rock block to crush or ride over them. As shown in Figure 2-6, which shows the relation between the shear stress and shear displacement of different joints under pseudostatic cyclic loading condition, the joint chatter behavior was not as pronounced at relatively lower normal stress level; in this figure, it is 1.0 MPa. However, when the input frequency was increased from 2.1×10^{-4} Hz for the pseudostatic cyclic tests to 0.5 Hz for the earthquake tests, or more than 1 Hz for the harmonic tests, the chatter behavior becomes increasingly pronounced, although the applied normal stress was 1 MPa (Figures 2-3 and 2-4). It is also interesting to note that, in some cases of the dynamic tests, the chatter behavior continues even after a number of cycles of shearing. Small shear displacement may be needed for the process of crushing or riding over the rock fragments since these rock fragments may not be fixed in place. Therefore, the stick component of the chatter behavior in this sense should be treated more broadly.

Figures 2-7 and 2-8 show the corresponding joint normal displacement versus shear displacement characteristic curves for Figures 2-3 and 2-4, respectively. The wear of the joint surfaces is a continuing process, as is evident in these figures, where the maximum joint normal displacement continues to decrease through the cycles of shearing. It is interesting to note that joint dilation (positive normal displacement) tends to decrease constantly during reverse shearing and may retain a small amount of dilation as the top rock block returns to its original position. The dilation curve is highly nonlinear but

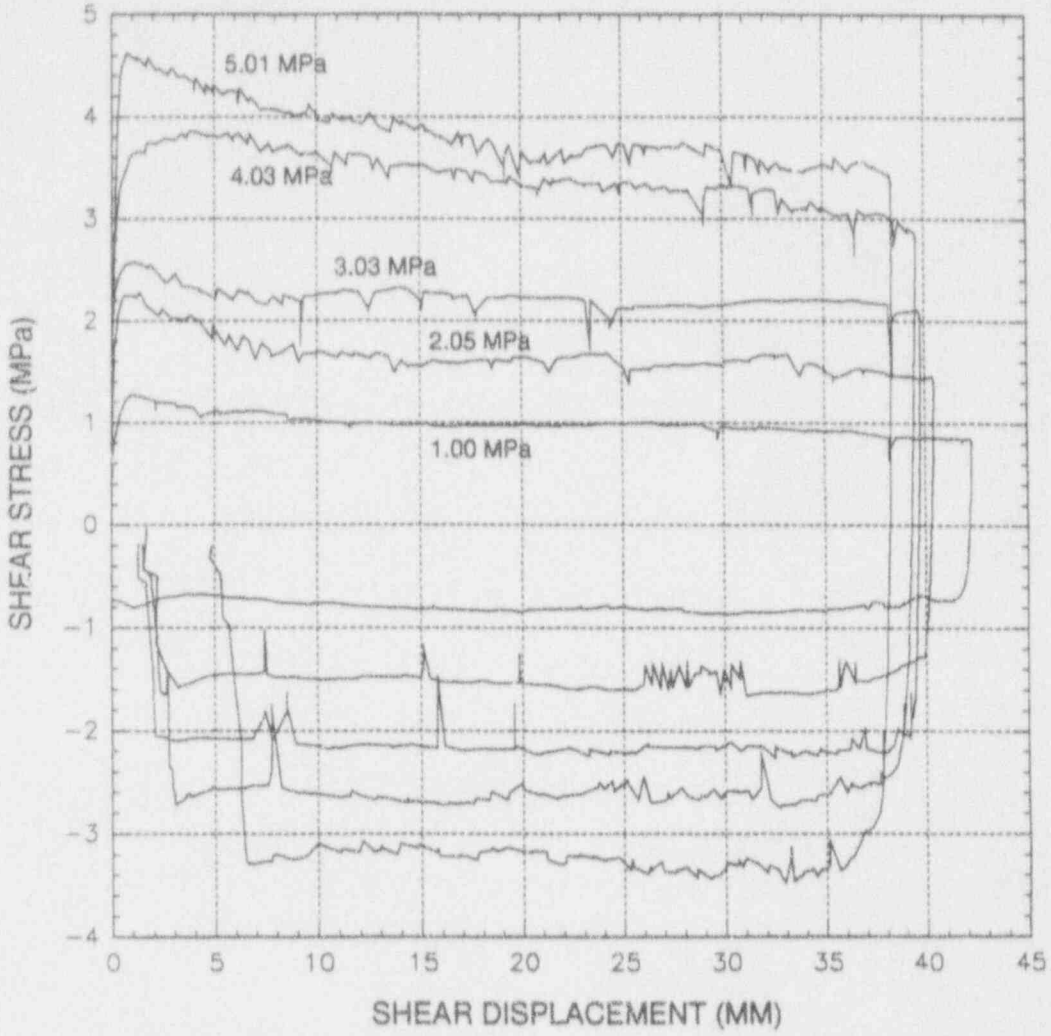

Figure 2-6. Shear stress versus shear displacement response as a function of applied normal load for various joint specimens

generally smooth for at least the first three cycles of the earthquake test results in Figure 2-8 as was that for the pseudostatic test (Figure 2-2). However, for the harmonic test as shown in Figure 2-7, many small-scale stick-slip oscillations that continued for many cycles were observed. This observation gives an indication of the potential impact of the input frequencies on joint dilation, which may be related to the existence of small-size rock fragments created in the process of shearing. Under pseudostatic conditions or smaller input frequency conditions, shear stress tends to crush these rock fragments instead of riding over them. However, under conditions of high input frequencies or high shear velocity for that matter, the rock fragments are stronger and tend to resist crushing and thus result in a temporary increase in normal displacement (the top block riding over these fragments). It is commonly understood that rock strength depends on loading rate and generally increases with increased loading rate. Once the fragments are crushed, the normal displacement tends to return to the original path. Judging from the overall joint shear behavior, the effect of the chatter component on the joint performance is considered to be limited.

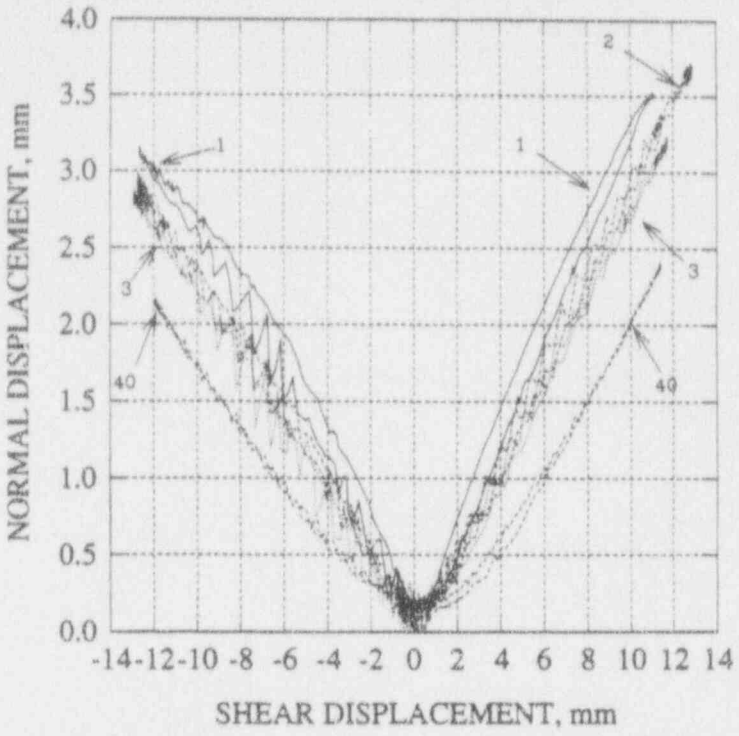

Figure 2-7. Joint normal displacement (dilation) versus shear displacement of a joint under a harmonic load with 1.4-Hz input frequency and 12.7-mm input displacement amplitude

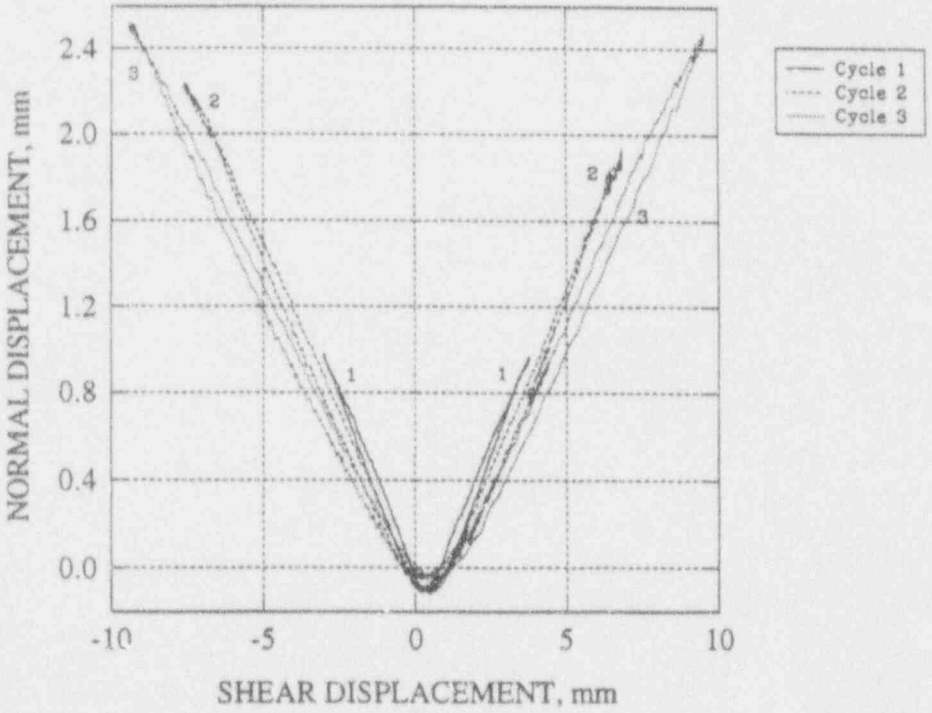

Figure 2-8. Joint normal displacement (dilation) versus shear displacement of a joint under an earthquake load with a maximum input displacement amplitude of 25.4 mm

In summary, two important distinct features for a joint during shearing have been identified; one is that the shear strength upon reverse shearing is smaller than that of forward shearing, and the other is that the joint dilation resulting from forward shearing recovers during reverse shearing. These two features on the joint behavior occur under various loading conditions. It should be emphasized again that both joint forward and reverse shearing are important phenomena of a rock joint. Reverse shearing can result from an earthquake, thermal load, or both — all of which are expected to be experienced during the life of an HLW repository. Failure to consider these two features of the joint behavior in an underground structural design and performance analysis could result in (i) an overestimation of the stability of emplacement drifts and emplacement boreholes, and (ii) prediction of an incorrect pattern of near-field flow (including preferential pathways for water and gas).

Some discussions on the potential impact of dynamic input from the aspect of shear velocity on the peak joint shear strength and joint shear strength for the reverse shearing are provided. Since natural rock joints were used for performing direct shear tests under cyclic pseudostatic, harmonic, and earthquake loading conditions, a different joint specimen was needed for each test. As a result, the joint characteristic for each test was different. Therefore, it is impossible to evaluate directly the dynamic effect on the joint shear strength, unless some means is developed to account for the effect of different roughness. Figure 2-9 illustrates an approximate means for such an evaluation. Admittedly, the conclusion that can be drawn from this figure is at best an approximation, due to a number of uncertainties involved. However, it does give an indication of the potential dynamic effect on the peak shear strength. The horizontal axis of the figure represents the joint roughness coefficient (*JRC*) value calculated from the tilt test, while the vertical axis represents the *JRC* value calculated from the direct shear test results. Although it has been determined that the tilt test method grossly underestimates the real *JRC* value, it has been shown, through the Spearman's rank correlation coefficient test, that the *JRC* value from the tilt test has a strong positive correlation with the corresponding *JRC* values calculated from the pseudostatic cyclic shear test results with a correlation coefficient, R^2, of about 0.85 (Hsiung et al., 1993b). It is, therefore, possible to develop an empirical expression relating the *JRC* values from the two methods. The dotted line in Figure 2-9 shows a second order polynomial fit between *JRC* values from the pseudostatic cyclic test results and the corresponding *JRC* from tilt tests with an R^2 of 0.82. This polynomial fit should provide sufficient confidence in estimating the *JRC* for the Apache Leap tuff joints using the tilt test. Subsequently, the estimated *JRC* can be used to estimate the "pseudostatic" peak joint shear resistance with reasonable confidence. Assuming that the peak joint shear strength will be affected by dynamic loads (e.g., induce a higher peak shear strength than the peak shear strength if the same specimen was tested under pseudostatic condition), then the *JRC* value calculated from the "dynamic" joint shear strength should be larger than the *JRC* value from the pseudostatic shear strength. In other words, the dynamic *JRC* should fall above the second polynomial curve if plotted in Figure 2-9. Figure 2-9 includes the dynamic *JRC* from the harmonic and earthquake test results. Examination of the figure indicates that, in general, the dynamic *JRC* values do not significantly differ from the corresponding pseudostatic *JRC* values, except for one data point from a harmonic test result. This observation is an indication that the dynamic input may not have an appreciable influence on the peak joint shear strength.

Figure 2-10 shows the effect of joint roughness on the joint shear stress reduction during reverse shearing for the dynamic tests. The horizontal axis represents the *JRC* values that were calculated using the dynamic peak shear strength results. The vertical axis is the ratio of the approximate shear strength during reverse shearing to the corresponding peak shear strength for forward shearing. There are two curves for each type of the dynamic tests in the figure. The legend "Earthquake, 1" denotes that the data in the 1st and 4th quadrants of the shear stress versus shear displacement characteristic curves for the

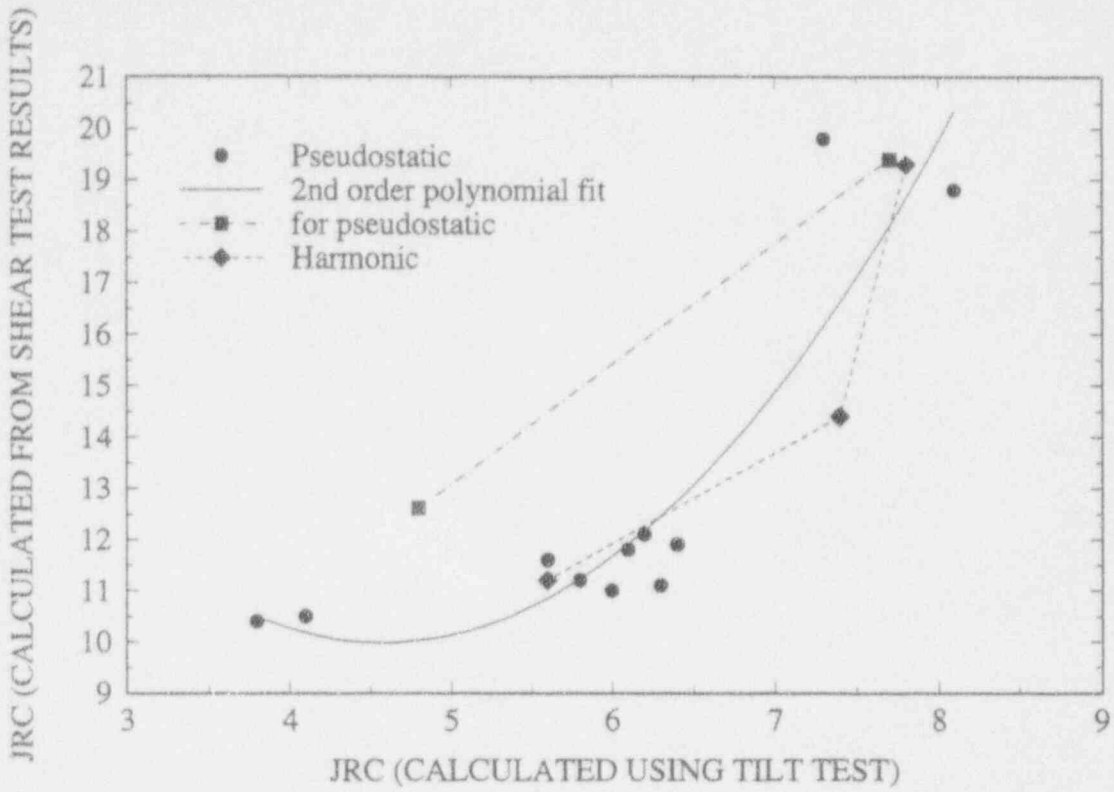

Figure 2-9. Effect of input frequency (shearing velocity) on peak joint shear strength

earthquake tests were used, while the legend "Earthquake, 2" denotes that the data in the 3rd and 2nd quadrants were used. The same approach was used for the harmonic tests. Figure 2-10 shows that the difference between the joint shear strength during reverse shearing and the peak shear strength will be larger for joints with rougher surfaces. The dynamic effect, on the other hand, is not clearly shown in the figure.

In summary, within the range of variation of the test input velocity or frequency, the test input velocity or frequency on the joint behavior is found to affect the chatter behavior for the Apache Leap tuff joints. As discussed earlier, the chatter behavior is believed to have limited effect on joint performance. No noticeable effect of the input frequency on the peak joint shear strength and the joint shear strength for the reverse shearing is observed. Consequently, it is possible not to consider the effect of shearing velocity variations, within a range from a velocity that is equivalent to a static condition to a velocity variation comparable to earthquakes, in evaluating joint behavior. However, the fact that the joint behavior in the reverse shearing is distinctly different from that of forward shearing, in the sense of joint shear strength, and the phenomenon that joint dilation recovers during reverse shearing deserve adequate representation by the rock joint models.

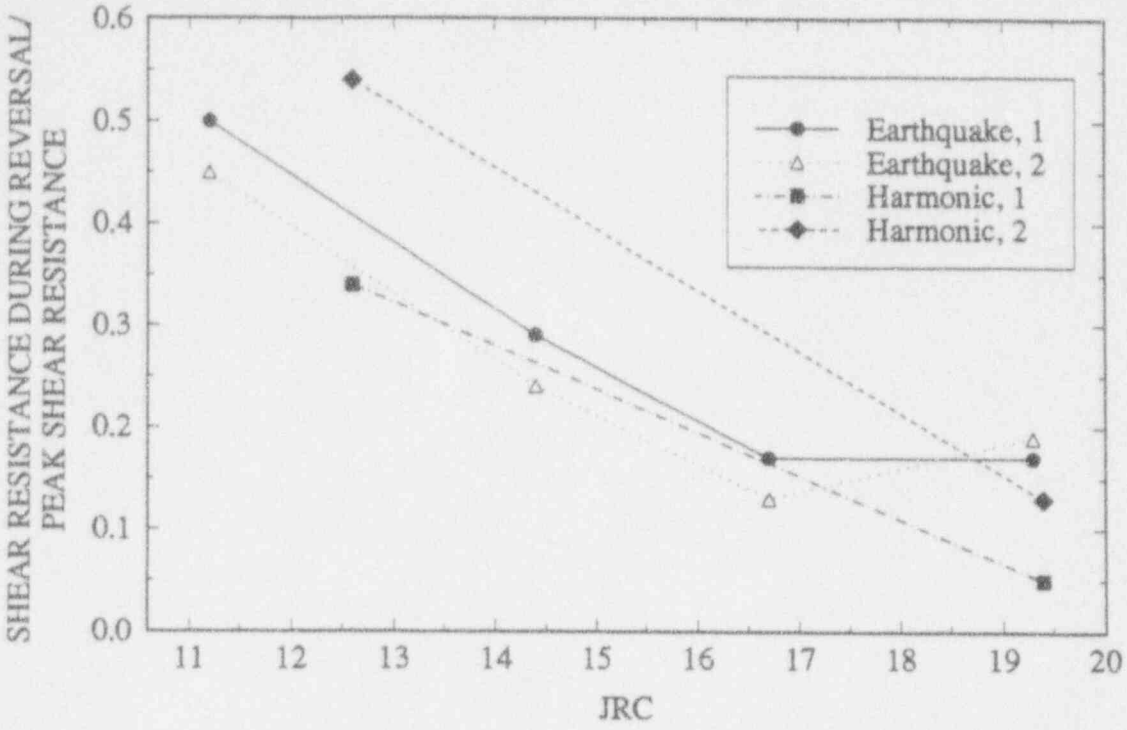

Figure 2-10. Effect of input frequency (shearing velocity) on joint shear strength during reverse shearing

3 EVALUATION OF ROCK JOINT MODELS

In this section, three commonly used empirical representations for jointed rock behavior are discussed and evaluated. This evaluation is carried out for each rock joint model by explicitly simulating the rock joint response using the respective constitutive equations. The implementation of these rock joint models in the UDEC code will be assessed in Section 5. These are the Mohr-Coulomb, Barton-Bandis, and Continuously-Yielding models. As mentioned in Section 2, these three models were developed based on the data obtained under unidirectional pseudostatic loading conditions. The relative merit of extending these models to include the joint shear behavior in the reverse direction is examined in this section.

3.1 MOHR-COULOMB MODEL

The simplest model for joint deformation and strength is the Mohr-Coulomb model, a linear deformation model that includes a shear failure criterion for a rock joint

$$\tau_o = C + \sigma_n \tan \phi \tag{3-1}$$

where τ_o is shear strength along the joint, σ_n is normal stress across the joint, C is cohesion, and ϕ is friction angle. Once the τ_o is reached, the joint assumes a perfectly plastic deformation. This equation does not offer directionality, thus suggests a homogeneous condition of joints, that is, the shear strength of a joint is the same in any direction. The joint shear response is governed by a constant shear stiffness K_s

$$\Delta\tau = K_s \, \Delta u_s^e \tag{3-2}$$

where $\Delta\tau$ is incremental shear stress and Δu_s^e is an elastic component of the incremental shear displacement. Based on Eqs. (3-1) and (3-2), $\Delta\tau$ becomes zero after the condition $|\tau| = \tau_o$ is reached, where τ is the shear stress on the joint. There is also a limiting tensile strength of the joint. If the tensile stress across the joint exceeds this value, the joint fails in tension and σ_n becomes equal to zero.

The Mohr-Coulomb joint model in its basic form does not consider the joint wear and dilation behavior. However, the dilation behavior may be added. In UDEC, the added dilation is restricted such that the dilation angle ψ is zero until shear stress has reached the shear strength of the joint (Figure 3-1), that is, joint dilation starts after the joint begins to deform plastically. A constant dilation angle is assumed for joint dilation. The dilation angle returns to zero after a critical shear displacement is reached. Mathematically, the relation is (ITASCA Consulting Group, Inc., 1992)

$$\text{if} \quad |\tau| < \tau_o, \quad \text{then} \quad \psi = 0 \tag{3-3}$$

and

$$\text{if} \quad |\tau| = \tau_o \quad \text{and} \quad |u_s| \geq u_{cs}, \quad \text{then} \quad \psi = 0 \tag{3-4}$$

where u_s is the joint shear displacement and u_{cs} is the critical shear displacement. Eq. (3-4) suggests that joint dilation should continue to increase even during reverse shearing.

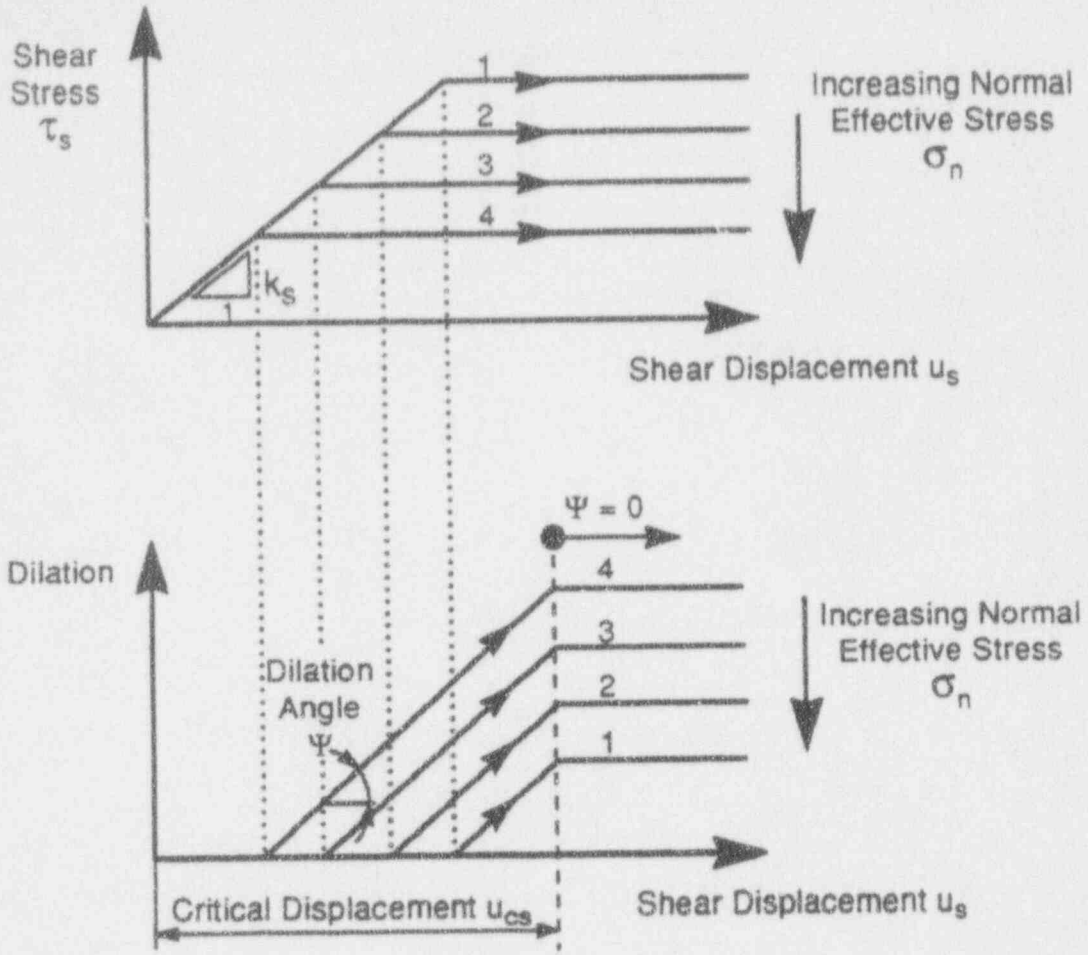

Figure 3-1. Schematic diagram of joint behavior in Mohr-Coulomb model of UDEC (ITASCA Consulting Group, Inc., 1992)

Assuming a joint with a shear stiffness, K_s, of 16.93 GPa, a friction angle, ϕ, of 38°, and a constant dilation angle, ψ, of 2.4°, the predicted joint behavior using the Mohr-Coulomb model subjected to a normal stress, σ_n, of 3 MPa can be illustrated in both Figures 3-2 and 3-3. In both figures, the cohesion C for the joint is assumed to be zero. For Figure 3-2, the critical shear displacement, u_{cs}, is not reached while it is about 10.52 mm for Figure 3-3. For shear loading (Figures 3-2 and 3-3), shear displacement is linear and reversible up to when the joint shear strength is reached and then perfectly plastic. Reverse shearing after plastic yield is accompanied by permanent shear displacement and hysteresis. Note that the shear strengths for both forward and reverse shearing are the same, an indication that the Mohr-Coulomb rock joint model cannot adequately represent joint shear behavior during reverse shearing as indicated in Figures 2-3 and 2-4. Two dilation curves are shown in either of the figures. Curve "Dilation 1" represents the dilation behavior following the definition of Eq. (3-4). Curve "Dilation 2" is obtained by assuming that joint dilation is shear-direction dependent. In this particular case, the sign of the dilation angle is changed to negative as the direction of shearing is reversed. As can be observed in both figures, if dilation follows the rule set by Eq. (3-4), it will continue to increase during reverse shearing. This phenomenon substantially departs from the laboratory observations (Figures 2-2, 2-6, and 2-8). On the other hand, if dilation involves a sign change in dilation angle during reverse shearing, it tends to recover, that is, it is conceptually in agreement with the laboratory observations.

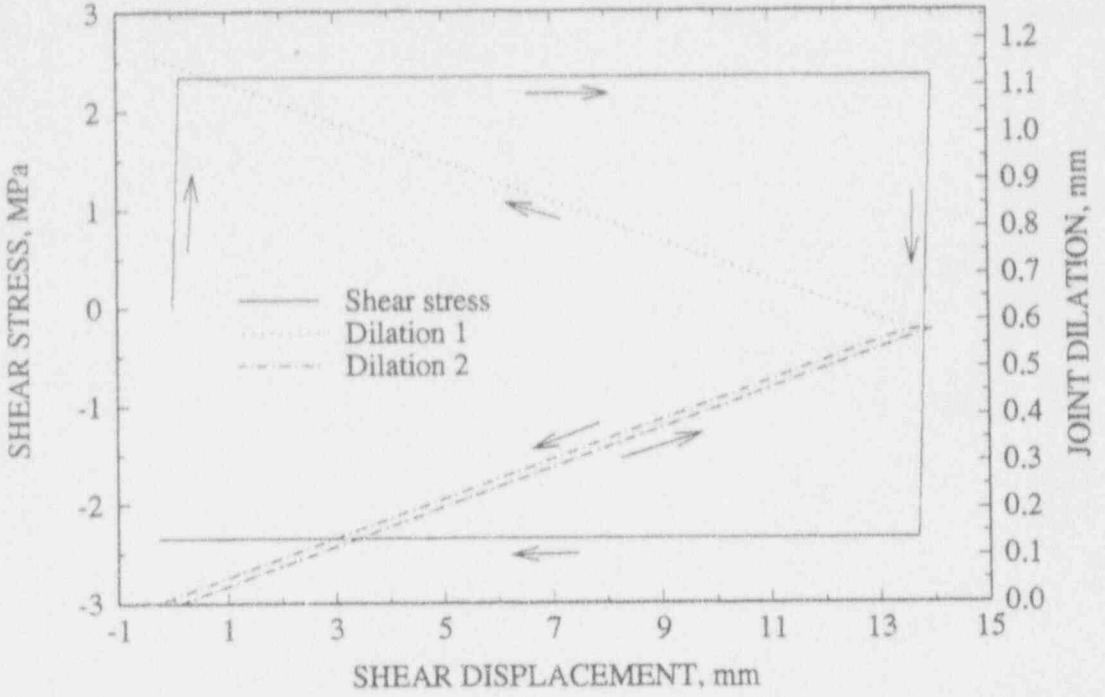

Figure 3-2. Prediction of joint behavior using the Mohr-Coulomb model assuming that shear stiffness = 16.93 GPa, friction angle = 38°, dilation angle = 2.4°, and normal stress = 3 MPa (assuming that the critical shear displacement is not reached)

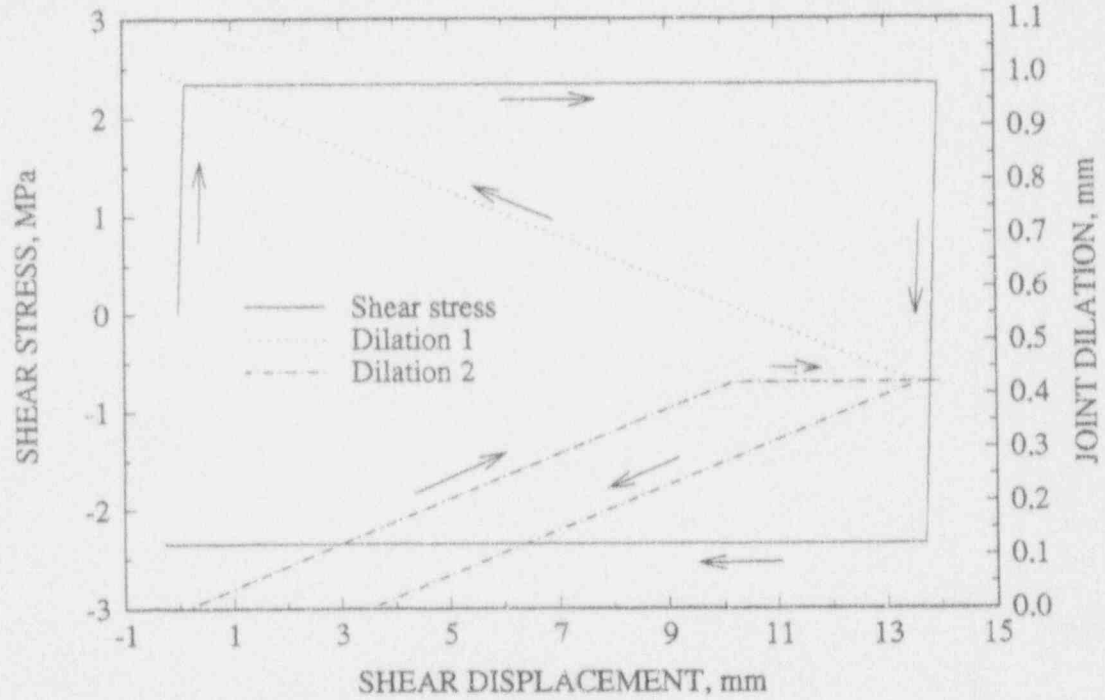

Figure 3-3. Prediction of joint behavior using the Mohr-Coulomb model assuming that shear stiffness = 16.93 GPa, friction angle = 38°, dilation angle = 2.4°, and normal stress = 3 MPa (assuming that the critical shear displacement has been reached)

3.2 BARTON-BANDIS MODEL

The Barton-Bandis model was proposed with the intent to take into consideration the effect of joint surface roughness on joint deformation and strength. The nonlinear joint strength criterion can be expressed as (Barton et al., 1985)

$$\tau_o = \sigma_n \tan \left[JRC \log_{10} \left(\frac{JCS}{\sigma_n} \right) + \phi_r \right] \tag{3-5}$$

where JRC is joint roughness coefficient, JCS is joint wall compressive strength, and ϕ_r is residual joint friction angle. The attrition of the surface roughness or reduction of the JRC is represented in a piece-wise linear manner as shown in Figure 3-4. The table in the figure governs the extent of the wear of the joint. When the joint is not sheared, it has a maximum JRC value, JRC_{peak}. However, as the joint begins to be sheared, the JRC value begins to become smaller as a result of roughness attrition. This JRC value is represented by JRC_{mob} in Figure 3-4. The symbol δ in Figure 3-4 denotes joint shear displacement while δ_p denotes the joint shear displacement at which the peak shear stress (shear strength) is reached. δ_p can be calculated by the following equation (Barton and Bandis, 1982)

$$\delta_p = \frac{L_n}{500} \left(\frac{JRC}{L_n} \right)^{0.33} \tag{3-6}$$

where L_n is the length of a test specimen.

Based on Eq. (3-5), the joint shear stress under a constant normal stress condition depends solely on the JRC value. When a joint is sheared in one direction, its roughness is reduced from JRC_{peak} to JRC_f. If, at this point, the direction of the shear is reversed, the initial shear stress required for the joint to be sheared in the reversed direction is controlled by the JRC_f value, following Eq. (3-5), which serves as the maximum JRC in the reverse direction. In other words, the Barton-Bandis model assumes that the shear strength at the initiation of the shear in the reverse direction is equal to the shear strength right before the forward shearing is stopped. Also, the data in the inset table in Figure 3-4 suggest that joint wear will stop after the JRC_{mob} becomes zero. This condition will be reached when ratio of the actual shear displacement δ to the shear displacement δ_p is greater than 100. Once the JRC becomes zero, the joint shear essentially resumes the Mohr-Coulomb model type of behavior.

The Barton-Bandis joint model (Barton et al., 1985) also recognized the dilation nature of joints and suggested that angle of dilation should be a function of JRC value. The relation between the JRC and dilation angle ψ can be expressed in the following form

$$\psi = 0.5\ JRC \log_{10} \left(\frac{JCS}{\sigma_n} \right) \tag{3-7}$$

This equation indicates that, as joint surface roughness wears, its angle of dilation decreases. In other words, the rate of dilation becomes smaller as joint shearing progresses. The dilation angle will eventually become zero, that is, there will be no further dilation, as δ/δ_p becomes greater than 100. Judging from

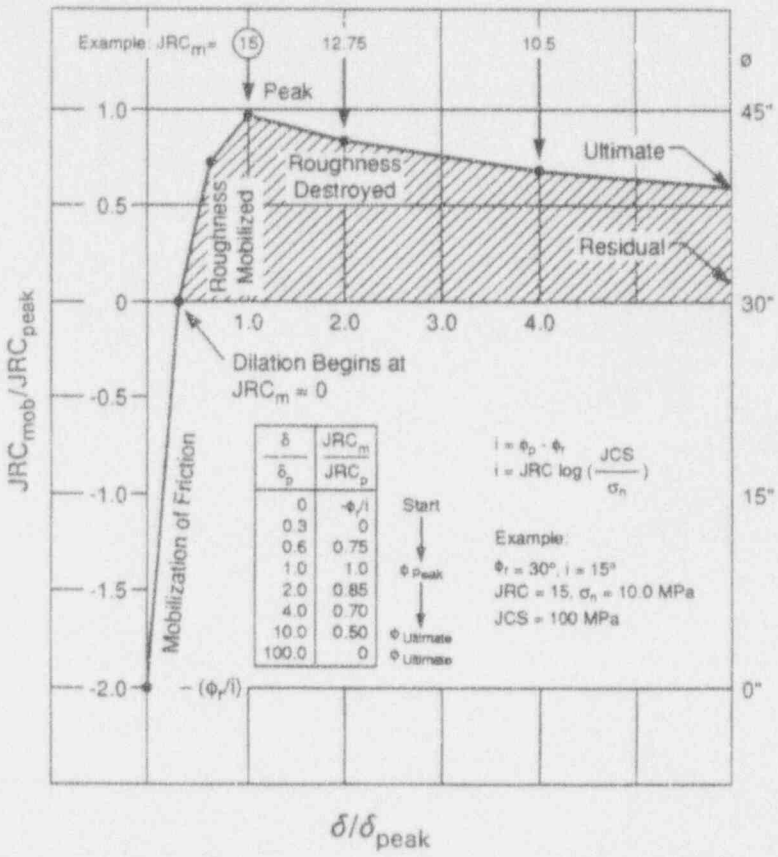

Figure 3-4. Barton-Bandis joint model for shear stress-displacement modeling, after Sharp (1970)

the nature of Eq. (3-7), ψ is always positive. Joint dilation will continue to increase, although at a gradually slower rate, even after the direction of shear has been reversed.

Assuming a joint with a *JCS* of 170.5 MPa, a *JRC* of 7.1, and a residual friction angle of 28.4°, the predicted joint behavior using the Barton-Bandis model subjected to a normal stress, σ_n, of 3 MPa can be illustrated as in Figure 3-5. Note that the *JRC* value of the joint at the beginning of reverse shearing in Figure 3-5 is half of the original *JRC*. Consequently, a distinct peak shear strength is observed in the process of reverse shearing. The peak shear strength for the reverse shearing is the same as the shear strength at the end of the forward shearing. This observation indicates that the Barton-Bandis rock joint model may not adequately represent joint shear behavior during reverse shearing. Two dilation curves are shown in Figure 3-5. Curve "Dilation 1" represents the dilation behavior following the definition of Eq. (3-7) in which the joint dilation continued to increase. If the sign of the dilation angle can be changed as the direction of shear reverses, joint dilation tends to decrease (recovery) during reverse shearing instead of increasing (curve "Dilation 2" in Figure 3-5). The rate of decrease in dilation or the extent of dilation recovery depends on the extent of joint wear. However, the recovery is not as extensive as that observed in the laboratory. Consequently, it will not be sufficient to explain the joint dilation behavior during reverse shearing at which dilation recovers at a much higher and increasing rate.

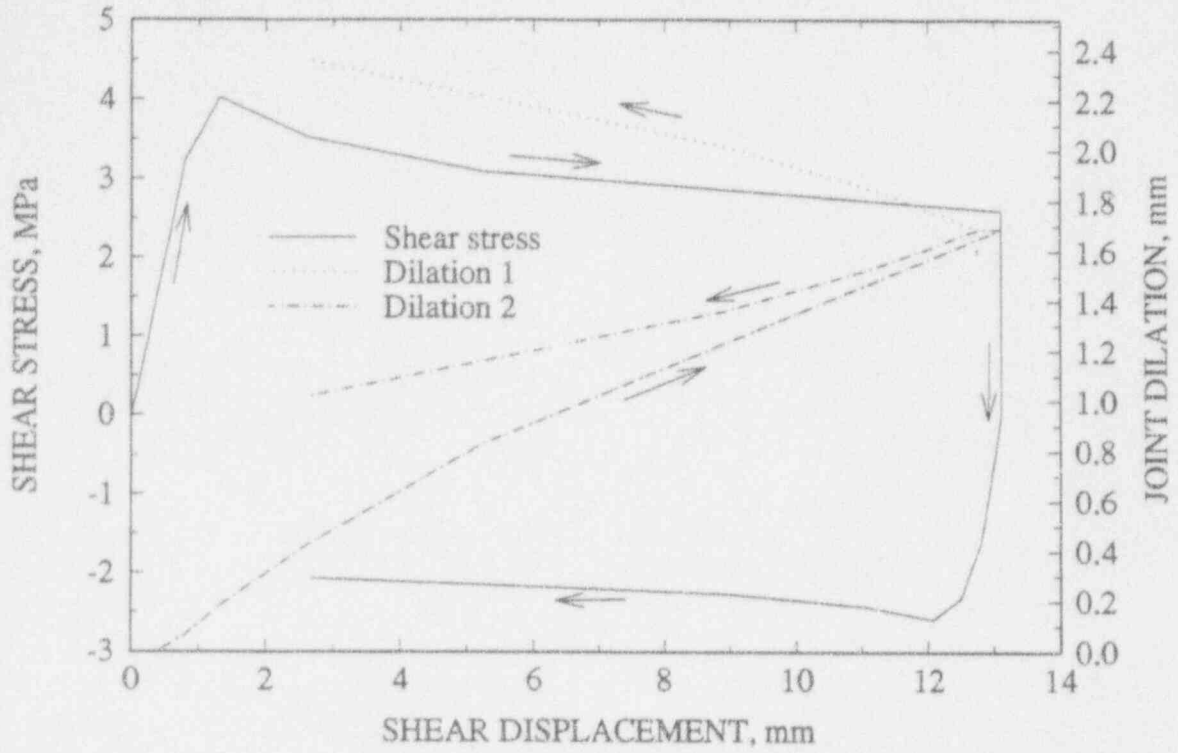

Figure 3-5. Prediction of joint behavior using the Barton-Bandis model assuming that joint wall compressive strength = 170.5 MPa, residual friction angle = 28.4°, joint roughness coefficient = 7.1, and normal stress = 3 MPa

3.3 CONTINUOUSLY-YIELDING MODEL

The Continuously-Yielding model for rock joint deformation was developed by ITASCA Consulting Group, Inc. (ITASCA Consulting Group, Inc. 1992; Cundall and Lemos, 1988). The model can simulate, in a simple way, the progressive damage of the joint surface under shear displacement and displays irreversible nonlinear behavior from the onset of shear loading. The shear stress increment is described as

$$\Delta\tau = F\, K_s\, \Delta u_s \tag{3-8}$$

where the shear stiffness K_s may be a function of normal stress

$$K_s = a_s\, \sigma_n^{e_s} \tag{3-9}$$

Therefore, the change in shear stress due to change in shear displacement can be expressed as

$$\Delta\tau = F\, a_s\, \sigma_n^{e_s}\, \Delta u_s \tag{3-10}$$

where F is a factor that governs the shear stiffness, and parameters a_s and e^s in Eq. (3-9) are constants. F depends on the difference between the actual stress curve and the bounding strength curve τ_o and is given as

$$F = \frac{(1 - \tau/\tau_o)}{(1 - r)} \tag{3-11}$$

Therefore, $\Delta\tau$ is

$$\Delta\tau = \frac{(1 - \tau/\tau_o)}{(1 - r)} a_s \sigma_n^{e_s} \Delta u_s \tag{3-12}$$

The factor r is initially zero. It restores the elastic stiffness immediately after load reversal. That means r is set to τ/τ_o (F becomes 1) whenever the sign of ($\Delta\tau$) is not the same as the sign of ($\Delta u_{s\ old}$). In practice, r is restricted to a maximum value of 0.75 to avoid numerical noise when the shear stress is approximately equal to the bounding strength, τ_o. The bounding strength, τ_o, is

$$\tau_o = \sigma_n \tan \phi_m \text{ sign } (\Delta u_s) \tag{3-13}$$

where ϕ_m is the friction angle that would apply if the joint is to dilate at the maximum dilation angle and is initially equal to the joint initial friction angle, ϕ_{mo}. As damage accumulates, ϕ_m is continuously reduced according to

$$\phi_m = (\phi_{mo} - \phi)\, e^{\left(-\frac{u_s^p}{R}\right)} + \phi \tag{3-14}$$

where u_s^p is the plastic shear displacement and the plastic shear displacement increment, Δu_s^p is given by

$$\Delta u_s^p = (1 - F)|\Delta u_s| \tag{3-15}$$

and ϕ is the basic friction angle of the rock surface. R is a material parameter with a dimension of length that expresses the joint roughness. A large value of R produces slower reduction of ϕ_m and a higher peak. The peak is reached when the bounding strength equals the shear stress. After the peak, the joint is in the softening region and the value of F becomes negative.

Based on Eq. (3-13), joint bounding shear strength under a constant normal stress condition depends solely on the friction angle, ϕ_m. If a joint is sheared in one direction and its friction angle, ϕ_m, is reduced from its initial value ϕ_{mo} to ϕ_f, and at this point, the direction of the shear is reversed, the corresponding bounding shear strength in the reversed direction, according to Eq. (3-13), is controlled by the ϕ_f, which serves as the maximum ϕ_m in the reverse direction. In other words, the Continuously-Yielding model assumes that the maximum bounding shear strength during reverse shearing is the same as the bounding shear strength at the end of the forward shearing process.

The formulation of joint dilation angle in the Continuously-Yielding model is expressed as

$$\psi = \tan^{-1}\left(\frac{|\tau|}{\sigma_n}\right) - \phi \tag{3-16}$$

Dilation takes place whenever the shear stress is at the bounding shear strength level, and is obtained from the friction angle, ϕ_m (Cundall and Lemos, 1988). Examining Eq. (3-16) reveals that the joint dilation as treated in the Continuously-Yielding model should continue to increase regardless of whether a joint is sheared in the forward or reverse direction. However, the rate of dilation decreases gradually and is governed by the value of ϕ_m. After the bounding shear strength is reached, Eq. (3-16) can be rewritten as

$$\psi = (\phi_{mo} - \phi)\, e^{\left(-\frac{u_s^p}{R}\right)} \tag{3-17}$$

Note again the increasing nature of joint dilation as shown in Eq. (3-17).

Assuming a joint with a constant shear stiffness, K_s, of 29.312 GPa/m, initial friction angle, ϕ_{mo}, of 39.3°, basic friction angle, ϕ, of 33.5°, and roughness parameter, R, of 0.0175, the predicted joint behavior using the Continuously-Yielding model subjected to a normal stress, σ_n, of 3 MPa can be illustrated in Figure 3-6. Note that the peak shear strength for the reverse shearing is not very different from the shear strength at the end of the forward shearing. This observation indicates that the

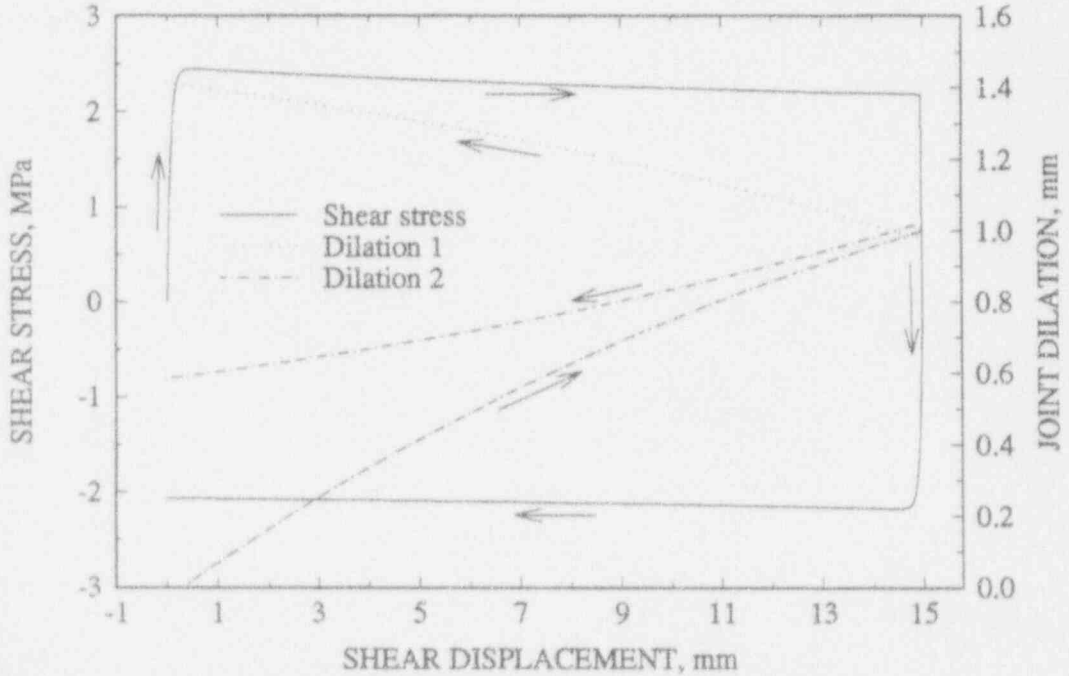

Figure 3-6. Prediction of joint behavior using the Continuously-Yielding model assuming that a constant shear stiffness = 29.312 GPa/m, initial friction angle = 39.3°, basic friction angle = 33.5°, roughness parameter = 0.0175, and normal stress = 3 MPa

Continuously-Yielding rock joint model may not adequately represent the joint shear behavior during reverse shearing observed in the laboratory. Two dilation curves are shown in Figure 3-6. Curve "Dilation 1" represents the dilation behavior following the definition of Eq. (3-17) in which the joint dilation continued to increase. If the sign of the dilation angle was changed as the direction of shear reverses, joint dilation tends to decrease (recovery) during reverse shearing instead of increasing (curve "Dilation 2" in Figure 3-6). However, the extent of the recovery is not as extensive as that observed in the laboratory.

3.4 SUMMARY

Careful examination of the respective equations representing the Mohr-Coulomb, Barton-Bandis, and Continuously-Yielding rock joint models has revealed that all three models were essentially developed for unidirectional shearing. They assume the same joint behavior in both forward and reverse shearing directions. With this assumption, the same shear strength criterion is applicable in both shearing conditions. This is not consistent with the measured shear strength in laboratory experiments. The shear strength during reverse shearing was always smaller than that in the forward direction.

The Mohr-Coulomb model calculates the dilation based on a constant dilation angle. Dilation starts when peak shear strength is reached and ceases when a critical shear displacement is reached. The Barton-Bandis and Continuously-Yielding models directly link joint dilation with shear displacement through the roughness properties. Since a joint continues to wear during shearing, the dilation angle used to calculate joint dilation continues to decrease. The constant decrease of dilation angle implies that the joint will eventually stop dilating when it is completely worn. All three models inherently assume an increase of joint dilation with increasing shear displacement irrespective of the direction of shearing. This is inconsistent with the joint dilation behavior observed in the laboratory.

4 NUMERICAL SIMULATION OF LABORATORY DIRECT SHEAR EXPERIMENTS USING UDEC

In the previous section, the ability of the three rock joint models in their fundamental forms to model joint behavior under cyclic loading conditions was discussed, while the ability of these joint models as implemented in the UDEC computer code for modeling joint behavior is going to be discussed in Section 5. This section focuses on numerical simulation of laboratory experiments of single-joint rock specimens using UDEC. The UDEC code Versions 1.82 and 1.83 were used in the numerical simulation. UDEC was upgraded in the middle of this study. Version 1.82 was used to develop the model. All the analyses reported in Section 5 were carried out using Version 1.83. Changes made in Version 1.83 do not affect the rock joint models.

Figure 4-1 shows top and side views of the direct shear test apparatus used for testing single-joint rock specimens in both cyclic pseudostatic and dynamic shear tests. Detail discussion on the apparatus is given by Hsiung et al. (1993b). The direct shear tests were designed to maintain a normal stress throughout the test period. For cyclic pseudostatic tests, a constant shear velocity was applied at a 4.2×10^{-2} mm/sec (4.2×10^{-5} m/sec) rate and the shear velocity varied as a function of drive input for the harmonic and earthquake shear tests. In UDEC modeling, a simplified approach was taken to model the experiments by not explicitly simulating the test apparatus. Figure 4-2 shows such a UDEC model. This approach neglected the possible effect of the test apparatus. For the cyclic pseudostatic shear tests, this approach was justified since the applied shear velocity was so small and the possible effect of the apparatus was not in existence. For the typical range of input frequencies of the dynamic loadings used in the laboratory, that is, below 5 Hz, the response of the shear apparatus should not influence joint response significantly. A separate study using the 3DEC has indicated that neglecting the effect of the test apparatus can be tolerated if the input frequencies of a dynamic test are less than 50 Hz (Hsiung and Chowdhury, 1991).

As shown in Figure 4-2, a rigid block was attached to the left-hand side of the top rock block. The attachment of this rigid block made it possible to apply an input loading condition similar to the actual test condition. The force variation measured at the centroid of this loading block resulting from resisting joint shear was directly comparable to the shear force measured from the load cell (identified as circle 5 in Figure 4-1) that was used for joint shear stress calculation. A constant normal stress was applied at the top surface of the top block. After iterating the system to static equilibrium, a horizontal input velocity was applied to the centroid of the rigid loading block. The rigid loading block was 3 mm above the horizontal interface. As a result, the applied load (in the form of a constant velocity) through the centroid of the rigid loading block did not go through the centroid of the top rock block. Consequently, a moment was created about the centroid of the top rock block. This moment was considered small. Nevertheless, it does have some effects on simulation results that will be discussed later in this section. The sides of the bottom rock block were fixed to prevent displacement along horizontal direction and the bottom of the bottom rock block was set to not allow movement in vertical direction. Both the top and bottom rock blocks were assumed to be fully-deformable. The constitutive behavior of the horizontal interface between the top and bottom rock blocks is characterized by either of the three rock joint models described in Section 3. The vertical interface between the rigid loading block and the top rock block is governed by the Mohr-Coulomb model. Cohesion and coefficient of friction of this vertical interface were assumed to be zero to allow sliding along the interface. This sliding capability was considered critical in that the applied input velocity could be maintained in the horizontal direction throughout the entire simulation. An extremely large tensile strength was also assigned to this vertical interface to prevent detachment from the top rock block.

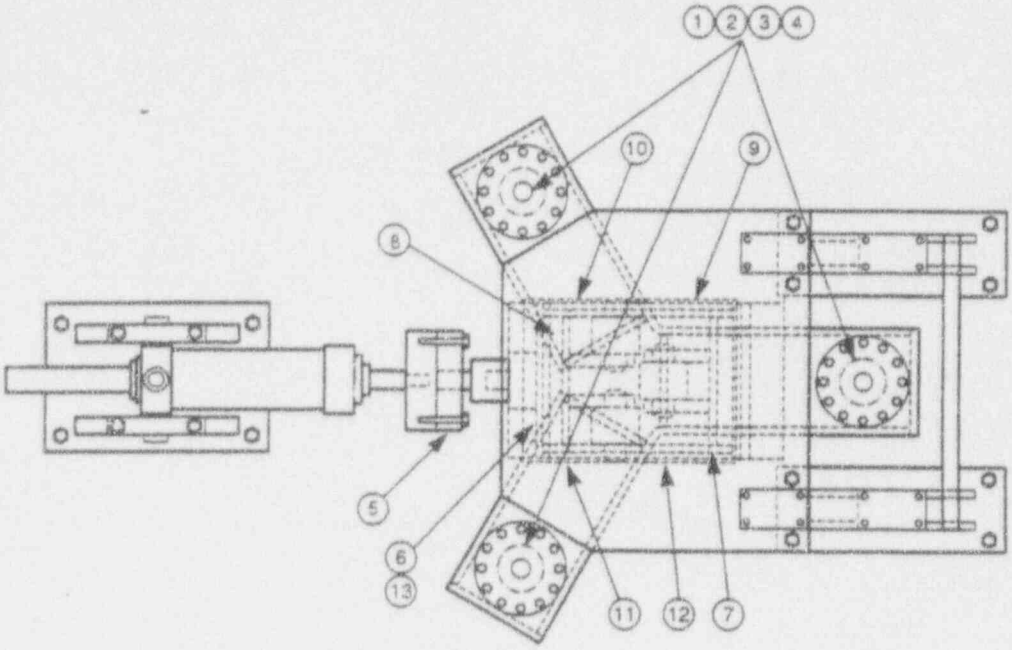

TOP VIEW

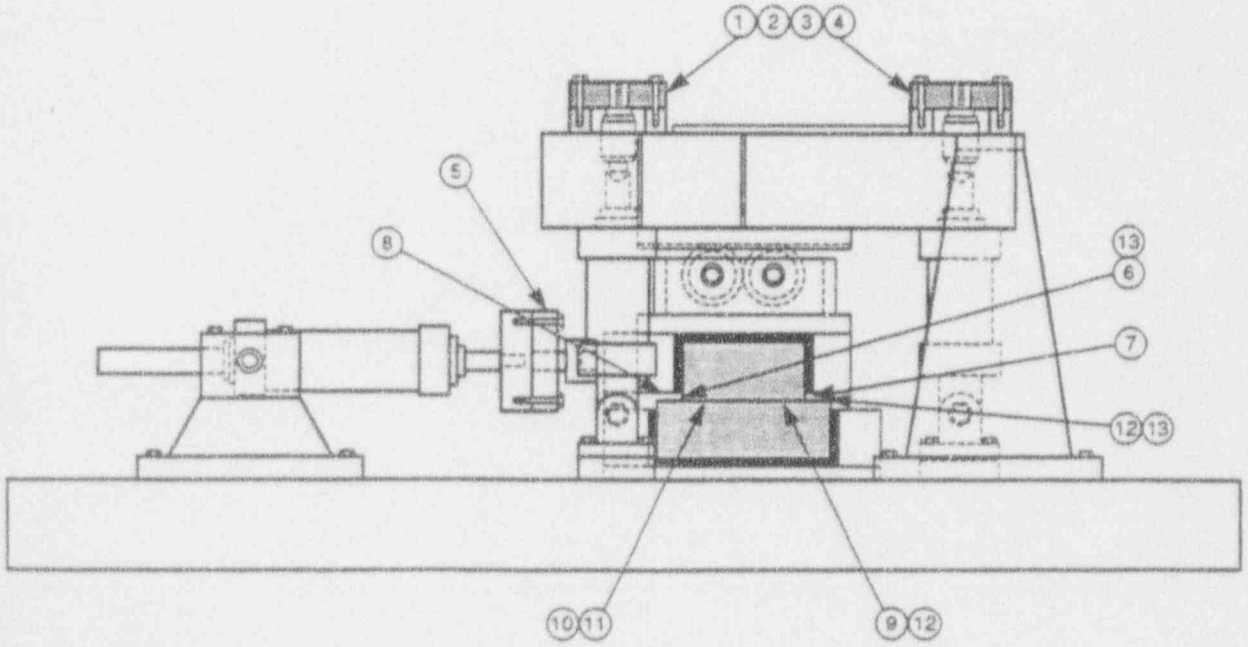

SIDE VIEW

Figure 4-1. Assembly and instrumentation diagram for direct shear test apparatus (numbers in circles refer to location of instrumentation)

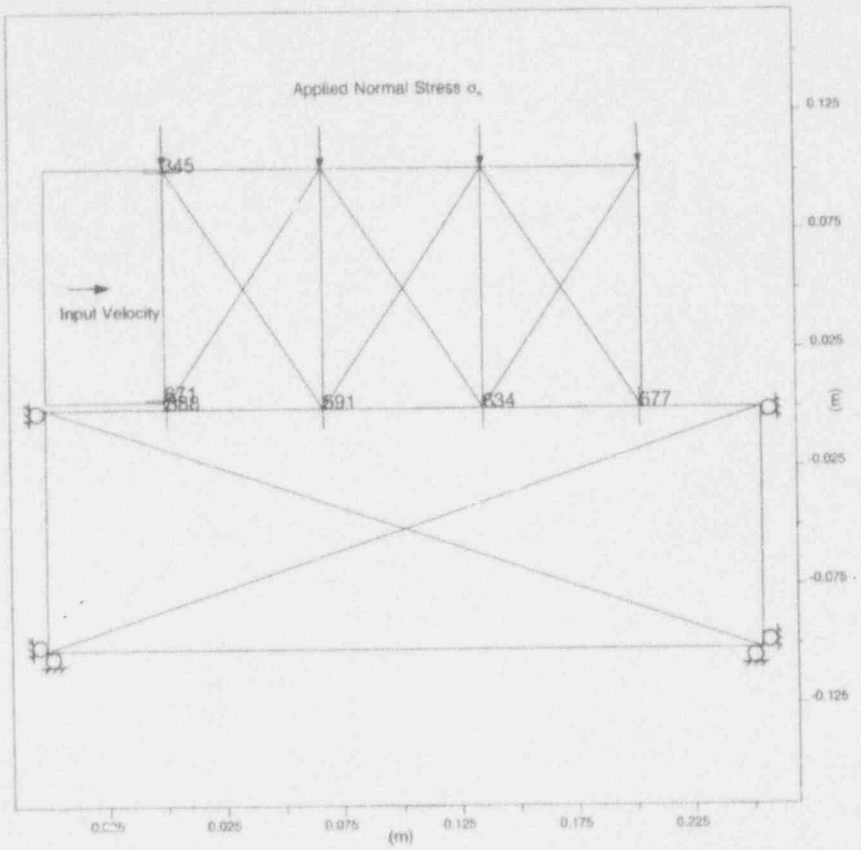

Figure 4-2. UDEC model for simulating laboratory test on single-joint specimen

The material properties used for the preliminary runs for evaluation of the UDEC model shown in Figure 4-2 are given as follows:

Rock material (both top and bottom blocks)

Density:	2,420 kg/m^3
Bulk Modulus K:	21,443 MPa
Shear Modulus G:	16,083 MPa

Vertical Interface

Joint Normal Stiffness (jkn):	200,000 MPa/m
Joint Shear Stiffness (jks):	20,000 MPa/m
Joint Tensile Strength (jten):	10^{10} MPa
Joint Cohesion (jcoh):	0 MPa
Joint Friction Coefficient (jfric):	0.0

Horizontal Joint Interface (using the Continuously-Yielding model)

Joint Normal Stiffness (jkn):	56,777 MPa/m
Minimum Joint Normal Stiffness (minjkn):	1,000 MPa/m
Maximum Joint Normal Stiffness (maxjkn):	100,000 MPa/m
Exponent of Joint Normal Stiffness (jen):	0.79
Joint Shear Stiffness (jks):	22,834 MPa/m
Minimum Joint Shear Stiffness (minjks):	22,834 MPa/m
Maximum Joint Shear Stiffness (maxjks):	22,834 MPa/m
Exponent of Joint Shear stiffness (jes):	0.0
Joint Tensile Strength (jten):	0 MPa
Joint Cohesion (jcoh):	0 MPa
Joint Initial Friction Angle (jif):	47.7°
Joint Residual Friction Angle (jfric):	39.8°
Joint Roughness Parameter (jr):	0.0138

In order to simulate the actual loading speed as was used in the laboratory, a constant horizontal velocity of 4.2×10^{-5} m/sec was applied to the centroid of the rigid loading block. The direction of the velocity was pointed toward the right-hand side of the model. This velocity combined with the small rock density resulted in an extremely small critical time step (5.337×10^{-6} sec). Based on this time step, it needed 178 million steps of calculation for the top rock block to displace 40 mm as it did for the laboratory tests. UDEC has been written in single-precision arithmetic specifically for IBM PC or compatibles. For single precision numbers, the last significant digit is in the seventh or eighth place after the decimal point. At the original applied velocity and the stable time step calculated by UDEC, the increments calculated for some variables at each time step were smaller than this precision. As a result, the numerical values of these variables did not get updated in each cycle. This numerical error was cumulative with every cycle. After a large number of cycles, may be more than a million or so, the cumulative error became excessive. This was confirmed by the peculiar result shown in Figure 4-3. This figure shows a distorted mesh of the top rock block as compared to that in Figure 4-2. This distortion was also associated with excessive counterclockwise rotation of the top rock block during joint shearing that caused loss of contact for most of the contact points between the top and bottom rock blocks with the exception of only one contact point located at the lower left corner of the top rock block.

To overcome this problem, the running time had to be shortened to reduce the number of calculations. There were two ways to reduce the total calculation numbers, by increasing the input velocity or rock density. It was decided to increase the input velocity. Although increase in input velocity deviates from the actual experimental condition, the modeling results were not significantly different from the experiment results since the Continuously-Yielding rock joint model is not velocity dependent. After some tests, a velocity of 100 mm/sec was used for further study. With this velocity, the numerical instability problem was eliminated. Caution needed to be exercised to ensure adequate damping (i.e., Rayleigh) to the model. The natural frequency required for the Rayleigh damping was determined by running the UDEC model with no shear load.

Figure 4-4 shows the relation between the shear stress and shear displacement at three contact points along the joint interface (refer to Figure 4-2 for the relative locations of these three contact points). The shear stress versus shear displacement curve for contact point 388 appears to be incorrect. This incorrect result is related to the logic used in the UDEC for the calculation of joint shear stress. At each time step, UDEC calculates forces and displacements at each contact point in the model. The shear stress at each

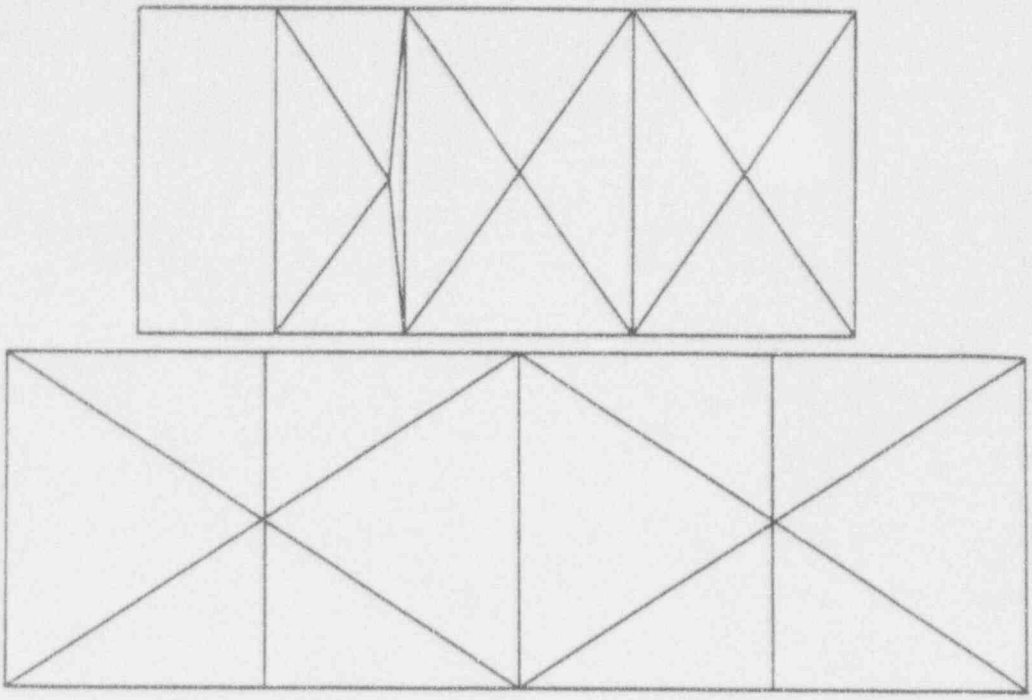

Figure 4-3. Plot showing distorted mesh of the top block due to numerical instability resulting from large number of calculations

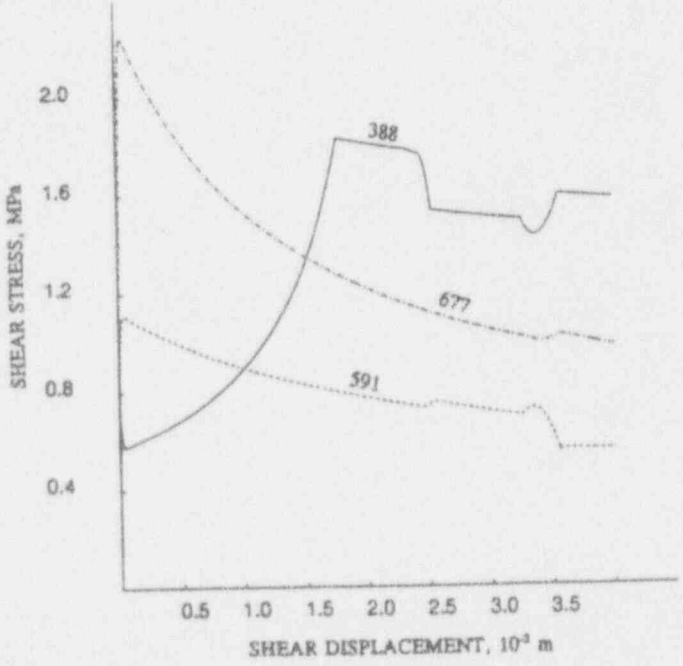

Figure 4-4. Joint shear stress versus shear displacement plot using model in Figure 4-2

contact point along a joint interface, if required, is then calculated by dividing the shear force at the point by its associated joint length. The joint length of a contact point is equal to the sum of half distances from this point to the immediate contact points on both sides. For example, in Figure 4-2, the joint length for contact point 558 is one-half the length between contact points 634 and 591. If one looks carefully, the joint length for contact point 388 is half the length between only this point and contact point 634 since contact point 388 is at the edge of the top rock block. As the top block moves to the right, contact point 388 follows. However, since contact point 634 is located at the bottom block, it remains stationary. As a result, the joint length at contact point 388 tends to decrease and, at some point, becomes zero when contact points 388 and 634 overlap each other. Since the joint shear force at contact point 388 does not decrease at the same rate as its joint length, the resulting shear stress tends to increase as indicated in Figure 4-4. This situation can be avoided by adopting a model as shown in Figure 4-5, in which no contact points were assigned on the bottom rock block. Consequently, the joint length at contact point 388 remained constant during shearing. Figure 4-6 shows the shear stress versus shear displacement curves along the joint interface using the model in Figure 4-5. All four curves correctly reflect the joint behavior. Figure 4-6 also shows the effect of the misalignment between the centroids of the rigid loading and the top rock blocks. A large difference in the shear stress between contact points 388 and 677 can be observed from the figure.

The UDEC model in Figure 4-5 formed the basic model for simulating the laboratory experiments on single-joint rock specimens. Minor modifications to the model in Figure 4-5 were made as shown in Figure 4-7. The size of the rigid loading block was reduced such that the centroids for the rigid loading block and the top rock block were at the same horizon. This modification was intended to minimize the effect of misalignment. Another modification involved increasing the rounding length for block corners from 0.001 of the block edge length used in Figure 4-5 to 0.005 of the block edge length as shown in Figure 4-7. This increase was necessary since the rounding length had a direct link to total joint dilation allowable before the two surfaces at the opposite sides of the joint interface were treated as completely separated (i.e., loss of contact) by the UDEC code. The larger the rounding length is, the larger the joint dilation is allowed. Figure 4-8 shows the shear stresses at these contact points.

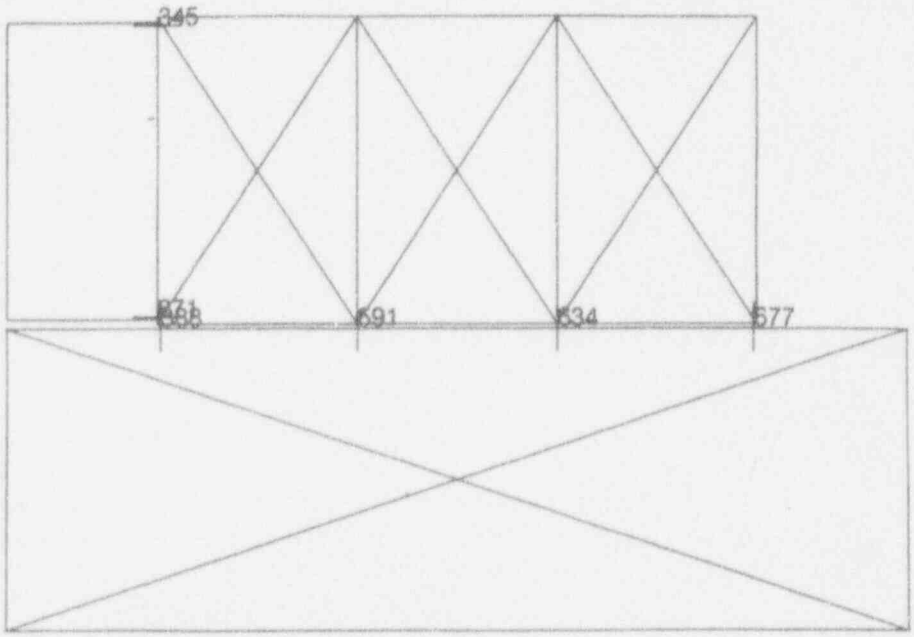

Figure 4-5. Modified UDEC model

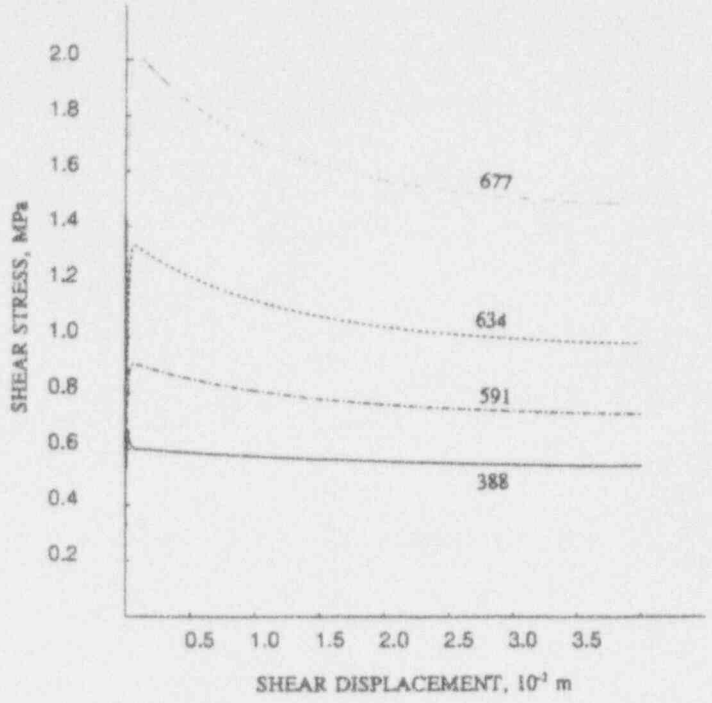

Figure 4-6. Joint shear stress versus shear displacement plot using model in Figure 4-5

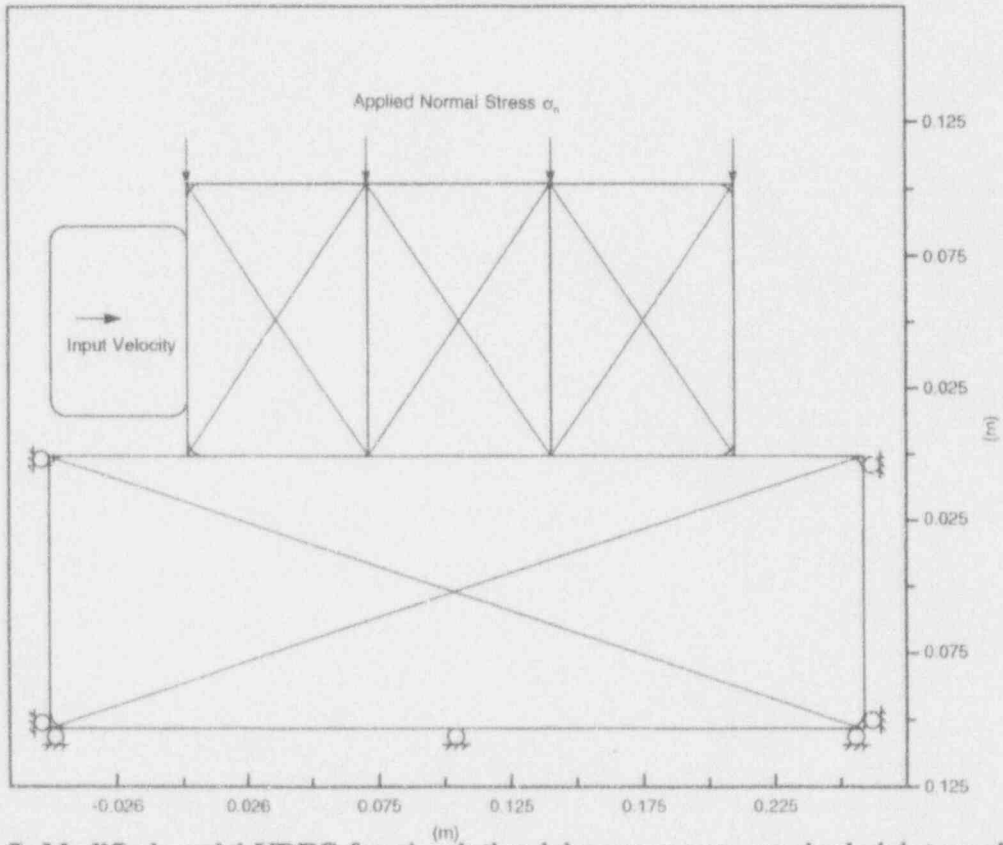

Figure 4-7. Modified model UDEC for simulating laboratory tests on single-joint specimens

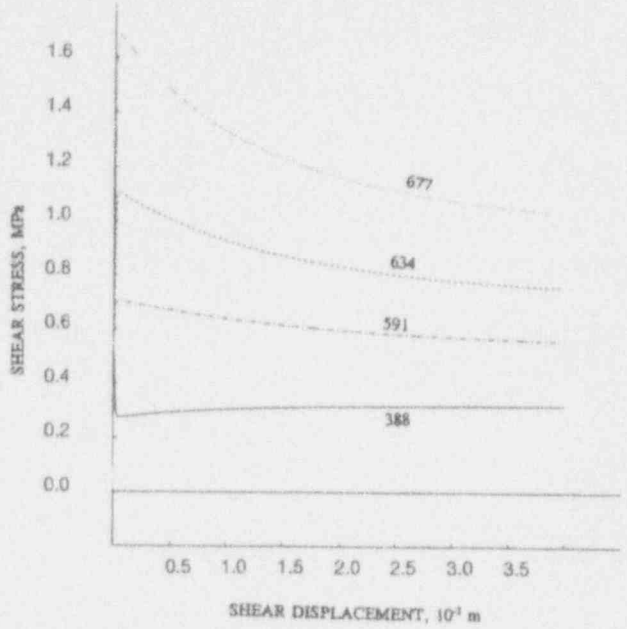

Figure 4-8. Joint shear stress versus shear displacement plot using model in Figure 4-7

Five cyclic pseudostatic tests, one harmonic test, and one earthquake direct shear test were simulated using the model in Figure 4-7. The results of these simulations are discussed in the following section. The material properties for rock matrix of each test are given in Table 4-1. These properties were obtained from testing cylindrical specimens taken from the intact rock near the joint to be tested. The joint material properties required for the three rock joint models are listed in Tables 4-2, 4-3, and 4-4. All these properties were calculated from the corresponding experimental results. Note that a detail discussion on the determination of these properties can be found in a report by Hsiung et al. (1993b).

Table 4-1. Material properties of rock matrix for joint specimens

Test Type	Test No.	Density (kg/m^3)	Bulk Modulus (GPa)	Shear Modulus (GPa)
cyclic pseudostatic	7	2418.8	20.13	16.34
cyclic pseudostatic	8	2418.8	23.72	17.79
cyclic pseudostatic	9	2418.8	20.96	14.41
cyclic pseudostatic	10	2418.8	23.37	14.02
cyclic pseudostatic	11	2418.8	20.00	13.17
harmonic	14	2418.8	21.86	17.10
earthquake	24	2418.8	19.93	14.96

Table 4-2. Joint properties for Mohr-Coulomb model used in UDEC

Test Type	Test No.	Normal Stress (MPa)	jkn (MPa/m)	jks (MPa/m)	jfric (degrees)	jcoh (MPa)	jdil (degrees)	z dilation (m)
cyclic pseudostatic	7	5.0	93926	16984	36.6	0.0	4.1	0.03725
cyclic pseudostatic	8	4.0	38278	11752	37.6	0.27	4.2	0.03799
		5.0	42267	11602	37.6	0.27	3.0	0.03663
cyclic pseudostatic	9	3.0	35964	16929	38.0	0.0	2.4	0.03815
		4.0	39861	13876	38.0	0.0	1.6	0.03785
		5.0	46109	13281	38.0	0.0	1.3	0.03749
cyclic pseudostatic	10	2.0	33323	8639	37.2	0.19	2.7	0.04032
		3.0	36220	9480	37.2	0.19	1.7	0.03811
		4.0	56634	9502	37.2	0.19	1.3	0.03698
		5.0	71282	9514	37.2	0.19	1.1	0.03696
cyclic pseudostatic	11	1.0	37778	5461	43.0	0.02	2.9	0.03701
		2.0	57389	2299	43.0	0.02	1.4	0.04284
		3.0	76538	10393	43.0	0.02	1.1	0.03990
		4.0	86560	25530	43.0	0.02	0.9	0.03480
		5.0	108021	12433	43.0	0.02	0.7	0.03806
harmonic	14	1.0	39141	7006	33.5	0.0	18.5	0.001097
earthquake	24	1.0	57405	28177	43.0	0.0	8.6	0.00198

Note: jkn = joint normal stiffness; jkn = joint shear stiffness; jfric = joint friction angle; jcoh = joint cohesion; jdil = joint dilation angle; z dilation = critical shear displacement

Test 4-3. Joint properties for Barton-Bandis model used in UDEC

Test Type	Test No.	jkn (MPa/m)	jks (MPa/m)	jcso (MPa)	sigmac (MPa)	jrco	phir (degrees)	lo (m)	ln (m)
cyclic pseudostatic	7	93926	18984	120.3	133.07	12.1	26.2	0.2032	0.2032
cyclic pseudostatic	8	37278	11752	144.9	151.00	11.0	27.0	0.2032	0.2032
cyclic pseudostatic	9	35964	16929	170.5	200.64	7.0	28.4	0.2032	0.2032
cyclic pseudostatic	10	33323	8639	112.5	120.46	11.8	26.2	0.2032	0.2032
cyclic pseudostatic	11	37778	5461	115.3	132.38	10.4	27.6	0.2032	0.2032
harmonic	14	39141	7006	106.3	157.07	19.5	24.7	0.2032	0.2032
earthquake	24	57405	28177	123.4	159.27	11.0	26.8	0.2032	0.2032

Note: jkn = joint normal stiffness; jks = joint shear stiffness; jcso = laboratory-scale joint wall compressive strength; sigmac = intact rock uniaxial compressive strength; jrco = laboratory-scale *JRC*; phir = residual angle of friction; lo = laboratory-scale joint length; ln = field-scale joint length

Test 4-4. Joint properties for Continuously-Yielding model used in UDEC

Test Type	Test No.	jkn (MPa/m)	minjkn (MPa/m)	maxjkn (MPa/m)	jen	jks (MPa/m)	minjks (MPa/m)	maxjks (MPa)	jes	jif (degrees)	jfric (degrees)	jr (m)
cyclic pseudostatic	7	57857	57857	93926	0.7086	23821	23821	23821	0.0	42.3	32.3	0.0172
cyclic pseudostatic	8	34045	34045	42267	0.5965	27218	27218	27218	0.0	44.7	35.8	0.0210
cyclic pseudostatic	9	29361	29361	46109	0.6783	29312	29312	29312	0.0	39.3	33.5	0.0175
cyclic pseudostatic	10	47801	33323	71218	0.5199	19398	19398	19398	0.0	44.3	36.1	0.0135
cyclic pseudostatic	11	56953	37778	108021	0.7304	22156	22156	22156	0.0	47.4	39.4	0.0136
harmonic	14	39141	57405	95000	0.6885	7006	7006	7006	0.0	57.6	32.8	0.0169
earthquake	24	57405	57405	93926	0.4404	28177	28177	28177	0.0	48.8	39.2	0.0211

Note: jkn = joint normal stiffness; minjkn = minimum value of jkn; maxjkn = maximum value of jkn; jks = joint shear stiffness; minjks = maximum value of jks; jen = exponent of joint normal stiffness; jes = exponent of joint shear stiffness; jif = joint initial friction angle; jfric = joint friction angle; jr = joint roughness parameter

5 RESULTS AND DISCUSSIONS OF UDEC MODELING

5.1 CYCLIC PSEUDOSTATIC EXPERIMENTS MODELING

Five pseudostatic direct shear experiments were simulated using UDEC code. Each ›eriment was analyzed using Mohr-Coulomb, Barton-Bandis, and Continuously-Yielding rock joint m s. These results were compared with those from the laboratory experiments to evaluate the implementat.on of these rock joint models in the UDEC computer code, and to assess the applicability of these joi:t models to simulate rock joint behavior under cyclic loading.

5.1.1 Mohr-Coulomb Joint Model

Figures 5-1 to 5-5 show joint shear stress versus shear displacement plots of UDEC modeling using the Mohr-Coulomb joint model for joint behavior simulation and laboratory test results for the five cyclic pseudostatic experiments. Notice that four tests (Figures 5-2 to 5-5) contain a different number of shear cycles. The shear cycle curve under the smallest applied normal stress is the first shear cycle in a figure, and the curve under the largest applied normal stress is the last shear cycle. The maximum normal stress applied on the top of the top rock block for both laboratory tests and modeling was about 5 MPa. The first shear cycle was initiated by shearing the top rock block, from its original position along one direction (forward shearing) for about 40 mm (portion of curve on the top half of Figures 5-1 to 5-5). Then the top rock block was sheared back (reverse shearing) to its initial position (portion of curve on the bottom half of Figures 5-1 to 5-5). After the completion of a shear cycle, the normal stress was released, and subsequently the next higher level of normal stress was applied, followed by the same shearing cycle as was conducted under the previous normal stress level. It should be noted that the Mohr-Coulomb rock joint model as implemented in the UDEC code assumes a constant normal stiffness for joint normal stress calculation. However, the results of cyclic normal loading/unloading tests on the Apache Leap tuff joints have indicated that joint normal stiffness is not constant at different normal stress levels. In order to properly model the test condition, different normal stiffnesses, calculated from the cyclic normal loading/unloading test results (Table 4-2), were used for different shear cycles.

The joint shear stress for the UDEC modeling was calculated using the horizontal force history at the centroid of the rigid loading block. As discussed earlier, this shear stress is comparable to the shear stress measured from the horizontal actuator during testing. As discussed in Section 3.1, the Mohr-Coulomb joint model assumes an elastic perfectly plastic behavior. Consequently, this model is not able to predict the strain softening behavior of a rock joint as is indicated in Figure 5-1. Nevertheless, this model does give a reasonable prediction in shear stress during joint forward shearing, except for the case shown in Figure 5-4 in which the predicted values of shear stress are substantially larger than the experimental results. The prediction of the shear stress in the period of reverse shearing, on the other hand, does not seem to be adequate.

Figures 5-6 to 5-10 illustrate the joint dilation behavior (normal displacement) for the five cyclic pseudostatic tests for which the joint shear stress versus shear displacement characteristics were shown in Figures 5-1 to 5-5. The joint dilation is equivalent to the positive normal displacement. The negative portion of the normal displacement is not dilation. Rather, it can be viewed as joint compaction. The joint dilation shown in the figures was an average value at the four contact points indicated in Figure 4-7. Note that, for all shear cycles, joint dilation reaches a maximum value that is controlled by the critical shear displacement, u_{cs} [Eq. (3-4)]. As discussed in Section 3.1 and confirmed in Figures 5-6 to 5-10, the joint

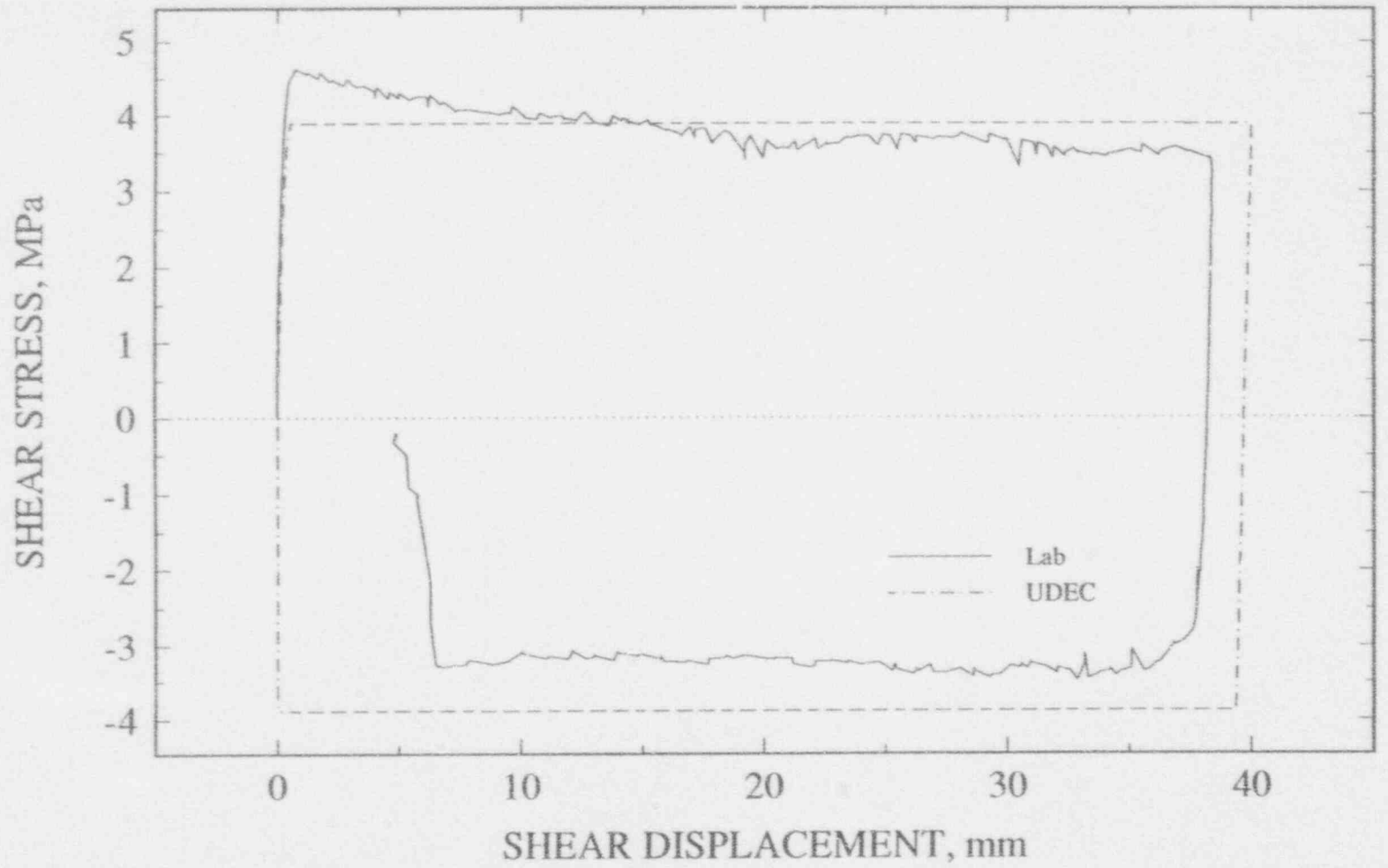

Figure 5-1. UDEC using Mohr-Coulomb joint model and laboratory test results of shear stress versus shear displacement plot for test no. 7 under normal stress of 5 MPa

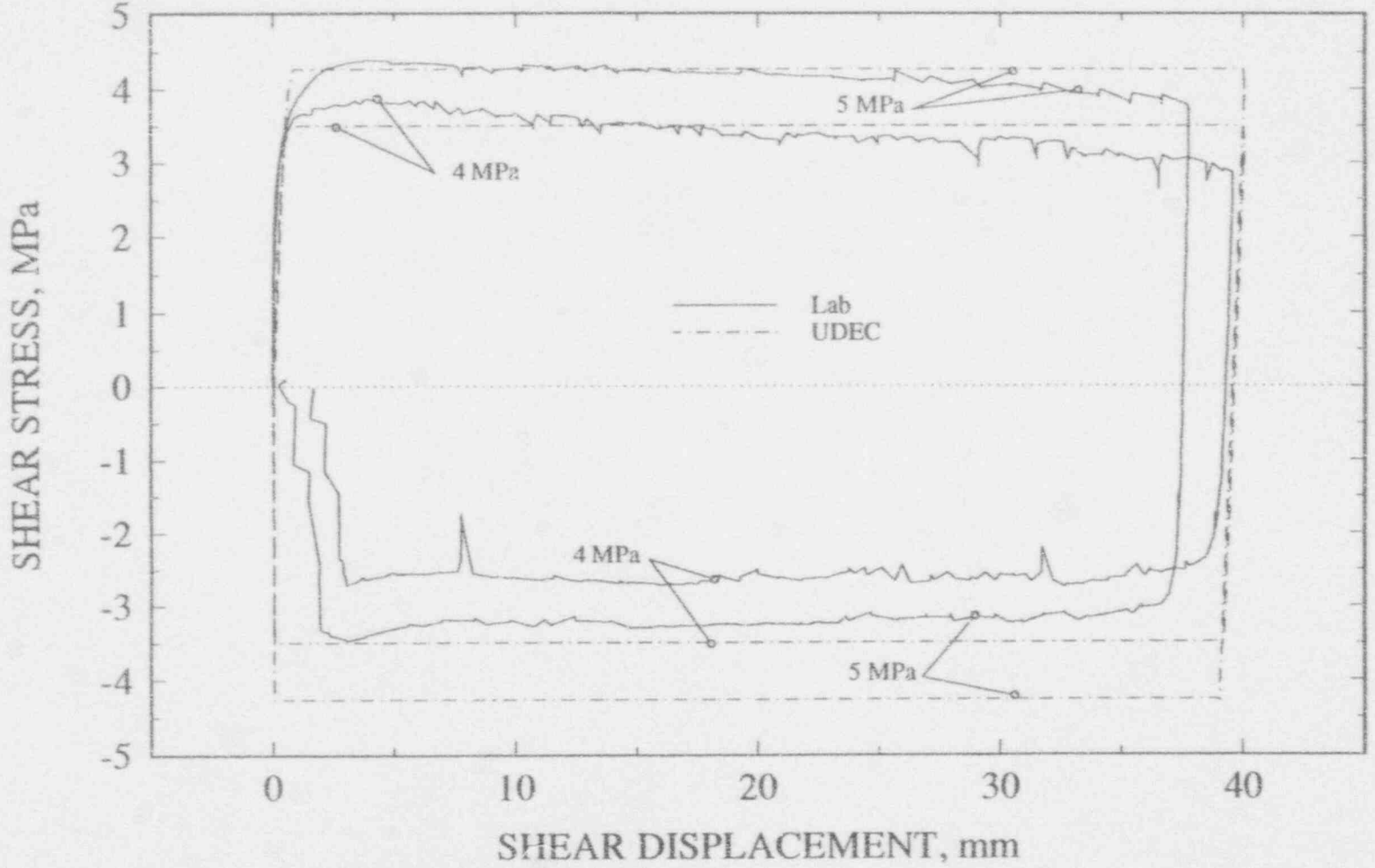

Figure 5-2. UDEC using Mohr-Coulomb joint model and laboratory test results of shear stress versus shear displacement plot for the same joint specimen as a function of normal stress for test no. 8

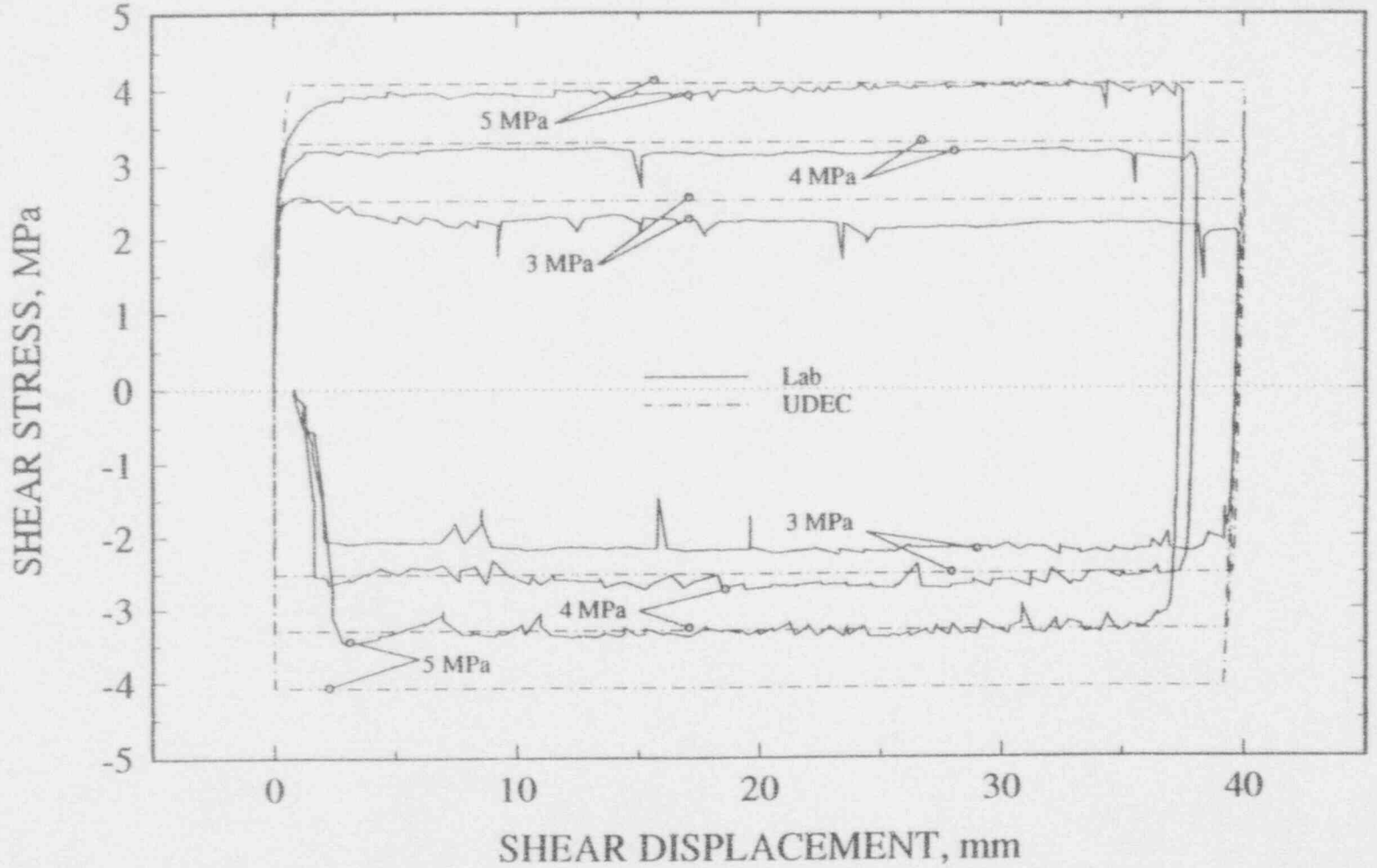

Figure 5-3. UDEC using Mohr-Coulomb joint model and laboratory test results of shear stress versus shear displacement plot for the same joint specimen as a function of normal stress for test no. 9

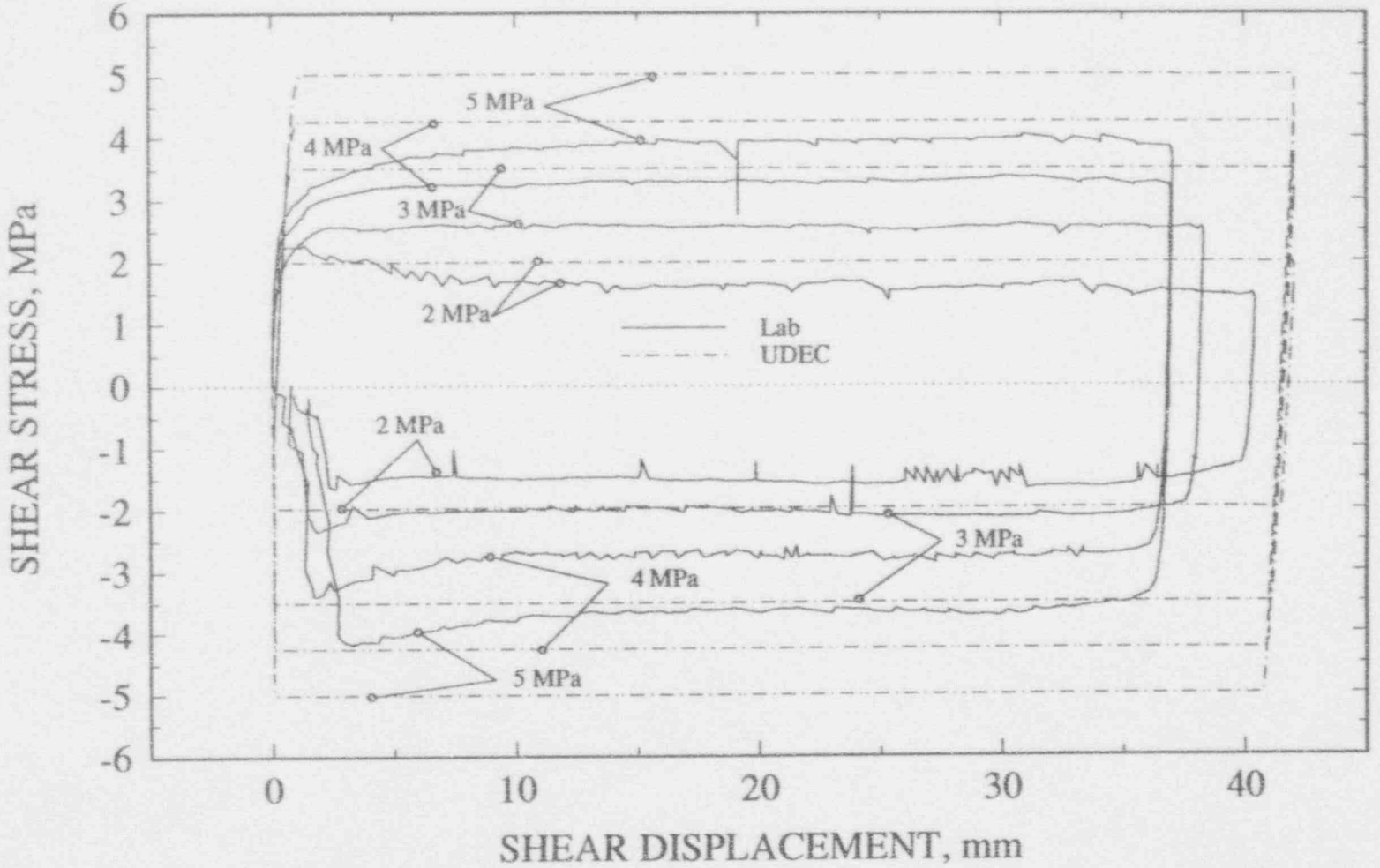

Figure 5-4. UDEC using Mohr-Coulomb joint model and laboratory test results of shear stress versus shear displacement plot for the same joint specimen as a function of normal stress for test no. 10

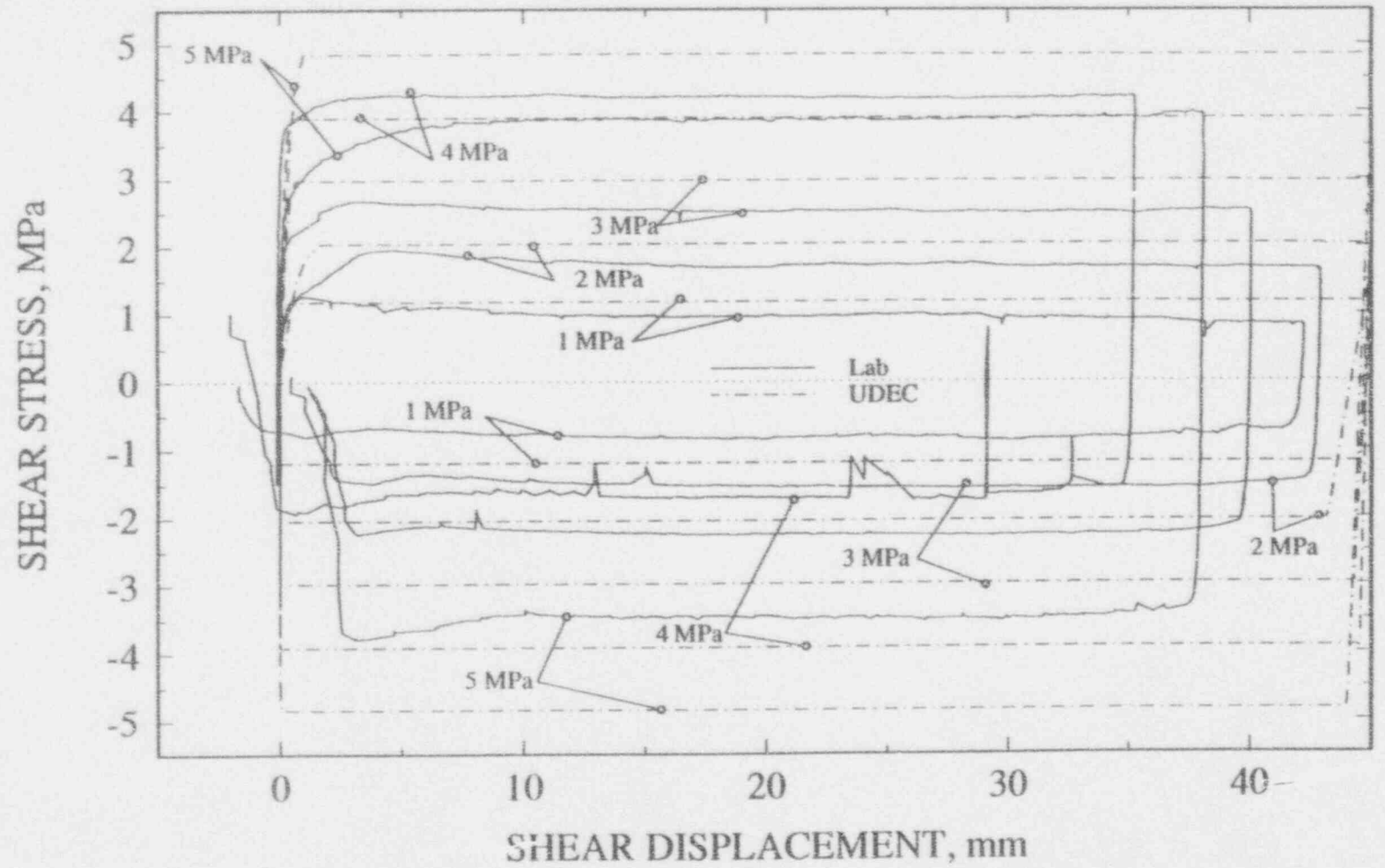

Figure 5-5. UDEC using Mohr-Coulomb joint model and laboratory test results of shear stress versus shear displacement plot for the same joint specimen as a function of normal stress for test no. 11

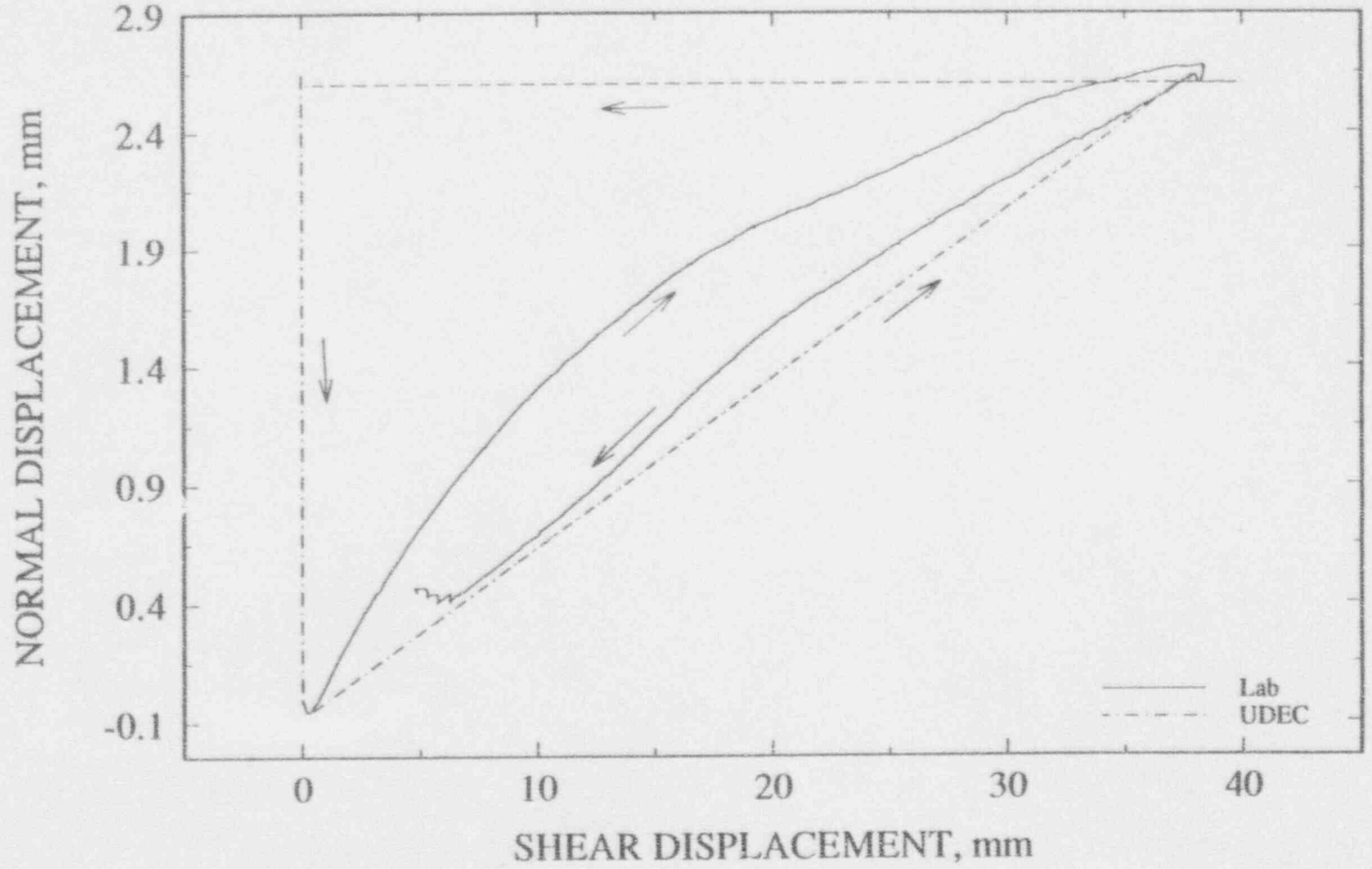

Figure 5-6. UDEC results using Mohr-Coulomb joint model and laboratory measurements of joint dilation for test no. 7 under normal stress of 5 MPa

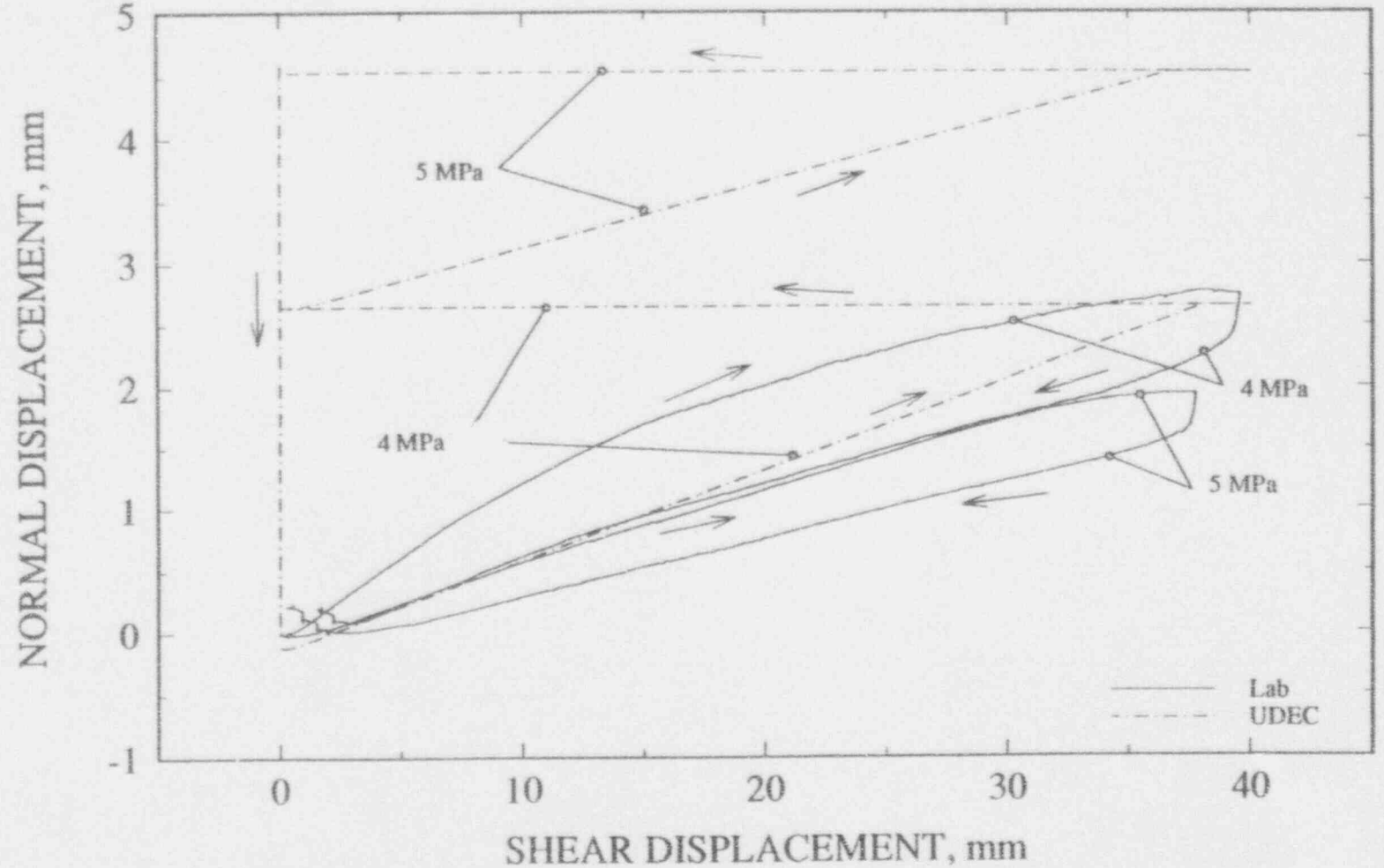

Figure 5-7. UDEC results using Mohr-Coulomb joint model and laboratory measurements of joint dilation plot for the same joint specimen as a function of normal stress for test no. 8

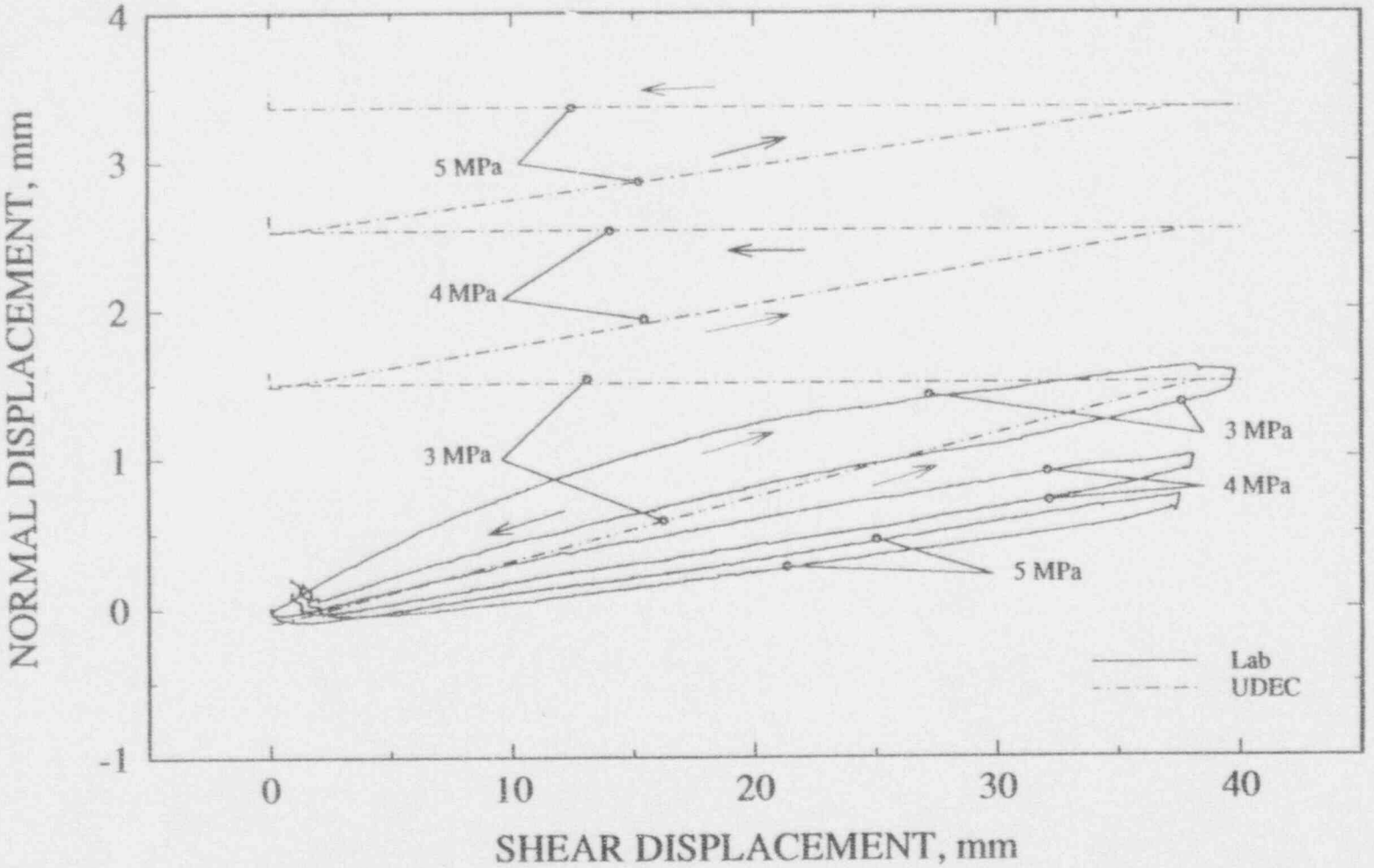

Figure 5-8. UDEC results using Mohr-Coulomb joint model and laboratory measurements of joint dilation plot for the same joint specimen as a function of normal stress for test no. 9

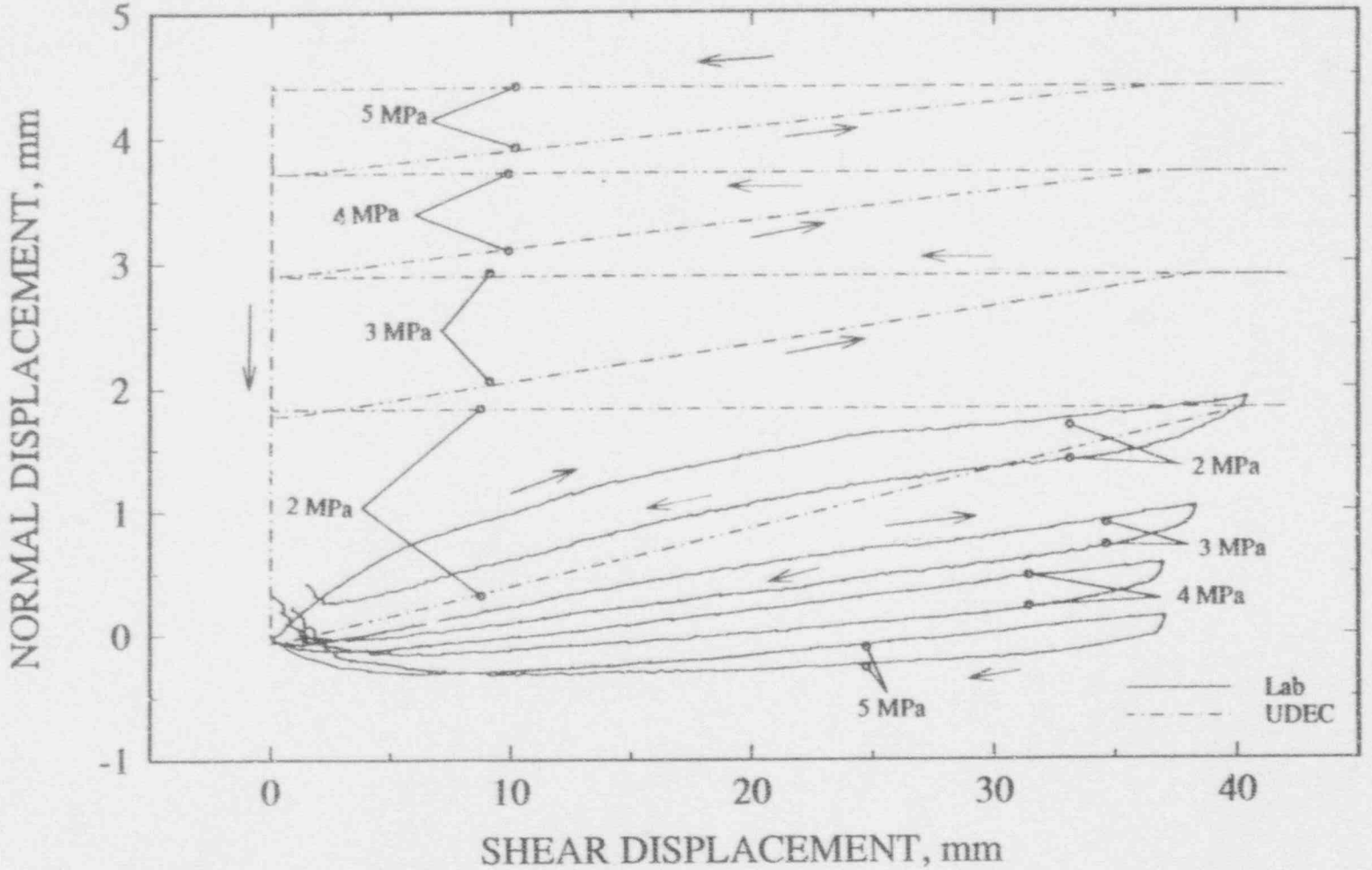

Figure 5-9. UDEC results using Mohr-Coulomb joint model and laboratory measurements of joint dilation plot for the same joint specimen as a function of normal stress for test no. 10

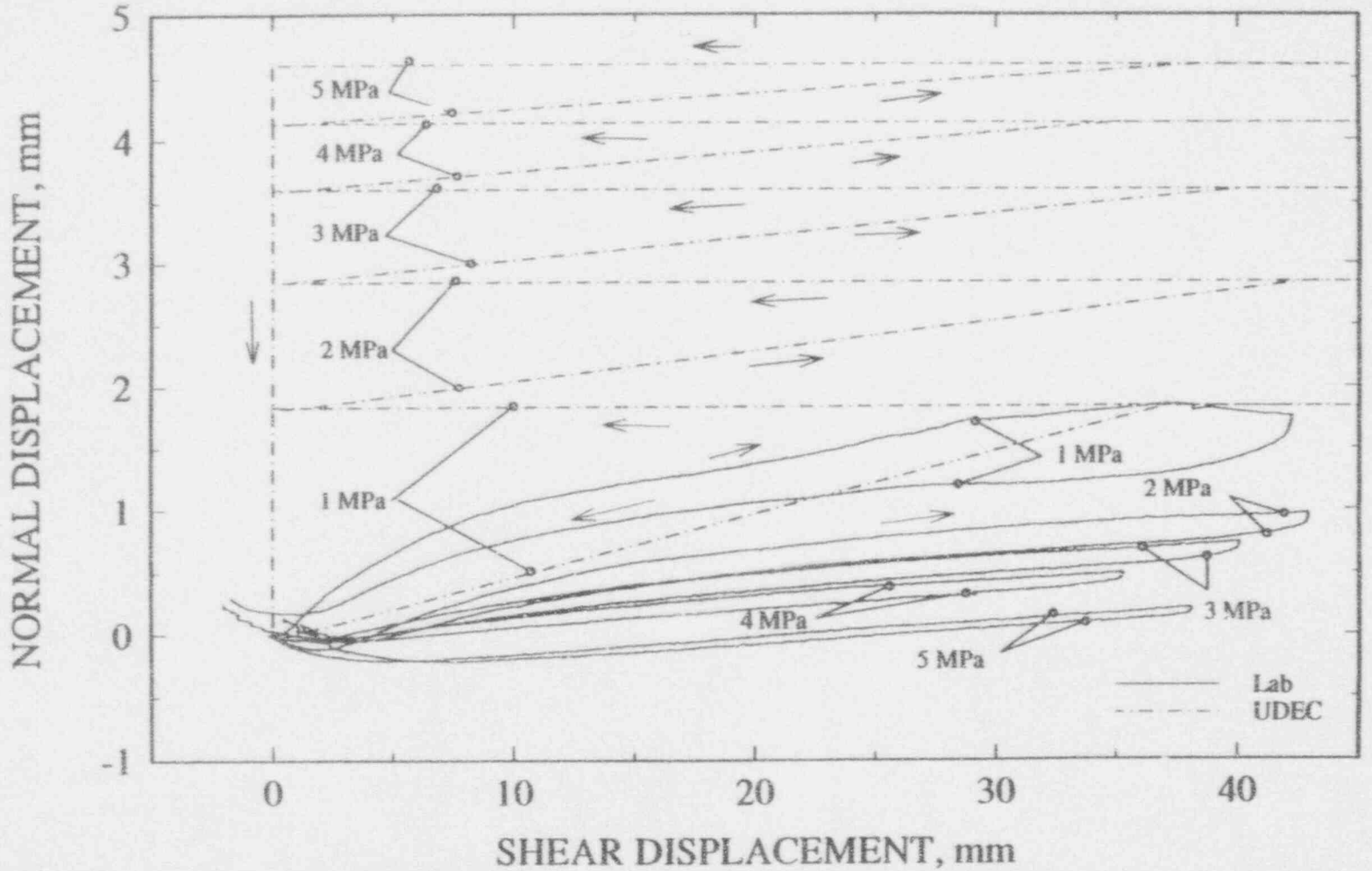

Figure 5-10. UDEC results using Mohr-Coulomb joint model and laboratory measurements of joint dilation plot for the same joint specimen as a function of normal stress for test no. 11

dilation, according to the Mohr-Coulomb model, ceases to increase when the shear displacement is greater than the u_{cs} value. The u_{cs} values for all shear cycles of all five experiments are listed in Table 4-2 under the "z dilation" column. The dilation behavior modeled using the Mohr-Coulomb model as implemented in the UDEC code further indicates that once the dilation ceases to increase during forward shearing, it will remain constant during the entire period of reverse shearing. This is probably an error in the implementation of Mohr-Coulomb model in the UDEC code. This dilation prediction departs from the dilation definition as provided in Eqs. (3-3) and (3-4) that indicate an increasing nature of joint dilation along both forward and reverse shearing directions (Figure 3-2). It is also different from the alternate concept that dilation angle changes sign because of the change in the direction of shear. Figures 5-7 to 5-10 further indicate that dilation begins to increase again during the forward shearing of the next shear cycle. Comparing the results from the UDEC simulation with those of the laboratory experiments, it is clear that the joint dilation prediction using the Mohr-Coulomb model as implemented in the UDEC code did not predict the dilation recovery during reverse shearing.

If the critical shear displacement, u_{cs}, is not reached during the course of forward shearing, the recovery of joint dilation can be predicted using the Mohr-Coulomb model as implemented in the UDEC code (Figure 5-11). This prediction indicates that the algorithm, as formulated in UDEC, for joint dilation calculations using Mohr-Coulomb involves a sign change of the dilation angle. Note that the temporary increase in joint dilation at the beginning of reverse shearing is not real. This temporary increase is a natural result of sign change in the dilation angle during reverse shearing. Bear in mind that the algorithm used in the UDEC code for dilation calculation for the Mohr-Coulomb model is the same for both forward and reverse shearing. As a result, what is originally the compaction behavior at the beginning of the forward shearing becomes the dilation at the beginning of reverse shearing due to sign change in dilation angle. In reality, similar compaction behavior, shown at the beginning of forward shearing, may also be observed at the beginning of reverse shearing. Careful examination of the experimental results for dilation seems to confirm this observation.

5.1.2 Barton-Bandis Joint Model

Figures 5-12 to 5-16 show joint shear stress versus shear displacement plots of UDEC modeling using the Barton-Bandis joint model for the same five cyclic pseudostatic tests which have been discussed in Section 5.1.1 for UDEC modeling using the Mohr-Coulomb rock joint model. The joint properties used for modeling of the various experiments are listed in Table 4-3. It can be noticed that distinct peak shear strengths were predicted by the UDEC code using the Barton-Bandis model for each cycle of shearing and for both forward and reverse shearing. The algorithm used in the UDEC code for shear stress calculation for the Barton-Bandis model is similar to that discussed in Section 3.2. As long as the joint roughness is not completely worn down, that is $JRC > 0$, a peak shear strength will be predicted for forward or reverse shearing and for consecutive shear cycles. The *JRC* value will become zero after the ratio of the actual shear displacement to the shear displacement at which the peak shear strength is reached is greater than 100. The prediction of peak shear strength for all shear cycles of the same specimen and also for reverse shearing is not consistent with the laboratory results in which peak shear strength was observed only for the forward shearing of the first shear cycle. If the assumption that *JRC* controls the existence of joint peak shear strength is correct, the laboratory results seem to indicate that the joints tested were completely worn during the first shear cycle before the shearing was reversed. While this speculation seems to be supported by the experimental results shown in Figures 5-12 to 5-16, it is not supported by the harmonic and earthquake test results as discussed in Section 2.3. Figures 2-3 and 2-4 show a continuing wear of joint roughness for at least several shear cycles. As can be observed

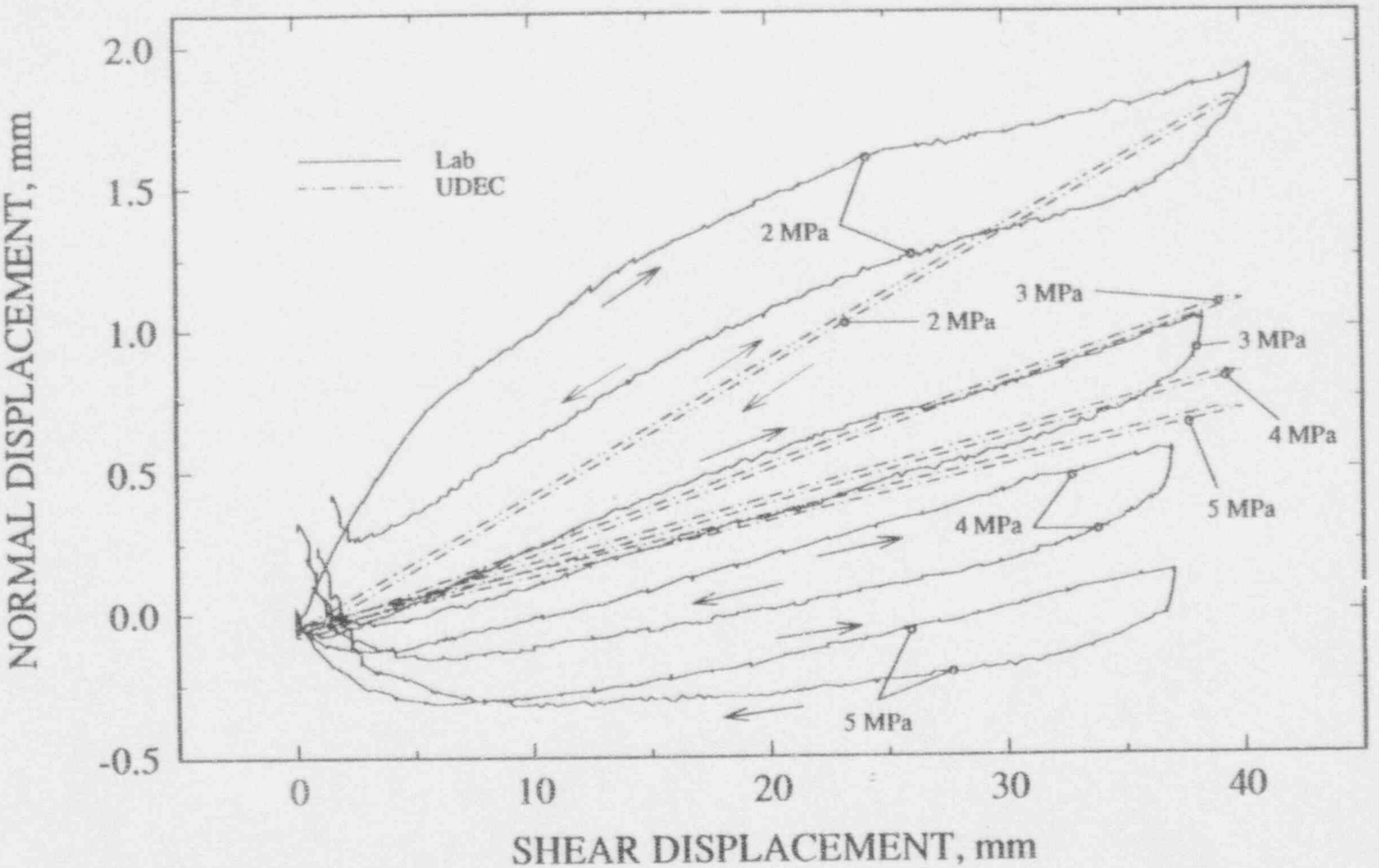

Figure 5-11. Typical joint dilation predicted by UDEC using Mohr-Coulomb joint model for test no. 10 when the critical shear displacement is not reached at all times

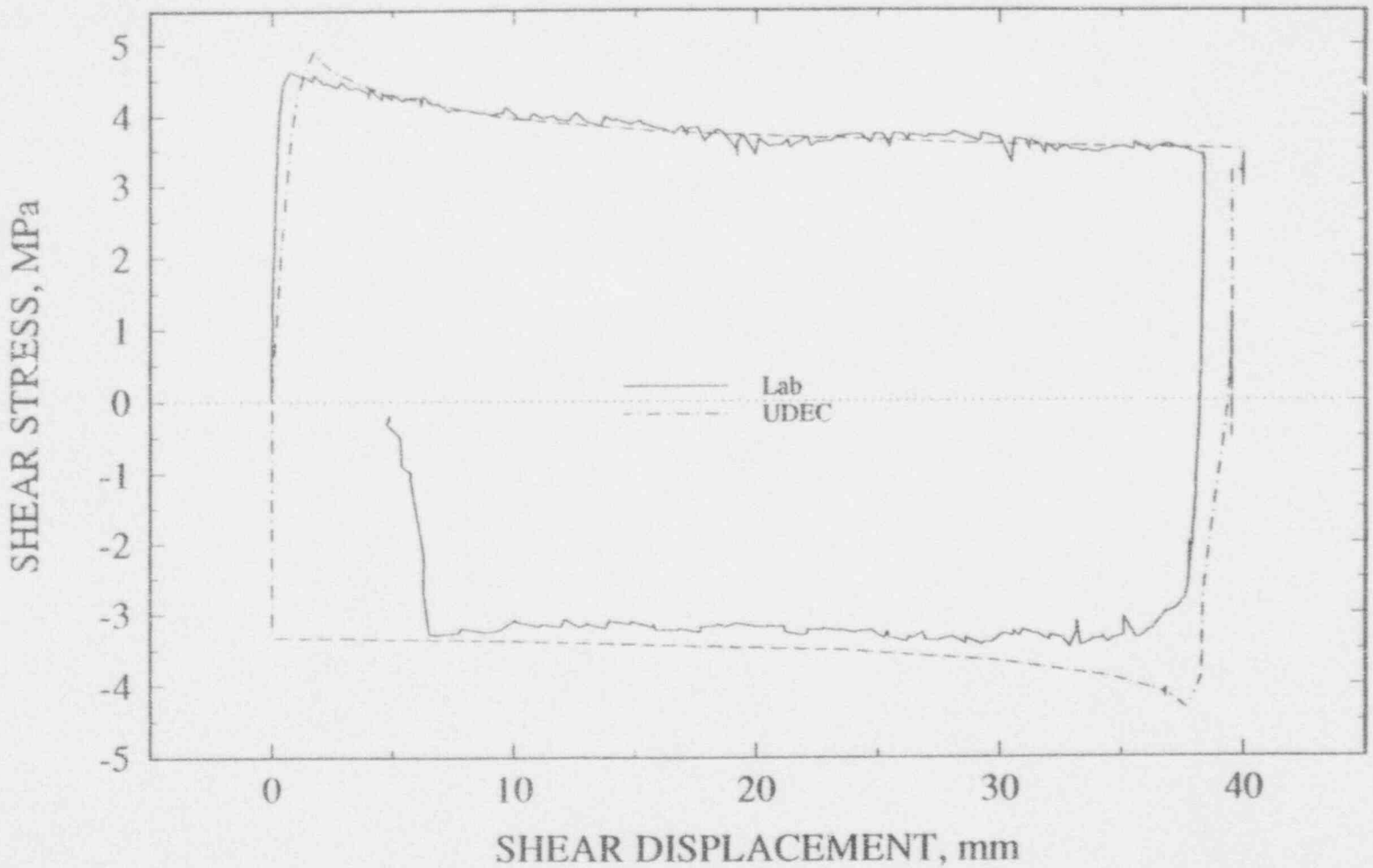

Figure 5-12. UDEC using Barton-Bandis joint model and laboratory test results of shear stress versus shear displacement plot for test no. 7 under normal stress of 5 MPa

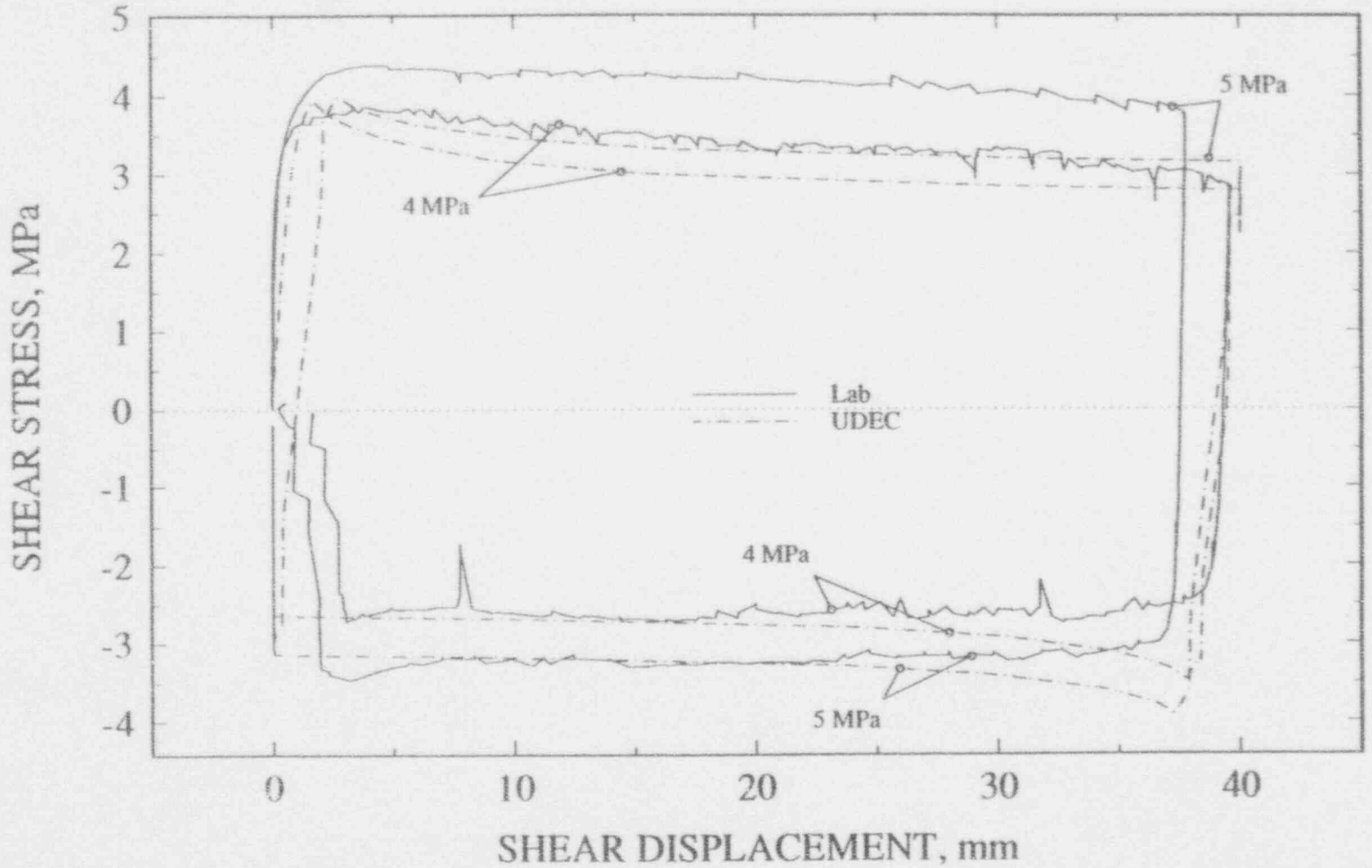

Figure 5-13. UDEC using Barton-Bandis joint model and laboratory test results of shear stress versus shear displacement plot for the same specimen as a function of normal stress for test no. 8

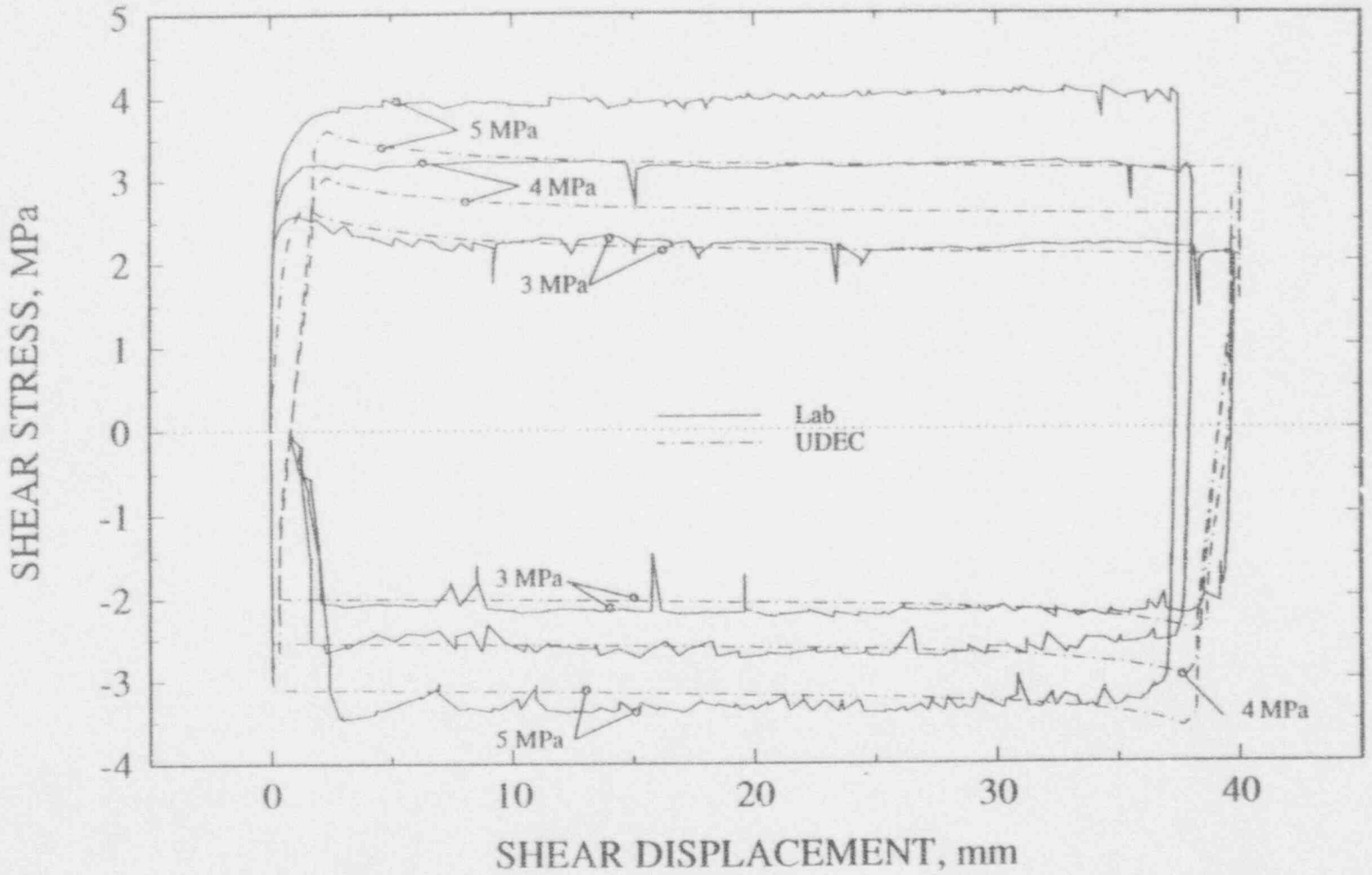

Figure 5-14. UDEC using Barton-Bandis joint model and laboratory test results of shear stress versus shear displacement plot for the same specimen as a function of normal stress for test no. 9

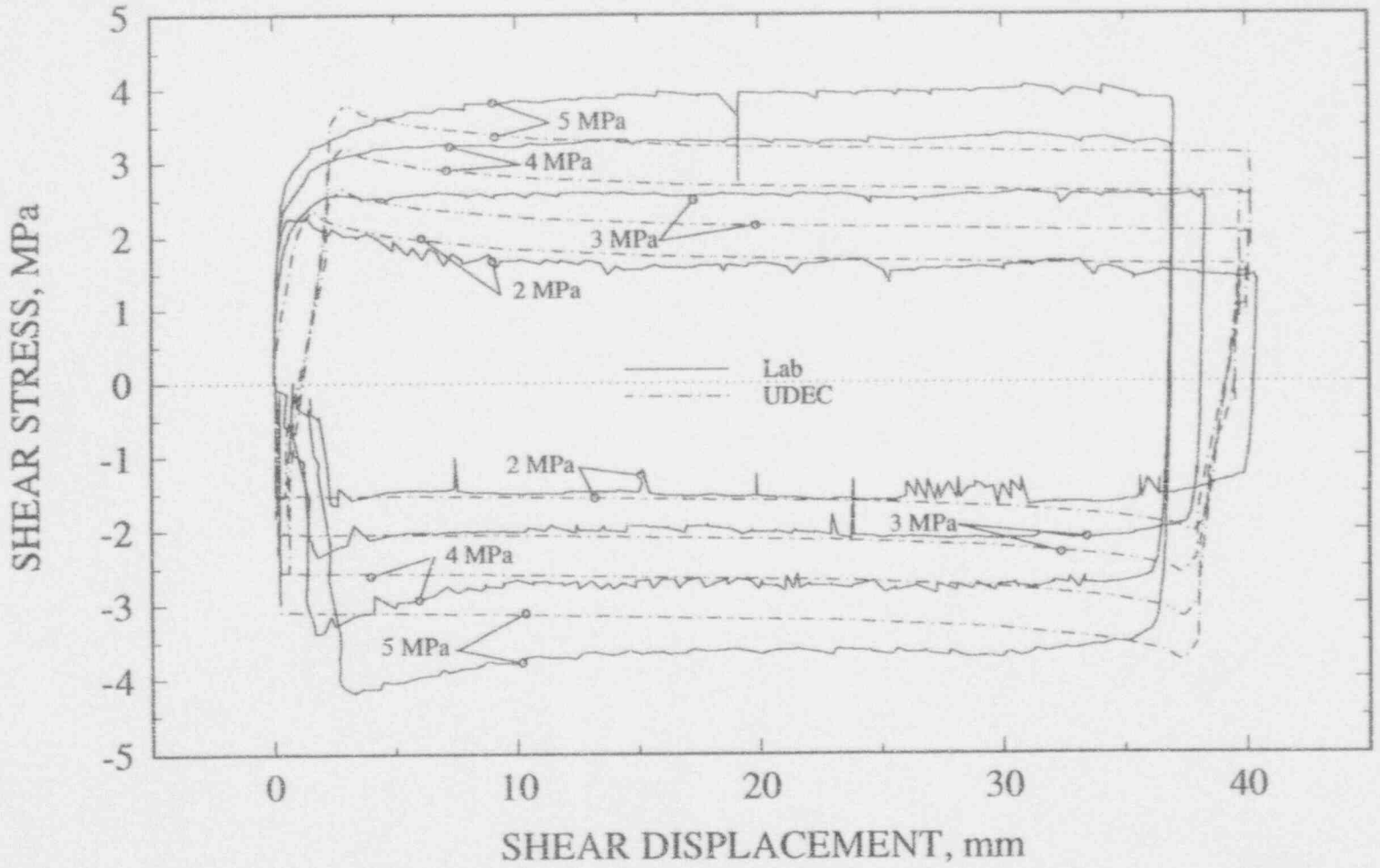

Figure 5-15. UDEC using Barton-Bandis joint model and laboratory test results of shear stress versus shear displacement plot for the same specimen as a function of normal stress for test no. 10

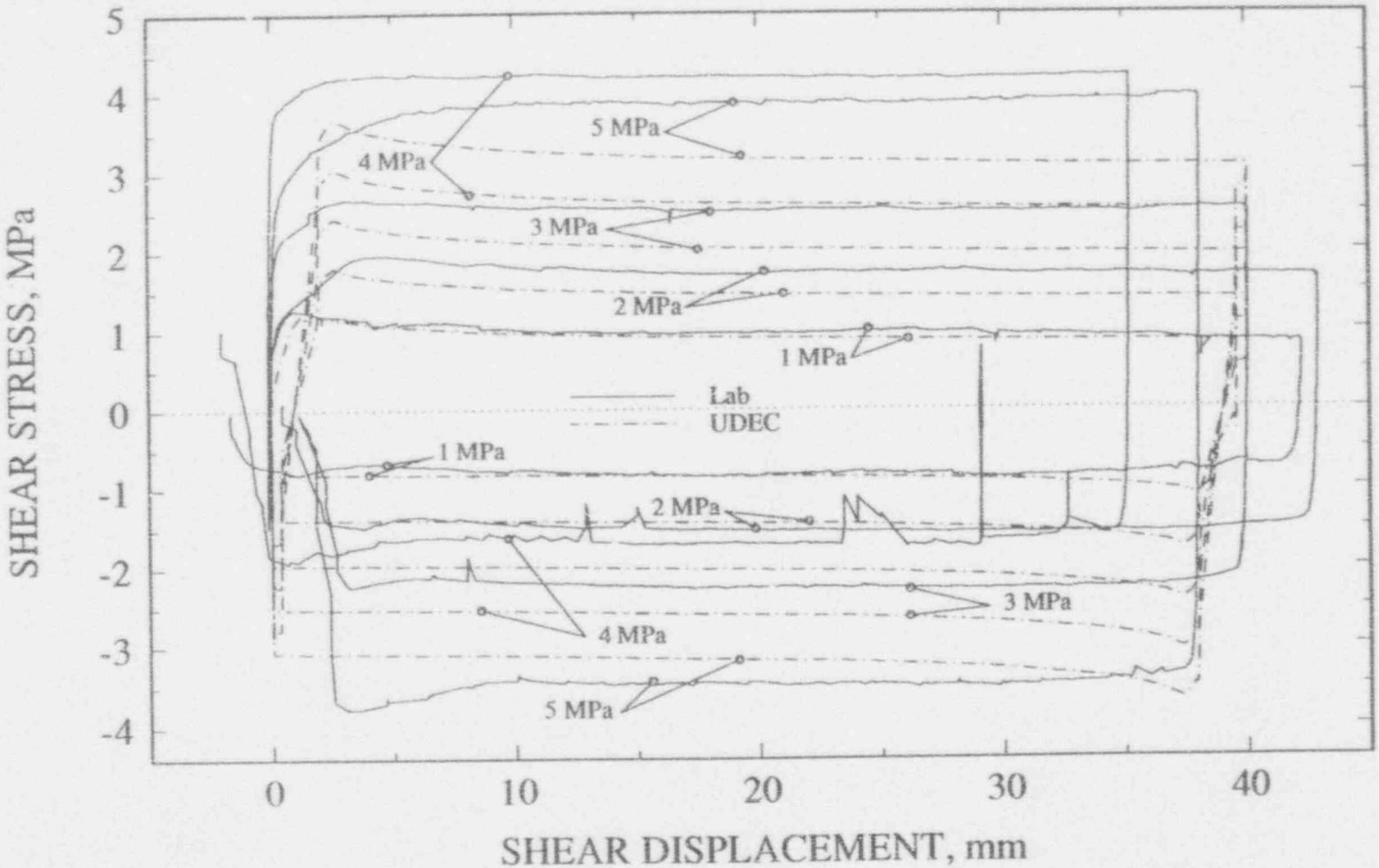

Figure 5-16. UDEC using Barton-Bandis joint model and laboratory test results of shear stress versus shear displacement plot for the same specimen as a function of normal stress for test no. 11

in Figures 5-12 to 5-16, the predicted peak shear strength during reverse shearing using the Barton-Bandis model is the same as the residual shear strength at the end of the forward shearing. This predicted phenomenon does not reflect the laboratory observation. It would seem from Figures 5-15 and 5-14 that the predicted shear strengths during reverse shearing match quite well with the laboratory results. This is because the shear strength prediction for the forward shearing was consistently underestimated as compared to the actual laboratory results except perhaps for the shear strength of the first shear cycle. Therefore, in reality, the same shear strength was predicted for both forward and reverse shearing.

Figures 5-17 to 5-21 show the predicted joint dilation. The dilation calculation using the Barton-Bandis model as implemented in the UDEC code as shown in the figures is clearly not correct. According to the calculation, the dilation is at least one order of magnitude less than the laboratory measured joint dilation depending upon the magnitude of the applied normal stress. Also, the calculated dilation indicates that dilation stops after a short period of sharp increase. This predicted behavior is not consistent with the dilation model proposed by Barton et al. (1985). According to the proposed dilation model, dilation angle is a function of *JRC*. Based on the calculation for shear stresses shown in Figures 5-12 to 5-16, the *JRC* was not zero even after several cycles of shearing, an indication that the associated joint dilation should not stop increasing as was illustrated in Figures 5-17 to 5-21. This incorrect calculation is related to the incorrect implementation of the dilation model in the UDEC code.

5.1.3 Continuously-Yielding Joint Model

Figures 5-22 to 5-26 show joint shear stress versus shear displacement plots of UDEC modeling using the Continuously-Yielding joint model for the five cyclic pseudostatic tests discussed in Sections 5.1.1 and 5.1.2. The joint properties used for modeling of the various experiments are listed in Table 4-4. Prediction of shear stress variation during forward shearing by the UDEC code using the Continuously-Yielding model produced mixed results. In some cases, (e.g., Figure 5-22) reasonably good agreement was observed between the modeling results and the laboratory measurements while, in other cases, the modeling results and the laboratory measurements (e.g., Figure 5-26) were quite different. In general, the prediction for the shear strength in the first shear cycle is quite close to the laboratory results for all the cyclic pseudostatic tests. This observation is expected since the joint parameters used for the Continuously-Yielding model in the UDEC code were back-calculated from the laboratory data. The shear strength prediction for reverse shearing in most cases is greater than that observed in the laboratory. Good agreement between the model and laboratory results for the shear strength during reverse shearing can be observed only when the difference in the shear strengths between forward and reverse shearing is small.

Figures 5-27 to 5-31 show joint dilation plots of UDEC results and test measurements. Although a good agreement is shown for dilation during forward shearing of the first shear cycle between the two sets of results, the prediction of dilation during reverse shearing using the Continuously-Yielding model is apparently inadequate. As can be seen in the figures, the dilation calculation in the Continuously-Yielding model, as implemented in the UDEC code, assumes a sign change in dilation angle during reverse shearing. As a result, some recovery in dilation is recognized. However, the amount of recovery is not sufficient to simulate the actual dilation recovery behavior observed experimentally. This gives an indication that the joint model implemented in the UDEC for calculation of shear dilation is inadequate.

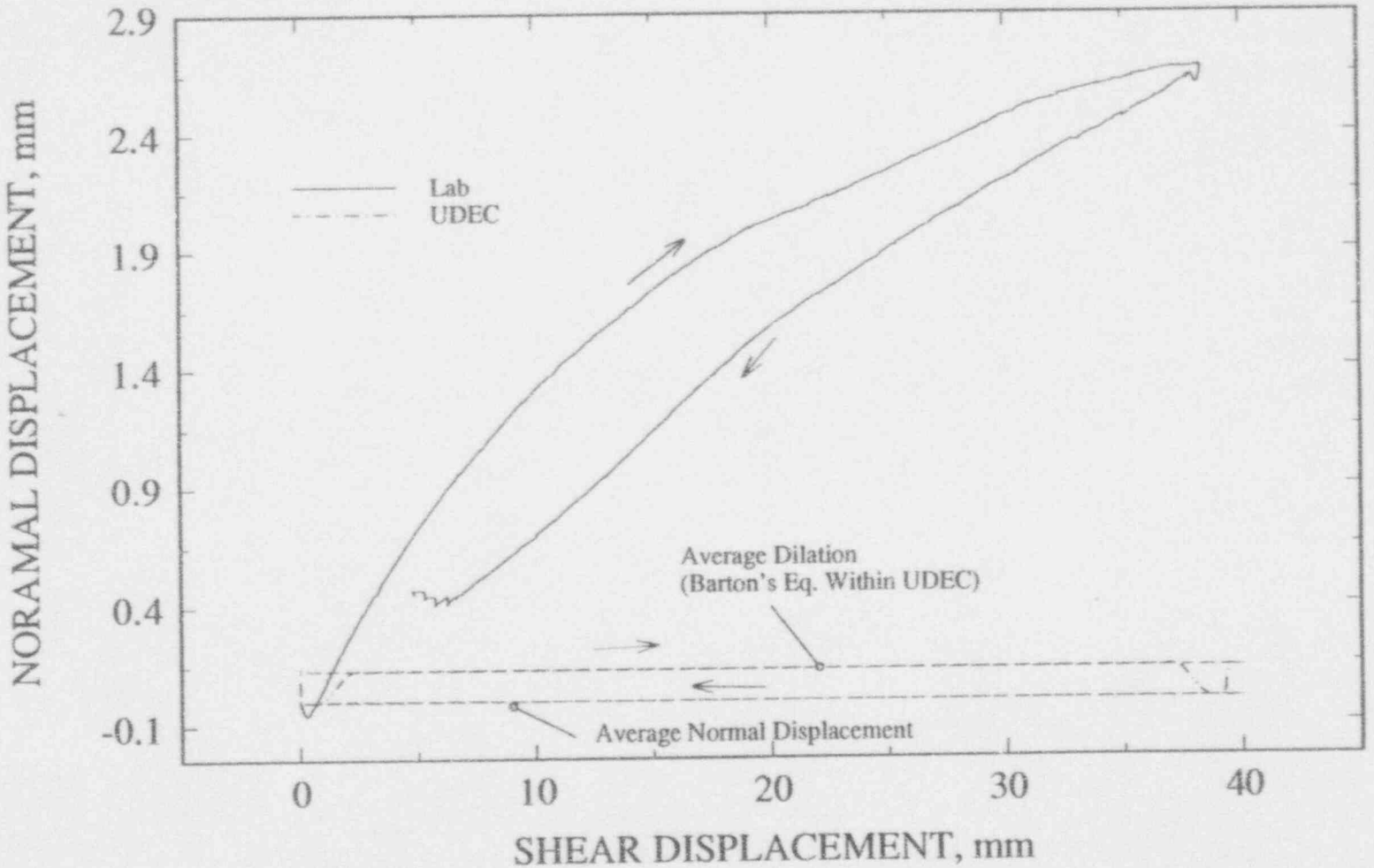

Figure 5-17. UDEC results using Barton-Bandis joint model and laboratory measurements of joint dilation plot for test no. 7 under normal stress of 5 MPa

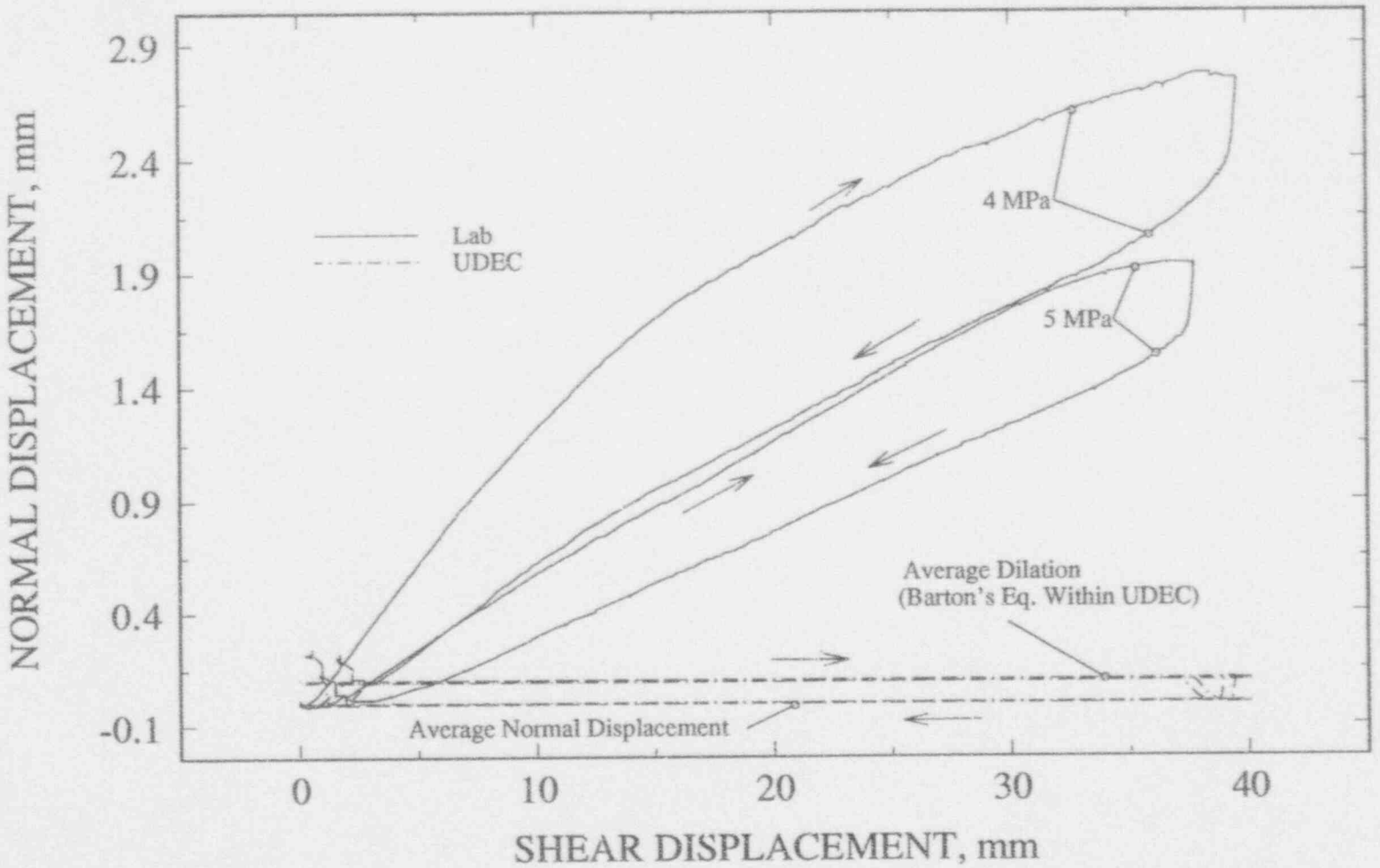

Figure 5-18. UDEC results using Barton-Bandis joint model and laboratory measurements of joint dilation plot for the same joint specimen as a function of normal stress for test no. 8

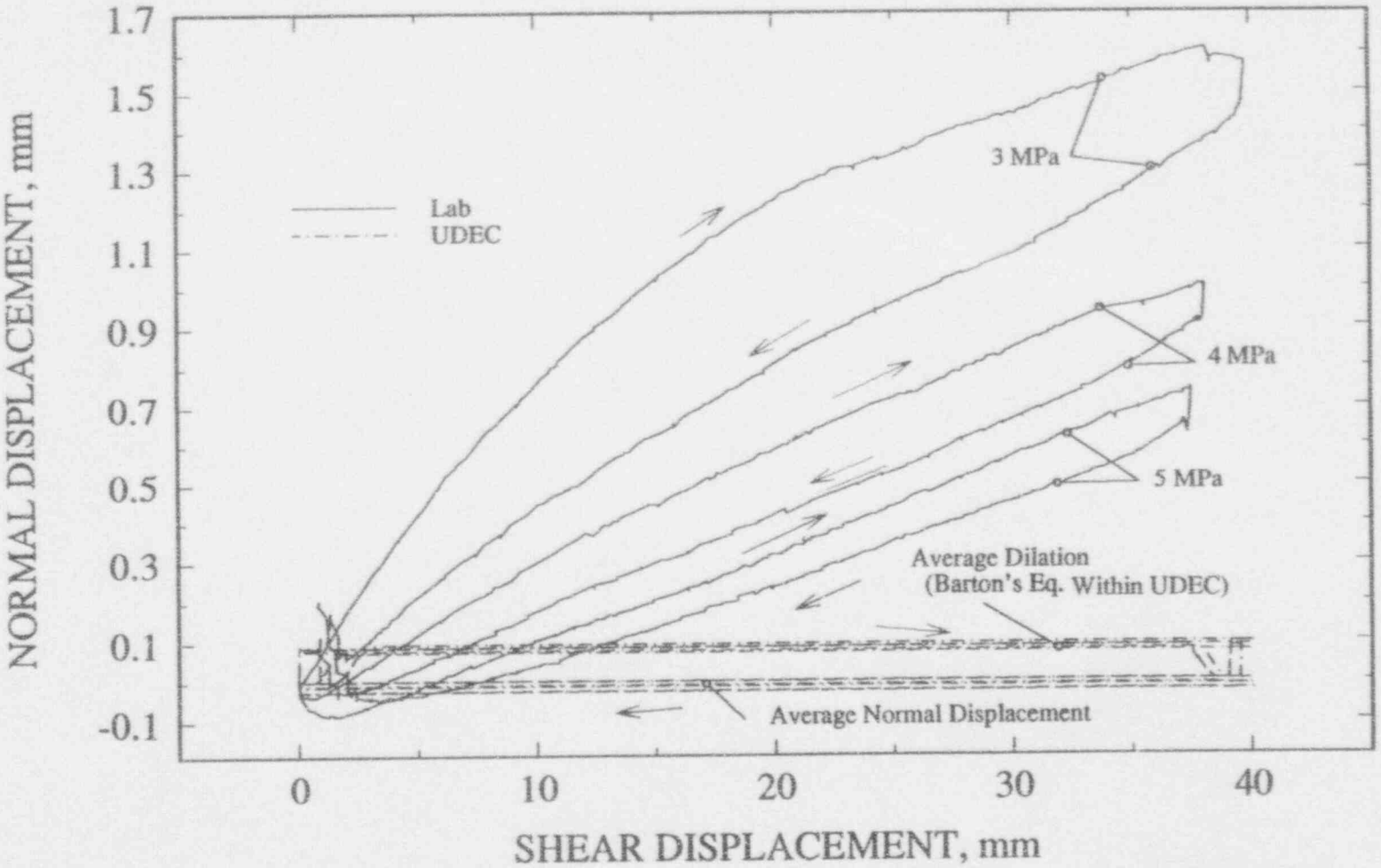

Figure 5-19. UDEC results using Barton-Bandis joint model and laboratory measurements of joint dilation plot for the same specimen as a function of normal stress for test no. 9

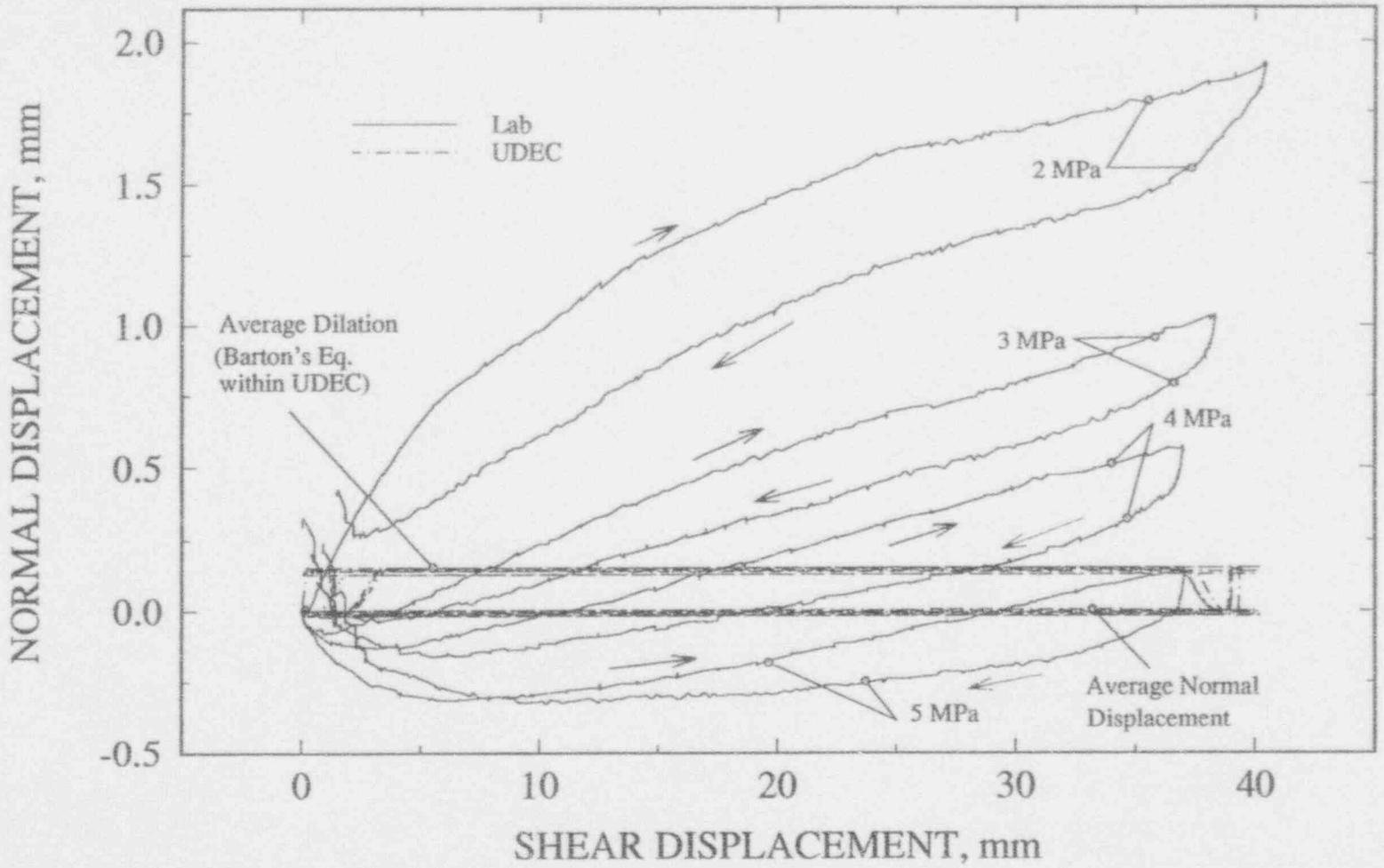

Figure 5-20. UDEC results using Barton-Bandis joint model and laboratory measurements of joint dilation plot for the same joint specimen as a function of normal stress for test no. 10

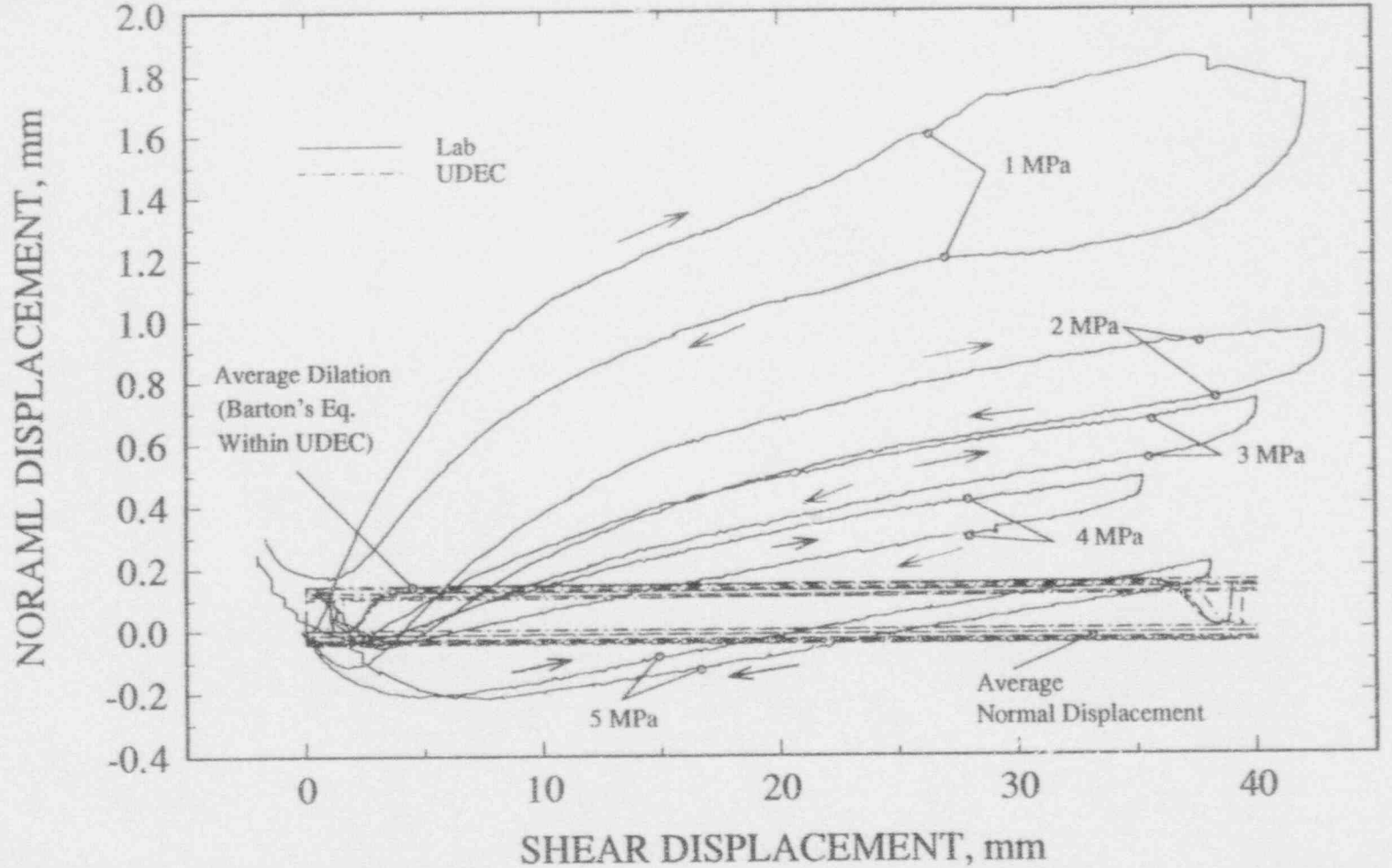

Figure 5-21. UDEC results using Barton-Bandis joint model and laboratory measurements of joint dilation plot for the same joint specimen as a function of normal stress for test no. 11

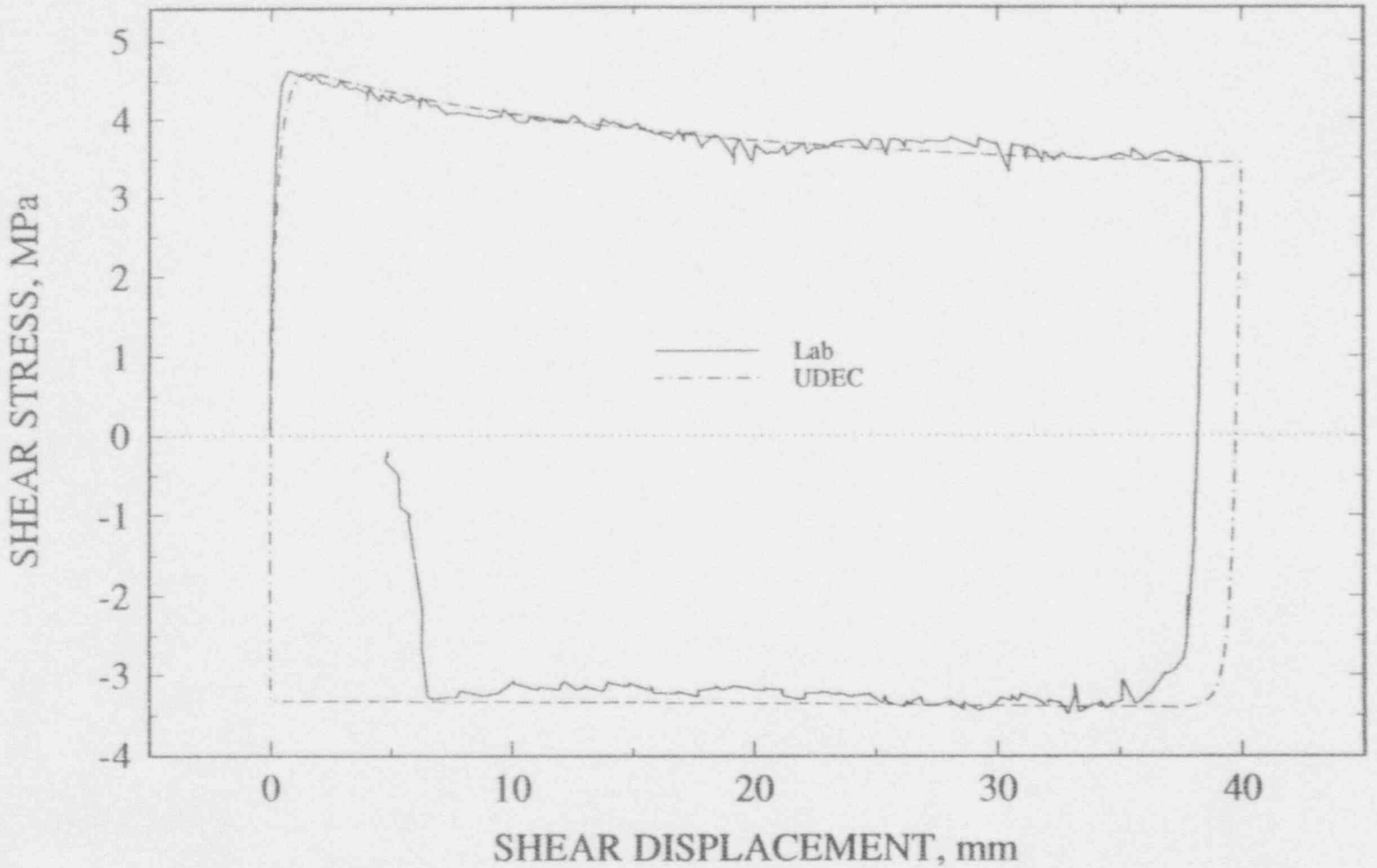

Figure 5-22. UDEC using Continuously-Yielding joint model and laboratory test results of shear stress versus shear displacement plot for test no. 7 under normal stress of 5 MPa

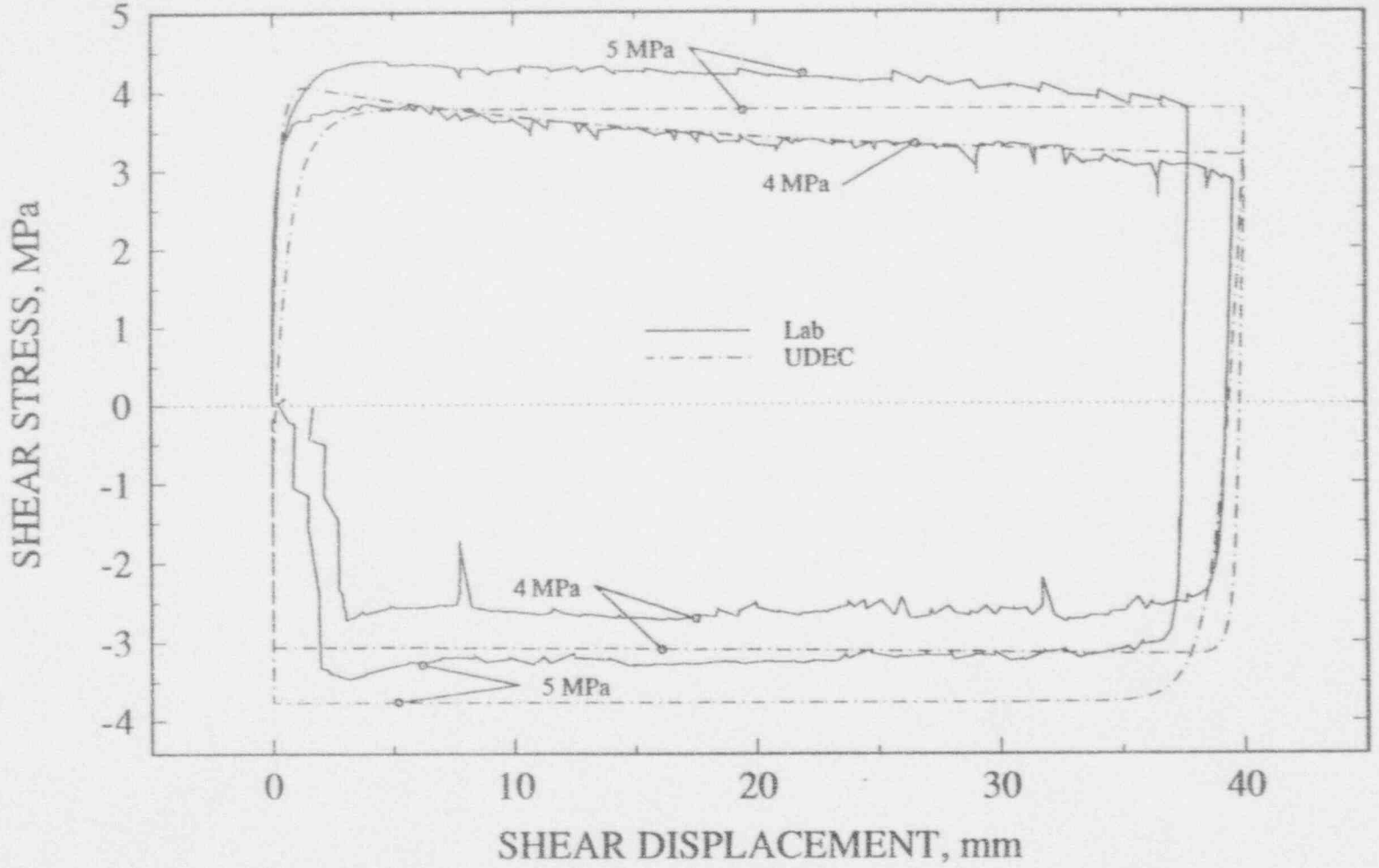

Figure 5-23. UDEC using Continuously-Yielding joint model and laboratory test results of shear stress versus shear displacement plot for the same specimen as a function of normal stress for test no. 8

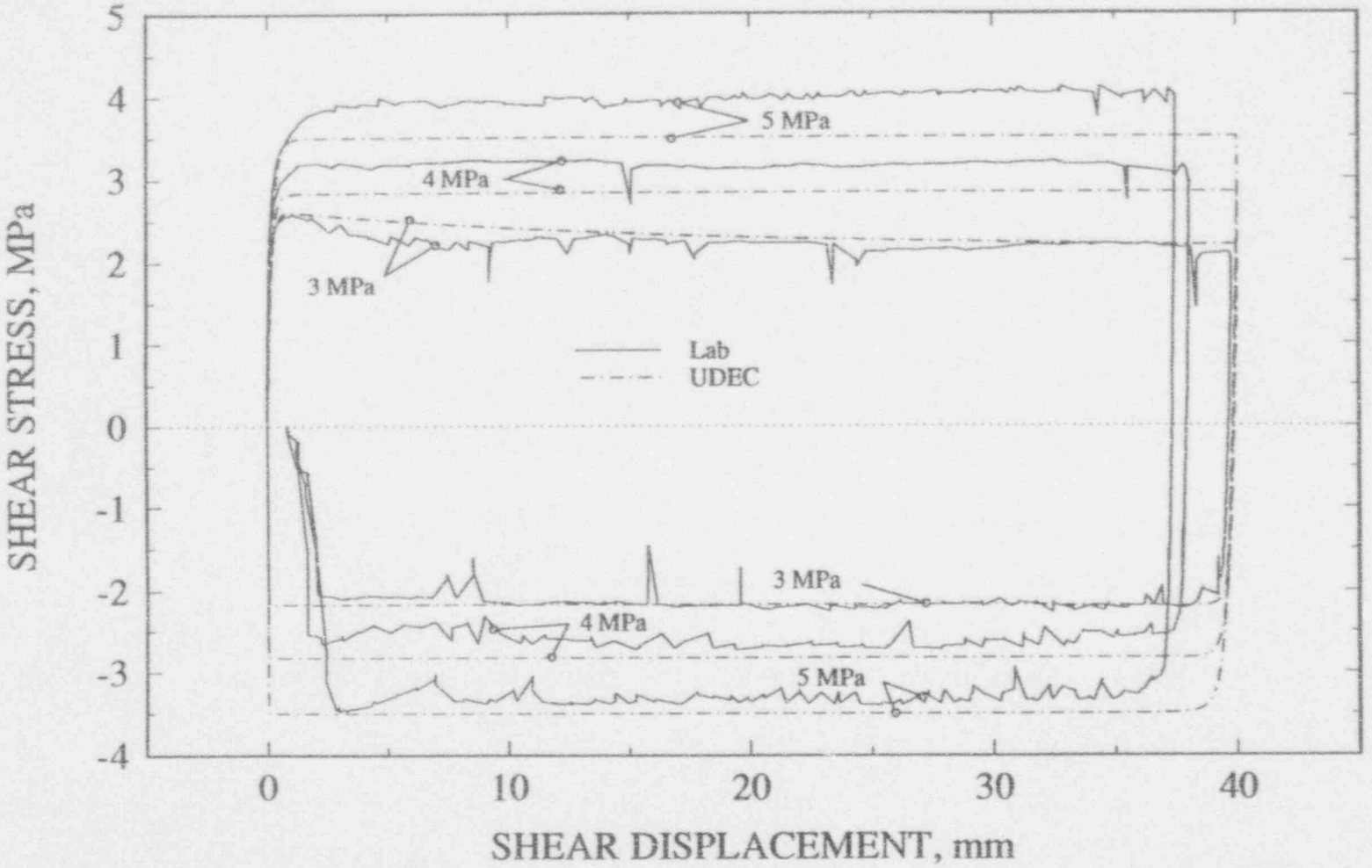

Figure 5-24. UDEC using Continuously-Yielding joint model and laboratory test results of shear stress versus shear displacement plot for the same specimen as a function of normal stress for test no. 9

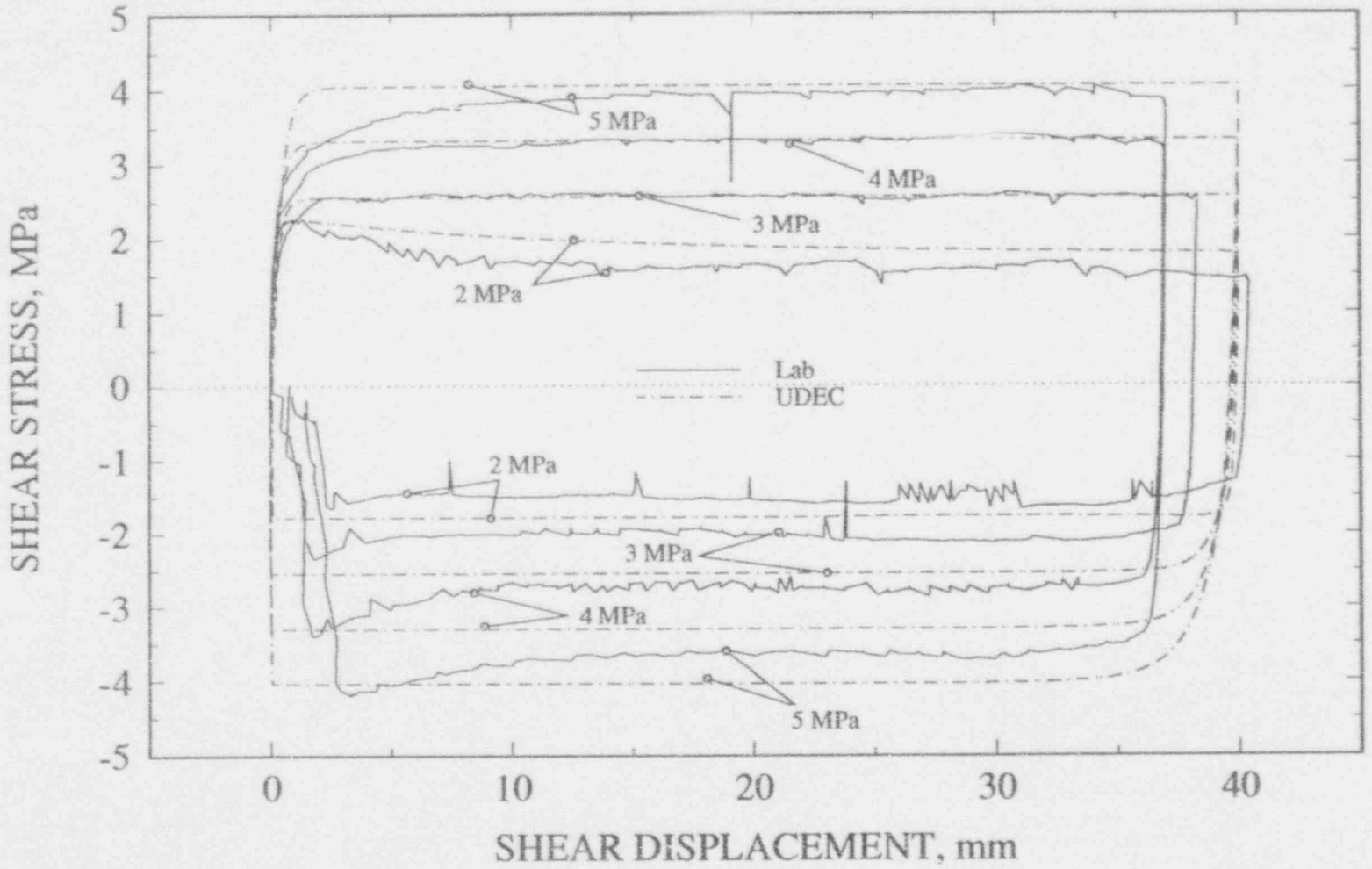

Figure 5-25. UDEC using Continuously-Yielding joint model and laboratory test results of shear stress versus shear displacement plot for the same specimen as a function of normal stress for test no. 10

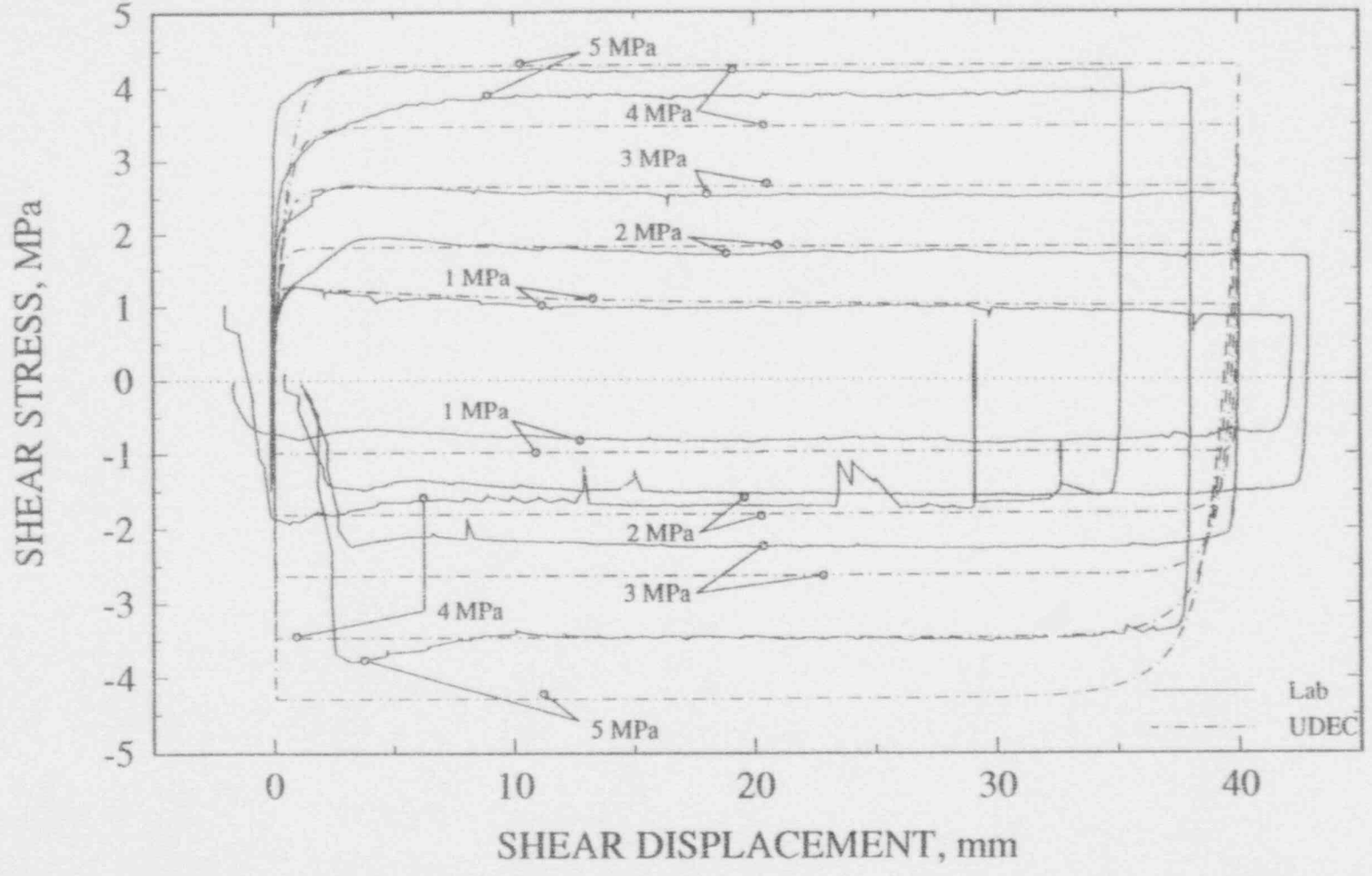

Figure 5-26. UDEC using Continuously-Yielding joint model and laboratory test results of shear stress versus shear displacement plot for the same specimen as a function of normal stress for test no. 11

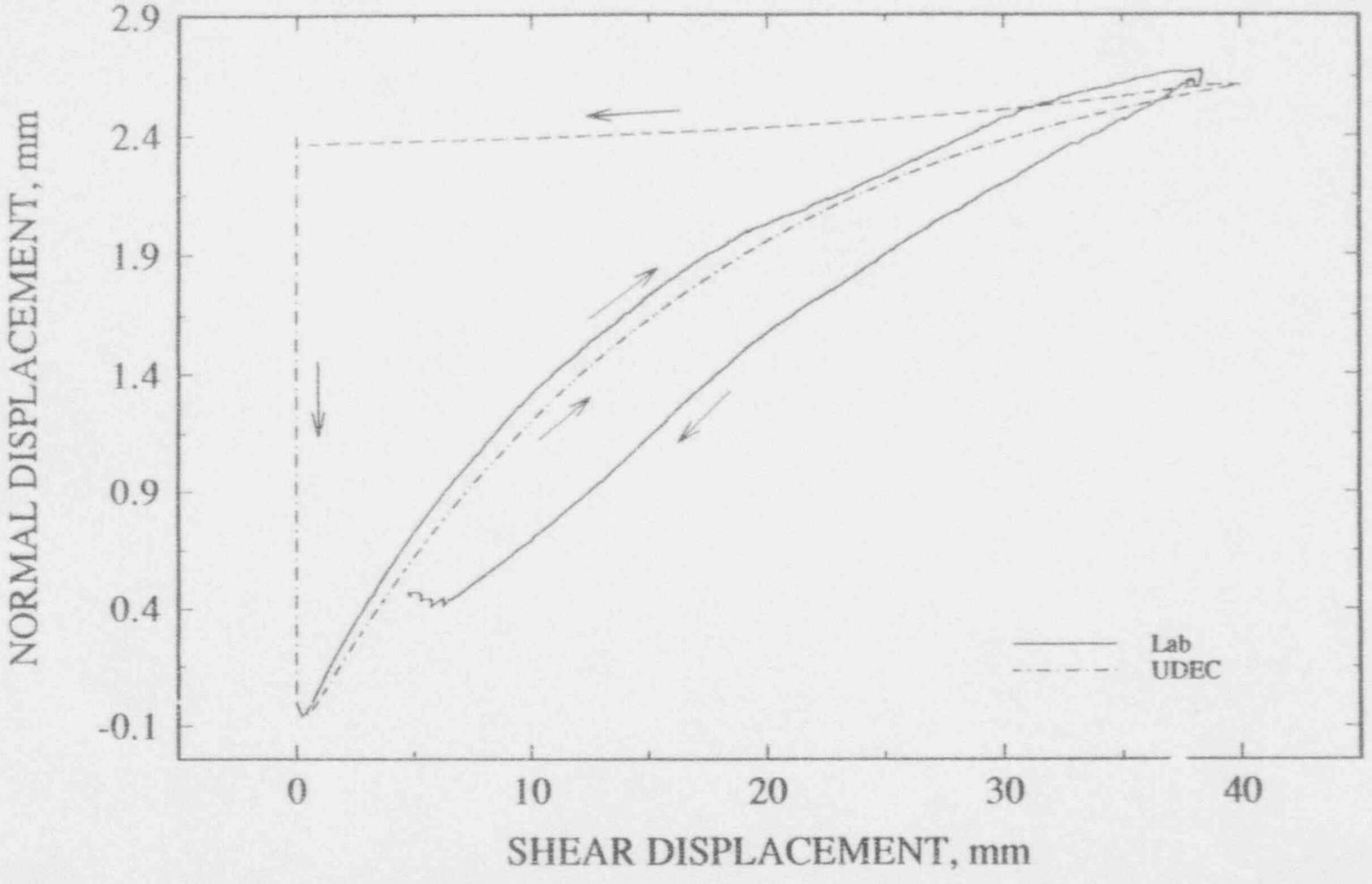

Figure 5-27. UDEC results using Continuously-Yielding joint model and laboratory measurements of joint dilation plot for test no. 7 under normal stress of 5 MPa

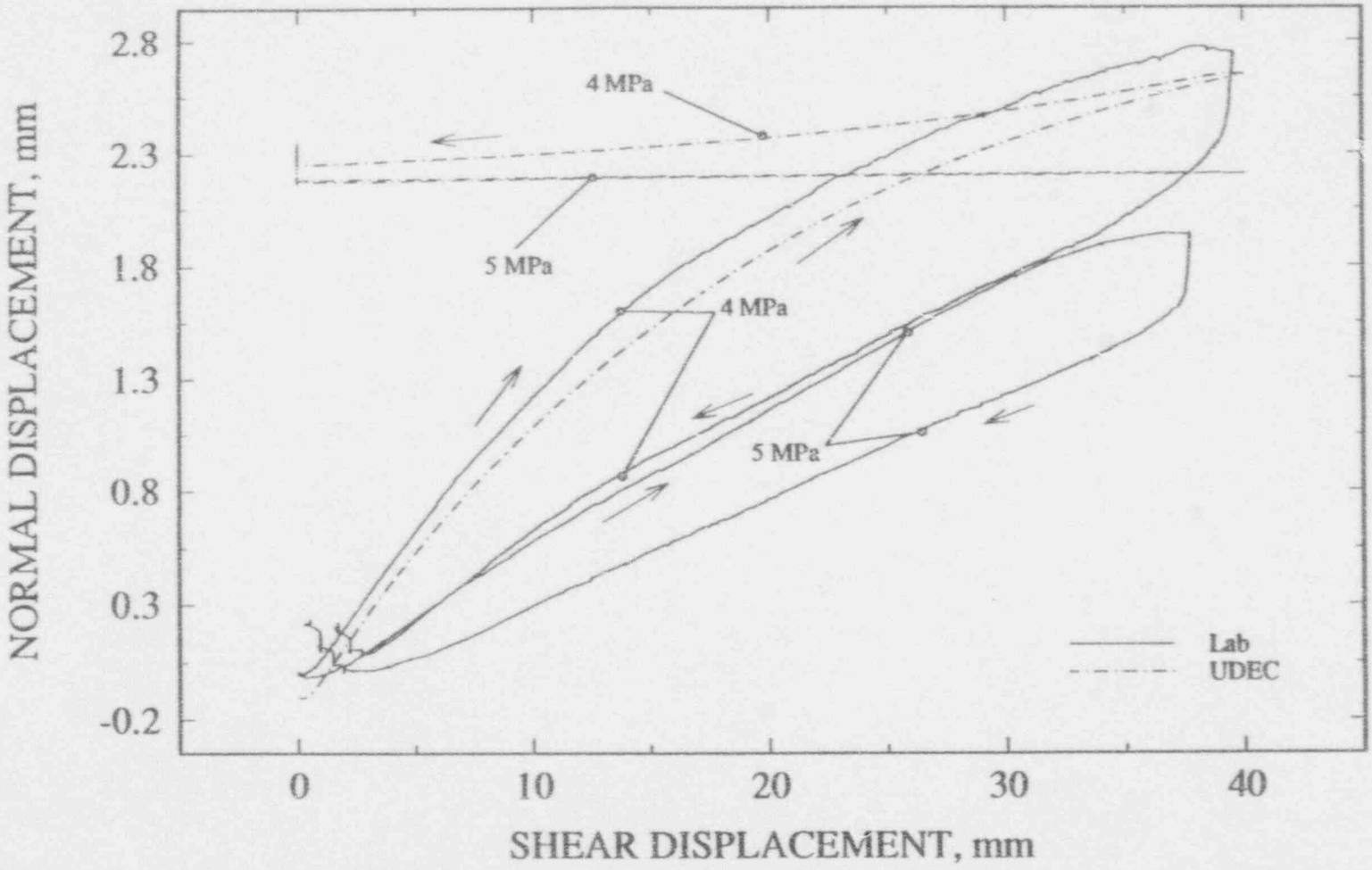

Figure 5-28. UDEC results using Continuously-Yielding joint model and laboratory measurements of joint dilation plot for the same joint specimen as a function of normal stress for test no. 8

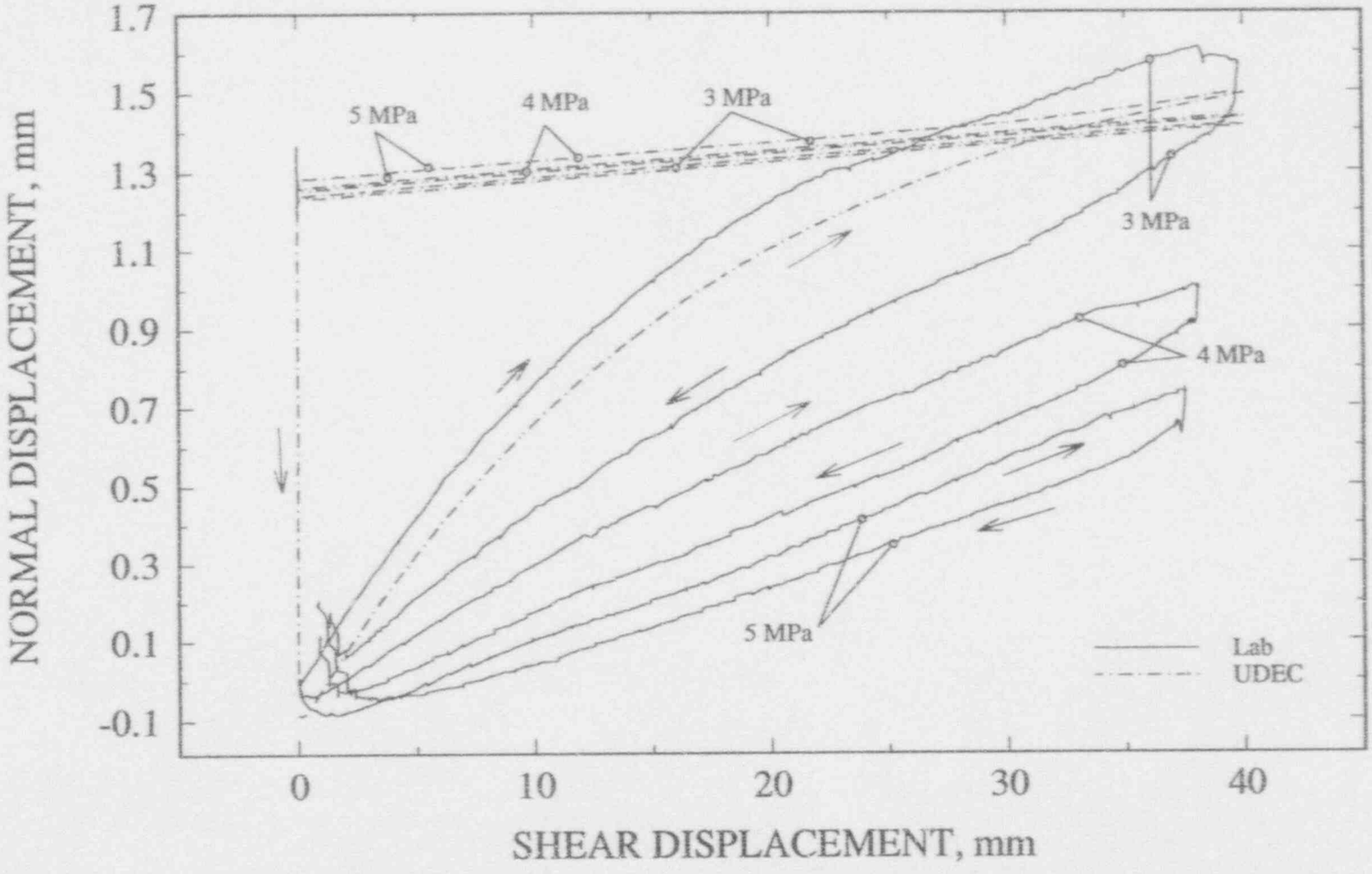

Figure 5-29. UDEC results using Continuously-Yielding joint model and laboratory measurements of joint dilation plot for the same joint specimen as a function of normal stress for test no. 9

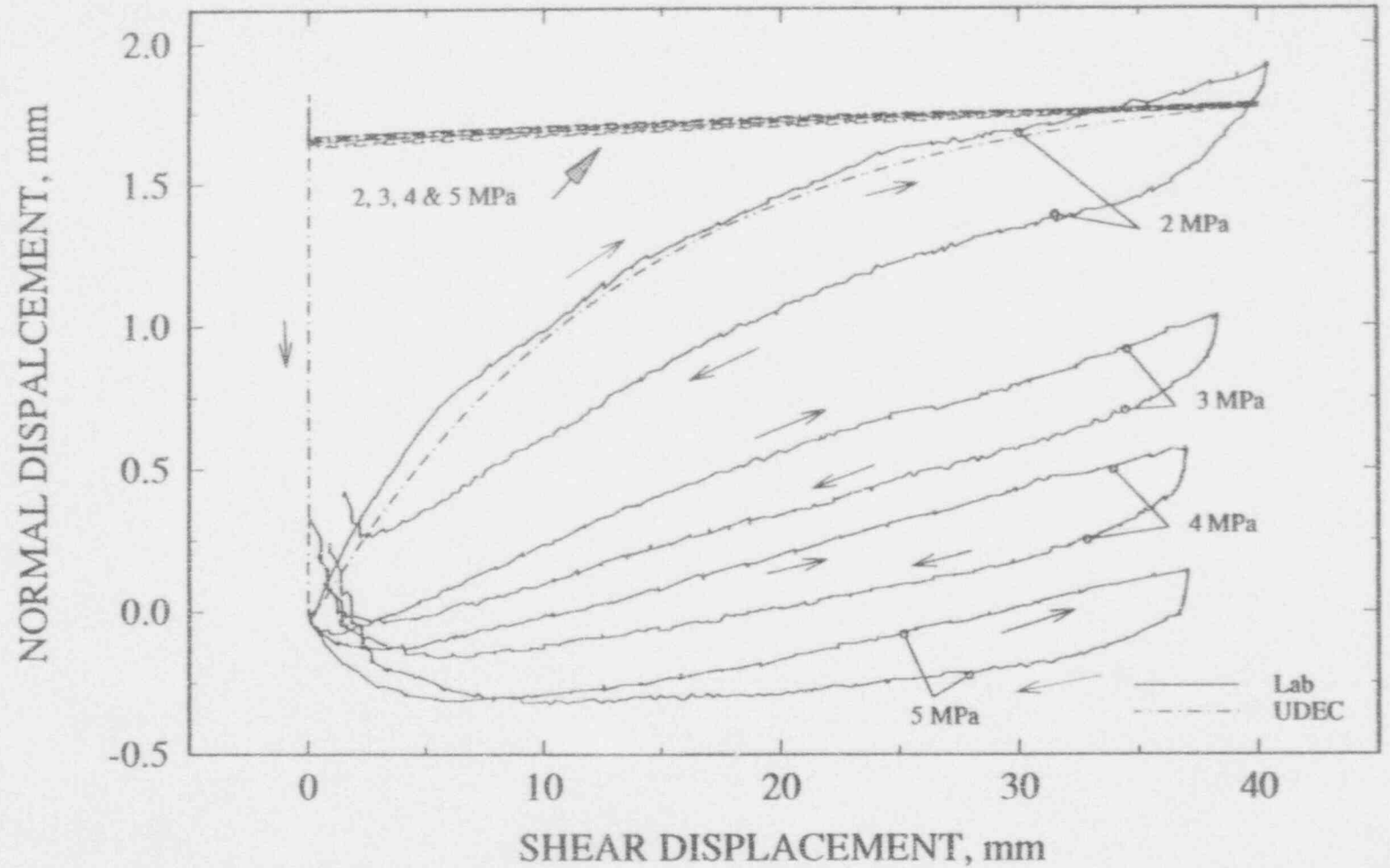

Figure 5-30. UDEC results using Continuously-Yielding joint model and laboratory measurements of joint dilation plot for the same joint specimen as a function of normal stress for test no. 10

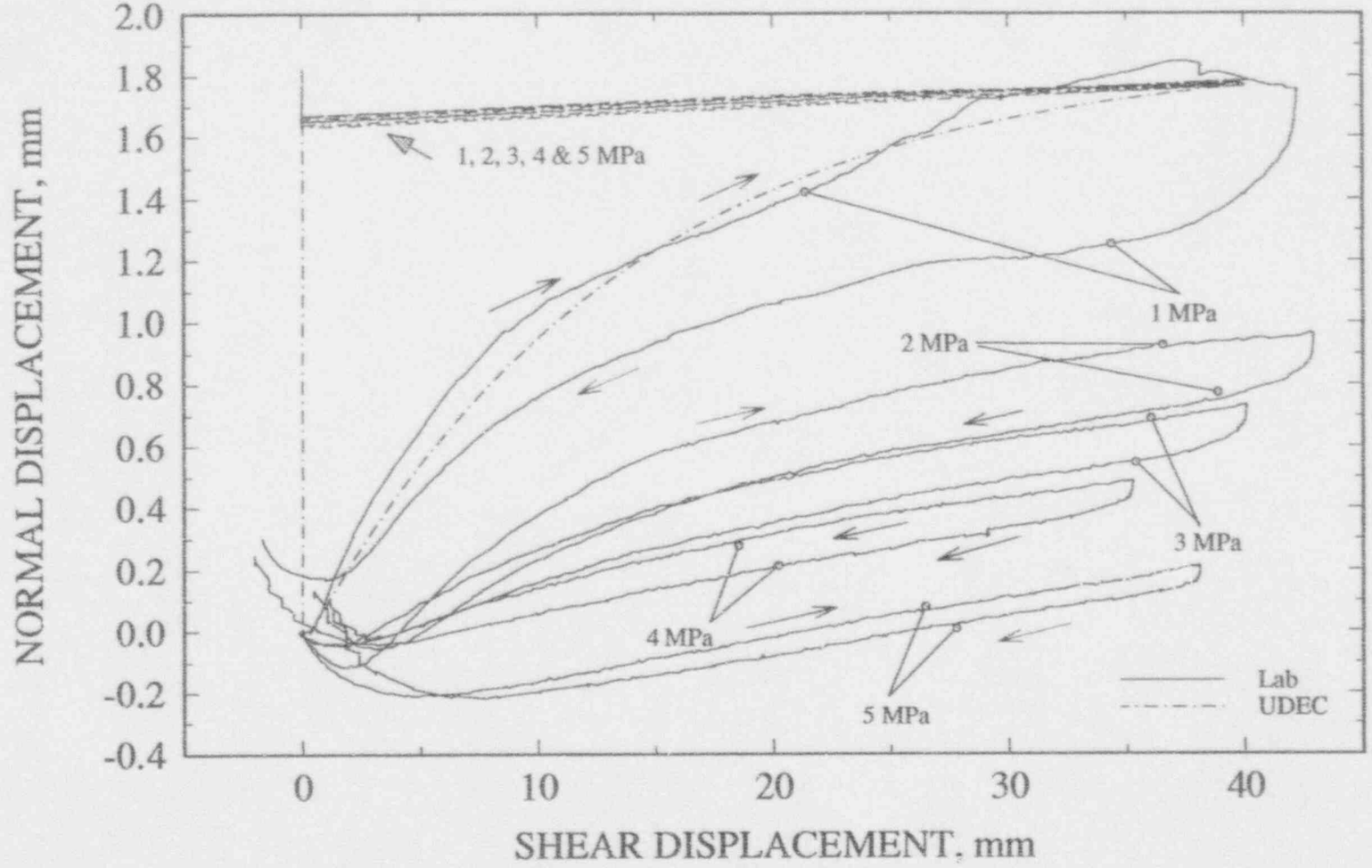

Figure 5-31. UDEC results using Continuously-Yielding joint model and laboratory measurements of joint dilation plot for the same joint specimen as a function of normal stress for test no. 11

5.2 DYNAMIC EXPERIMENT MODELING

One harmonic test and one earthquake direct shear tests were simulated by the UDEC code using the three rock joint models. The UDEC model used for the simulation is shown in Figure 4-7. The input velocity at the centroid of the rigid loading block was the first derivative of a sinusoidal wave which had a frequency of 1.4 Hz and amplitude of 12.7 mm for the harmonic experiment simulation. The input velocity for the earthquake experiment was the first derivative of the displacement input (Figure 2-5) for the laboratory experiment. It has been concluded in Section 2.3 that, within the range of variation of the test input velocity or frequency, there is no noticeable effect of the input frequency (shearing velocity) on the peak joint shear strength and the joint shear strength for the reverse shearing is observed. Consequently, it is possible to determine the joint properties for the rock joint models for the UDEC simulation using the experimental results directly. Tables 4-2, 4-3, and 4-4 list the calculated joint properties for the three rock joint models as required in the UDEC code.

Figures 5-32 to 5-34 show joint shear stress versus shear displacement plots of UDEC modeling using the three models for rock joint behavior simulation and the corresponding laboratory test results for the harmonic test while Figures 5-35 to 5-37 show the modeling results for the earthquake test. The first several cycles of the results are shown in the figures for clarity. From the laboratory harmonic and earthquake results shown in Figures 5-32 through 5-37, it can be found that the shear stress versus shear displacement curve in the third quadrant, for at least the first cycle, has a similar pattern to that in the first quadrant, that is, the presence of a peak shear stress. The reason for this similar characteristic is that the joint surface as represented in the third quadrant is "fresh" during the first cycle since it was not sheared earlier, as illustrated in Figure 5-38. As a result, a distinct peak value of the shear stress can be observed. This phenomenon cannot be properly modeled by UDEC since no mechanism is in place for properly simulating the two joint surfaces on the bottom block at both sides of the top block with different joint properties.

No substantial change in shear stress was observed during the process of joint shearing as shown in Figure 5-32 when the Mohr-Coulomb joint model was used in the UDEC simulation of the harmonic experiment. However, a substantial drop in shear stress was found after the first cycle of joint shearing for the UDEC modeling of the harmonic experiment using either the Barton-Bandis or Continuously-Yielding joint models (Figures 5-33 and 5-34). This difference may be explained by the fact that the "roughness" of a joint in the Barton-Bandis and Continuously-Yielding joint models is tied closely with the magnitude of shear displacement, while the Mohr-Coulomb joint model assumes no joint wear; that is, joint roughness is constant and will not decrease as a function of shear displacement. As discussed in Section 3, the link between the attrition of joint roughness and the amount of shear displacement has been provided in a tabular form as shown in Figure 3-4 for the Barton-Bandis joint model. For the Continuously-Yielding joint model, the link is based on Eq. (3-14). Both models assume that joint roughness will reduce substantially during the initial stage of shearing. For example, joint roughness reduces exponentially as a function of shear displacement according to the Continuously-Yielding joint model. In general, the reduction of joint roughness for the Continuously-Yielding model is at a relatively faster rate than that of the Barton-Bandis model. The results in Figures 5-33 and 5-34 indicate that the second cycle of shearing started after a total of 50 mm of previous shear displacement has taken place. Consequently, the joint roughness has been substantially reduced by the beginning of the second cycle. That is the reason for a large gap between the first and second cycle shear stress curves as shown in the first quadrant of both figures. For displacement cycles with relatively small displacement amplitudes, as was the case for the first few cycles of the results of the UDEC simulation on the earthquake experiment

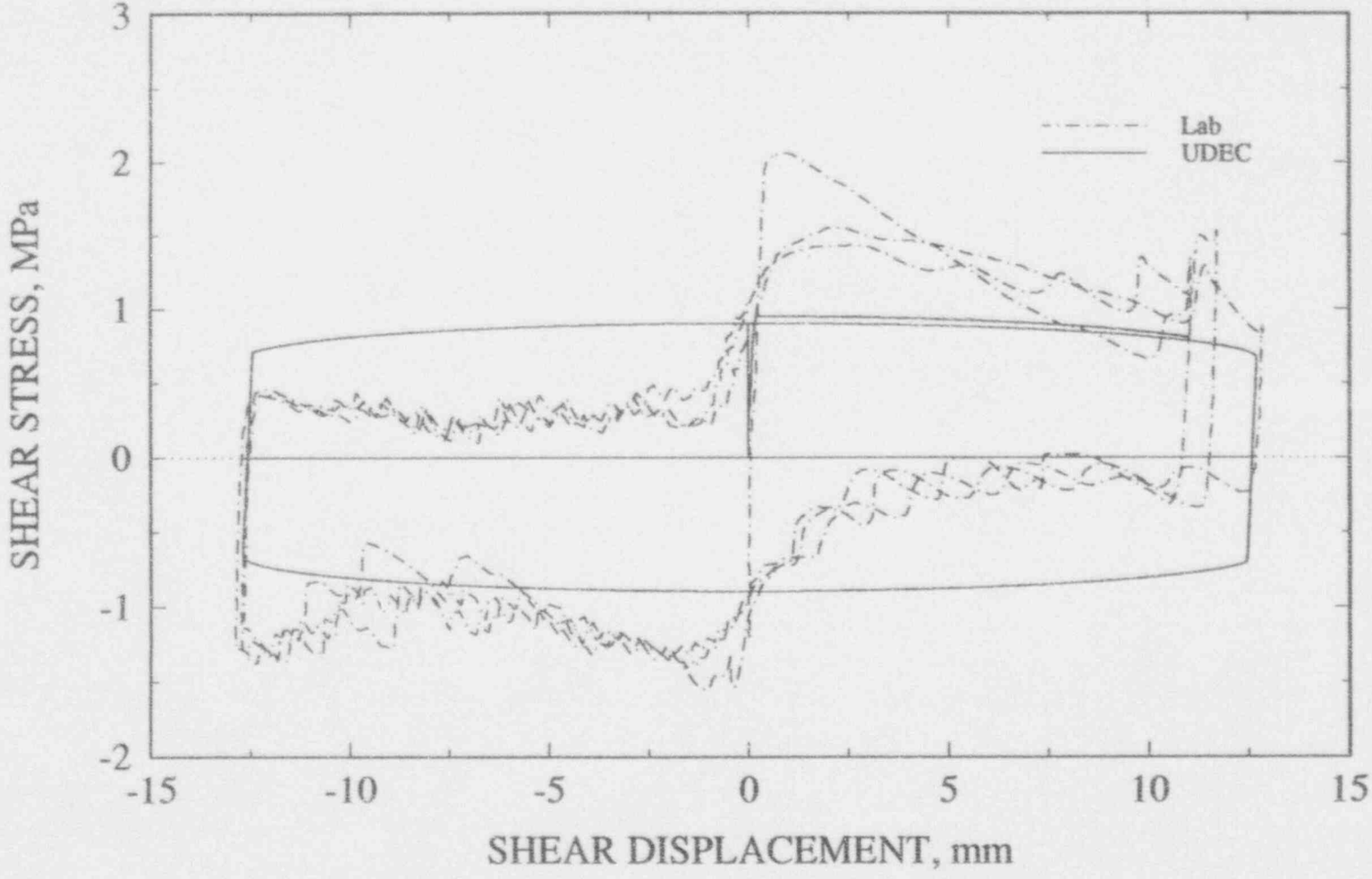

Figure 5-32. Laboratory results and UDEC prediction using Mohr-Coulomb joint model of shear stress versus shear displacement curve subjected to a harmonic load

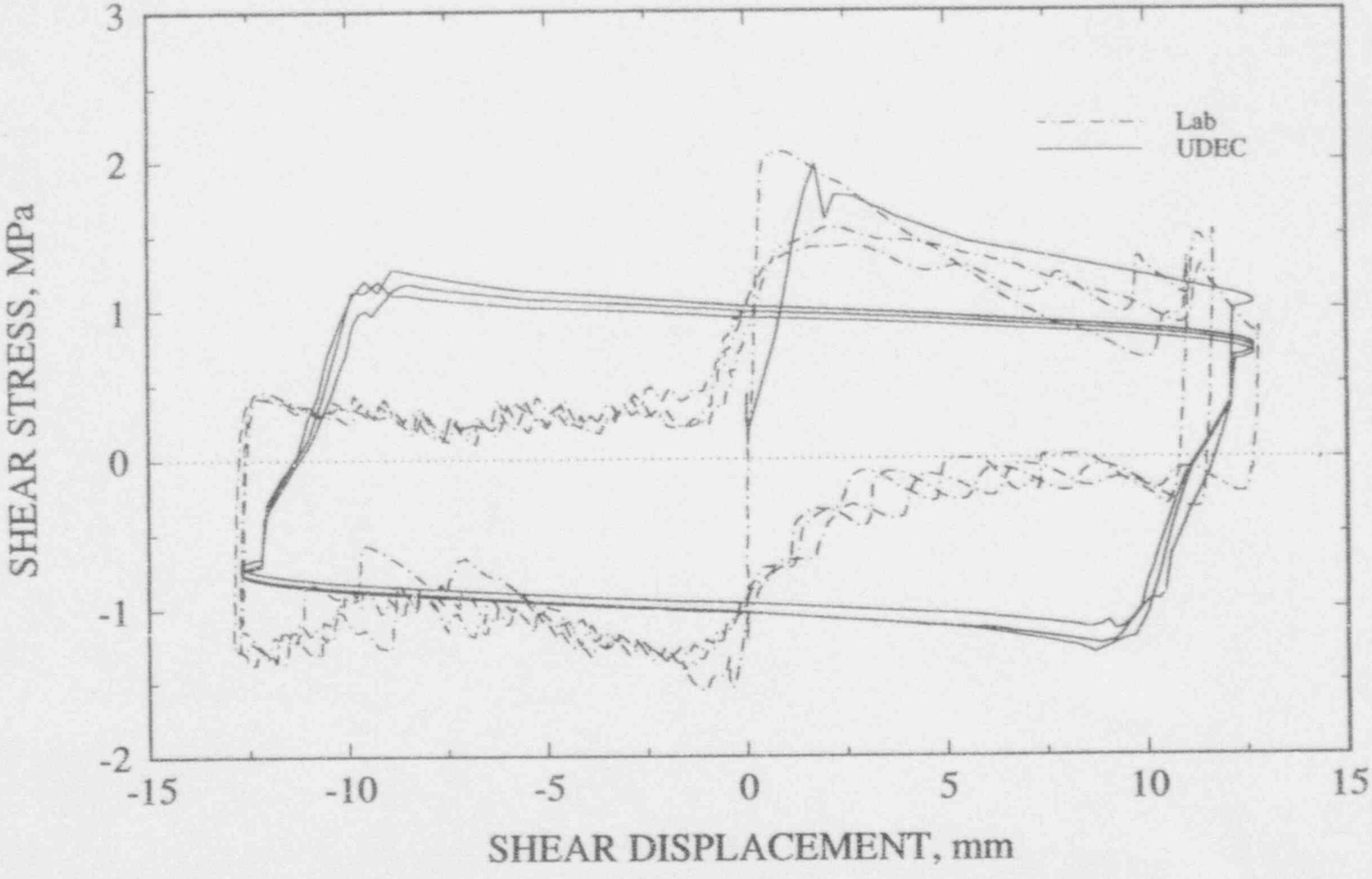

Figure 5-33. Laboratory results and UDEC prediction using Barton-Bandis joint model of shear stress versus shear displacement curve subjected to a harmonic load

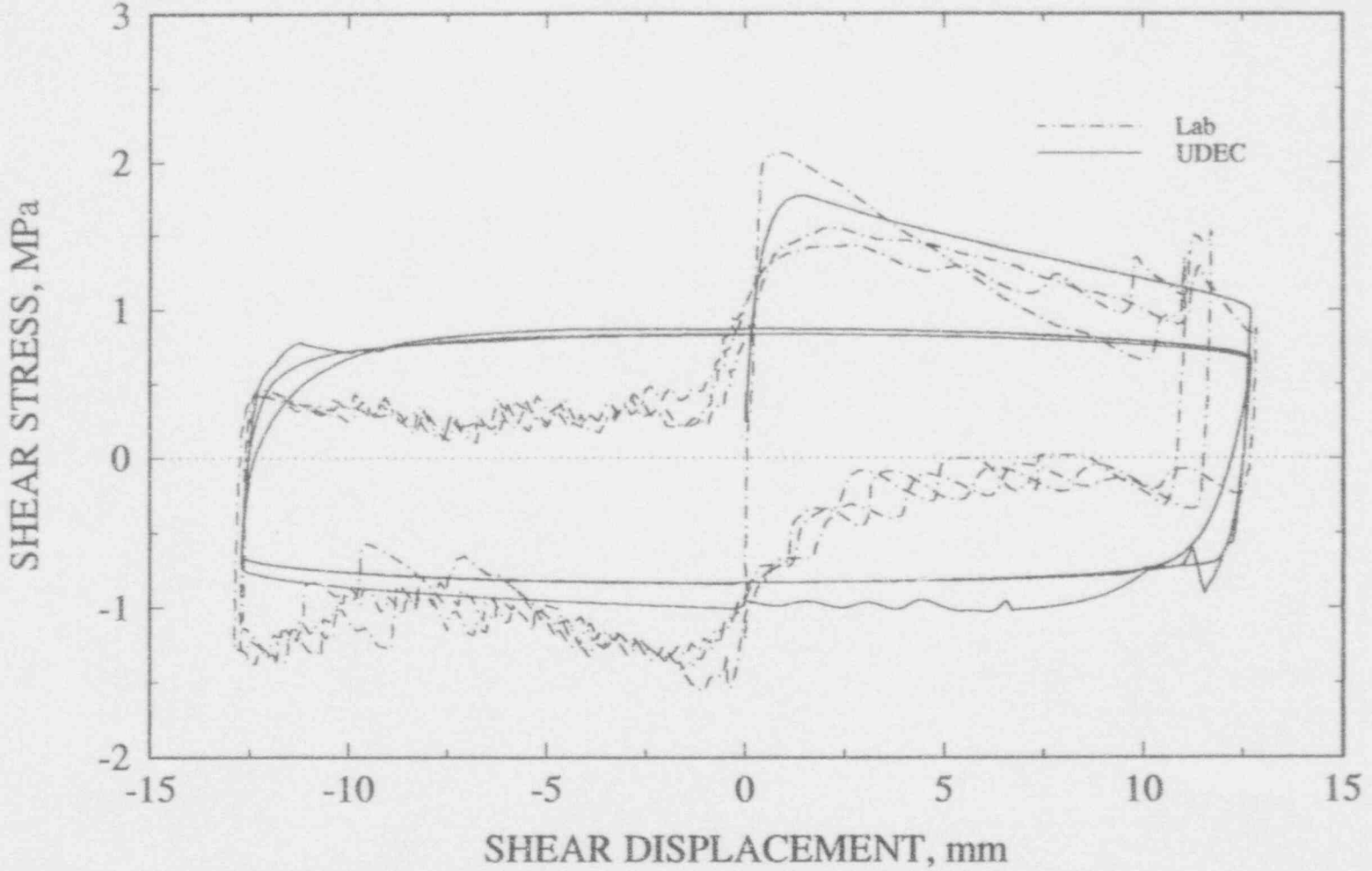

Figure 5-34. Laboratory results and UDEC prediction using Continuously-Yielding joint model of shear stress versus shear displacement curve subjected to a harmonic load

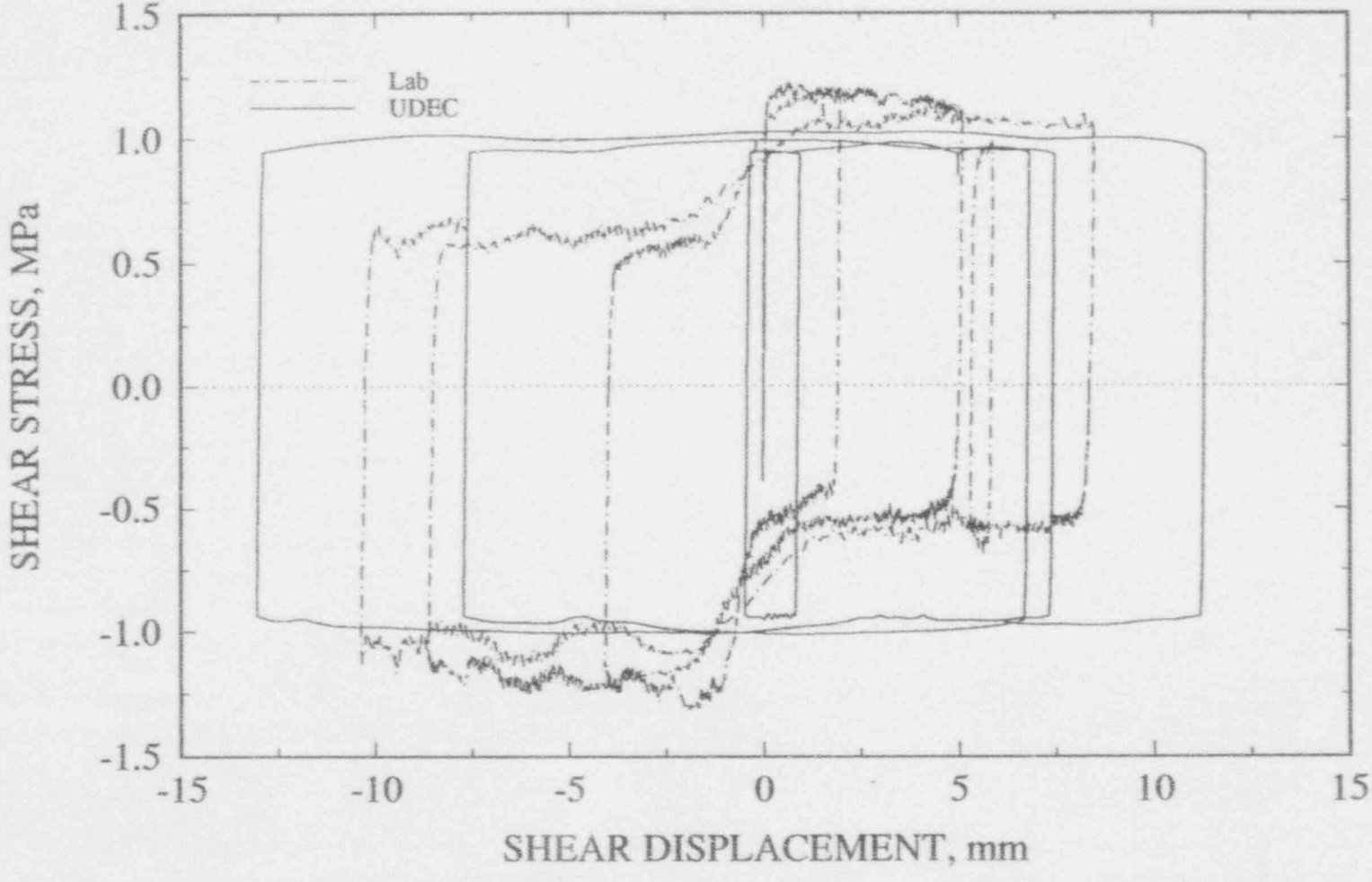

Figure 5-35. Laboratory results and UDEC prediction using Mohr-Coulomb joint model of shear stress versus shear displacement curve subjected to an earthquake load

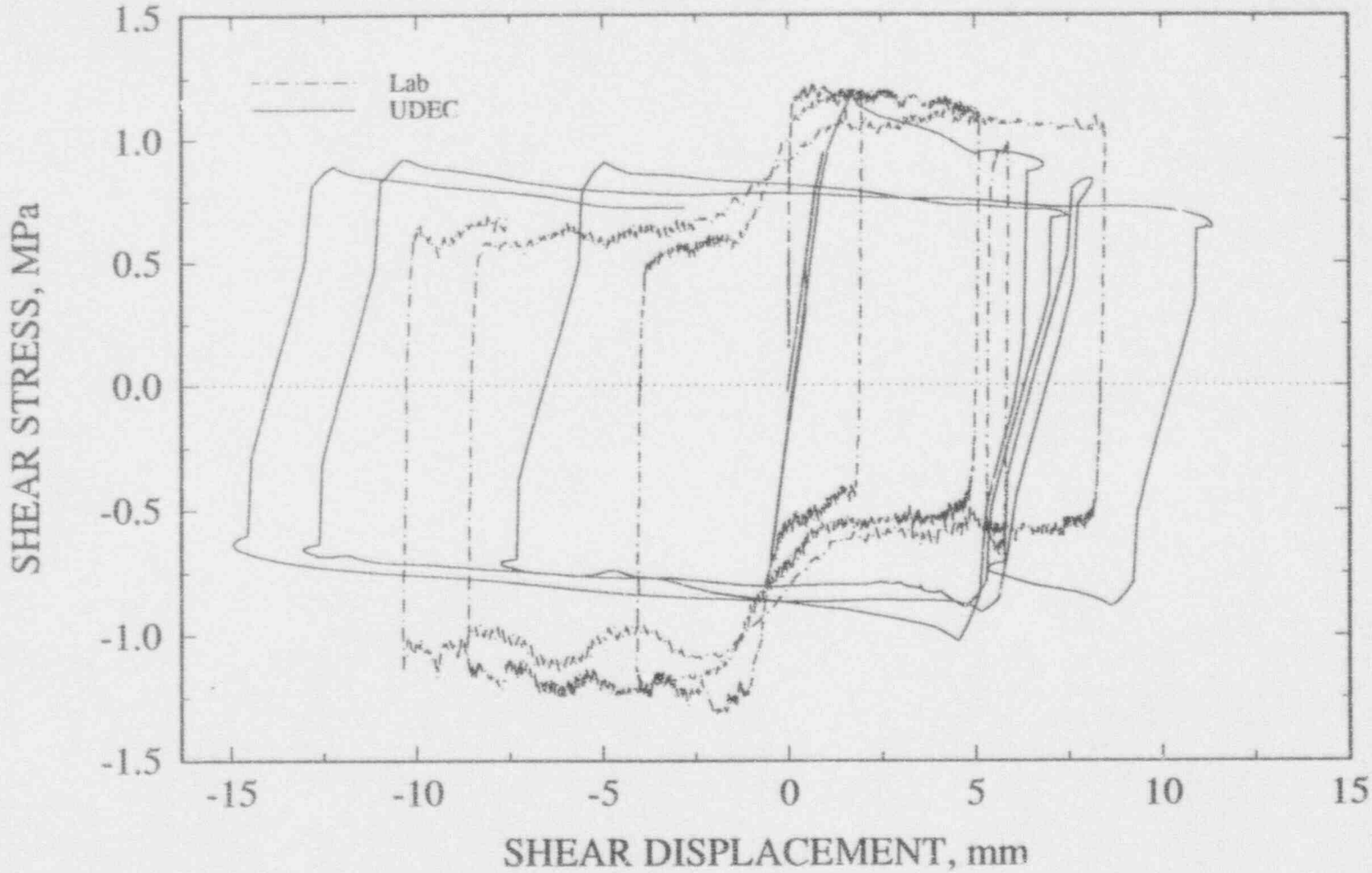

Figure 5-36. Laboratory results and UDEC prediction using Barton-Bandis joint model of shear stress versus shear displacement curve subjected to an earthquake load

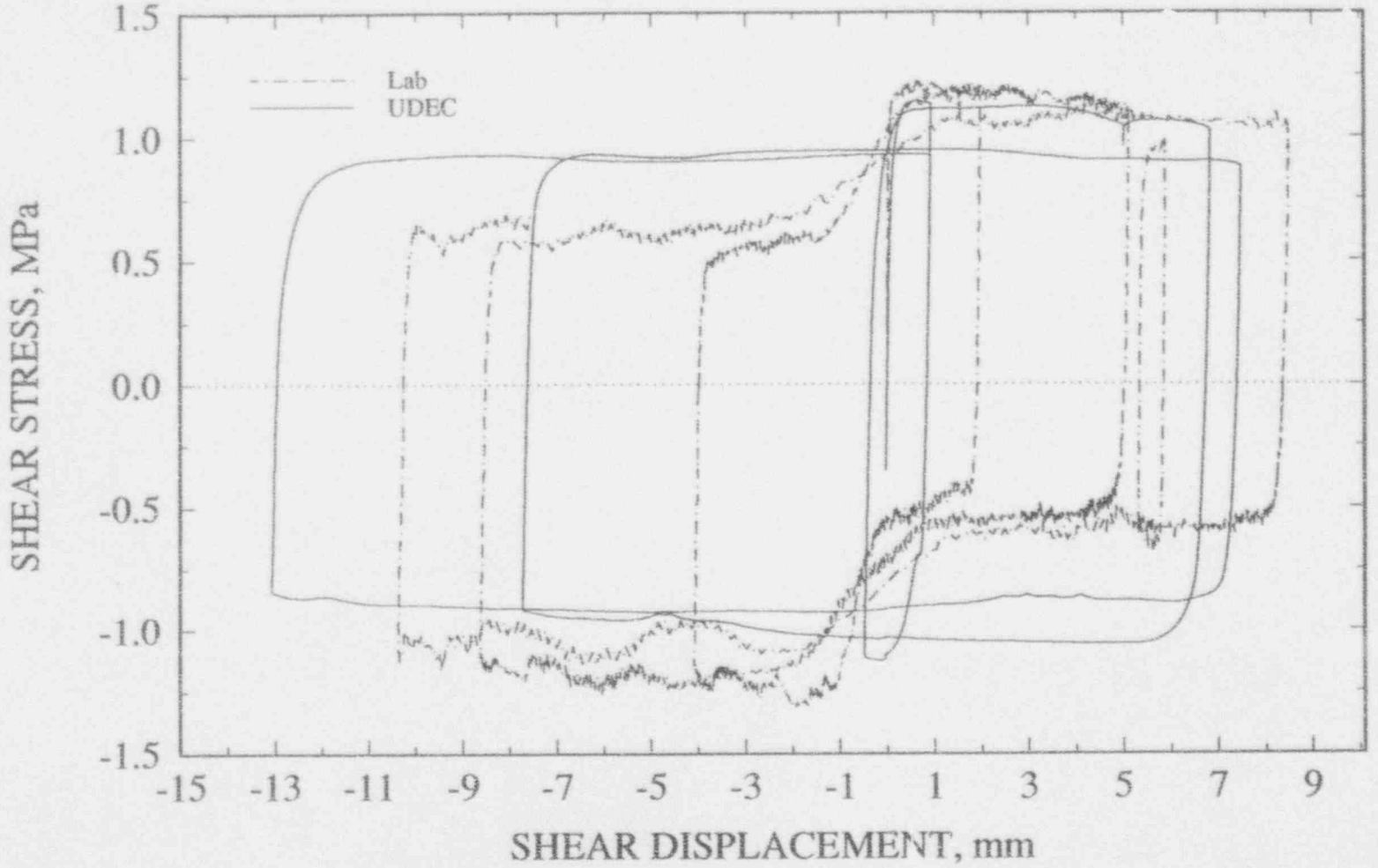

Figure 5-37. Laboratory results and UDEC prediction using Continuously-Yielding joint model of shear stress versus shear displacement curve subjected to an earthquake load

using the Continuously-Yielding model, this gap may be smaller. The large gap observed from the UDEC modeling results on the harmonic experiment using both the Barton-Bandis and Continuously-Yielding models is not consistent with the observation from the laboratory results that suggested a much slower rate in the wearing of joint roughness.

As can be observed from Figures 5-32 through 5-37, the predicted shear strength for reverse shearing is essentially the same as that for forward shearing for all three joint models used in the simulation, except perhaps for the first cycle of the shear stress versus shear displacement curve. This observation is not consistent with the laboratory results. The laboratory results for the harmonic and earthquake tests consistently showed a smaller shear strength upon reverse shearing than that of forward shearing.

Figures 5-39 to 5-41 show the predicted joint dilations of UDEC modeling of the harmonic experiment using the three rock joint models while Figures 5-42 to 5-44 show the modeling results for the earthquake experiment. The laboratory results are also included in each figure for comparison. These figures again demonstrate that the three rock joint models, as implemented in the UDEC computer code, cannot adequately describe the laboratory observed joint dilation behavior when cyclic shear loading is involved. It should be noted again that the dilation calculation using the Barton-Bandis joint model as implemented in the UDEC computer code is incorrect, judging by the unreasonable results produced.

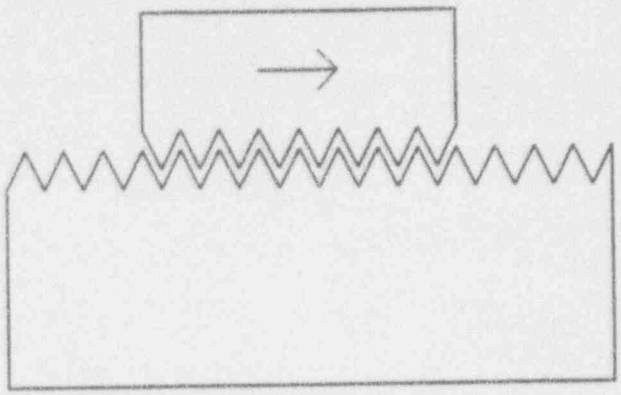

(a) Beginning of forward cycle

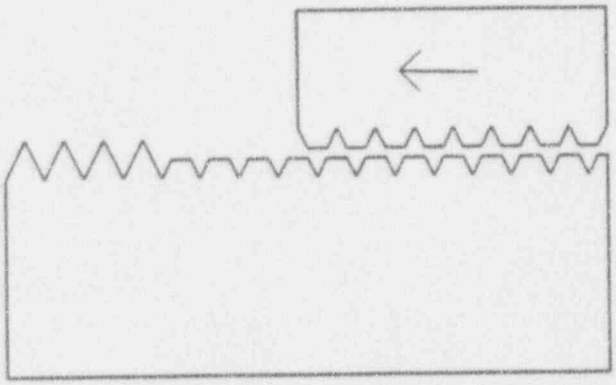

(b) Beginning of reverse cycle

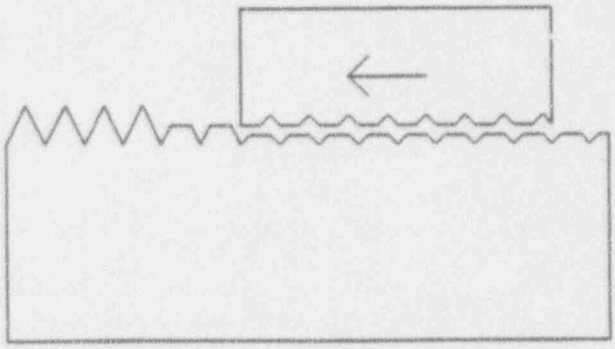

(c) Middle of reverse cycle

Figure 5-38. Schematic representation of roughness wearing of the rock joint in cyclic loading

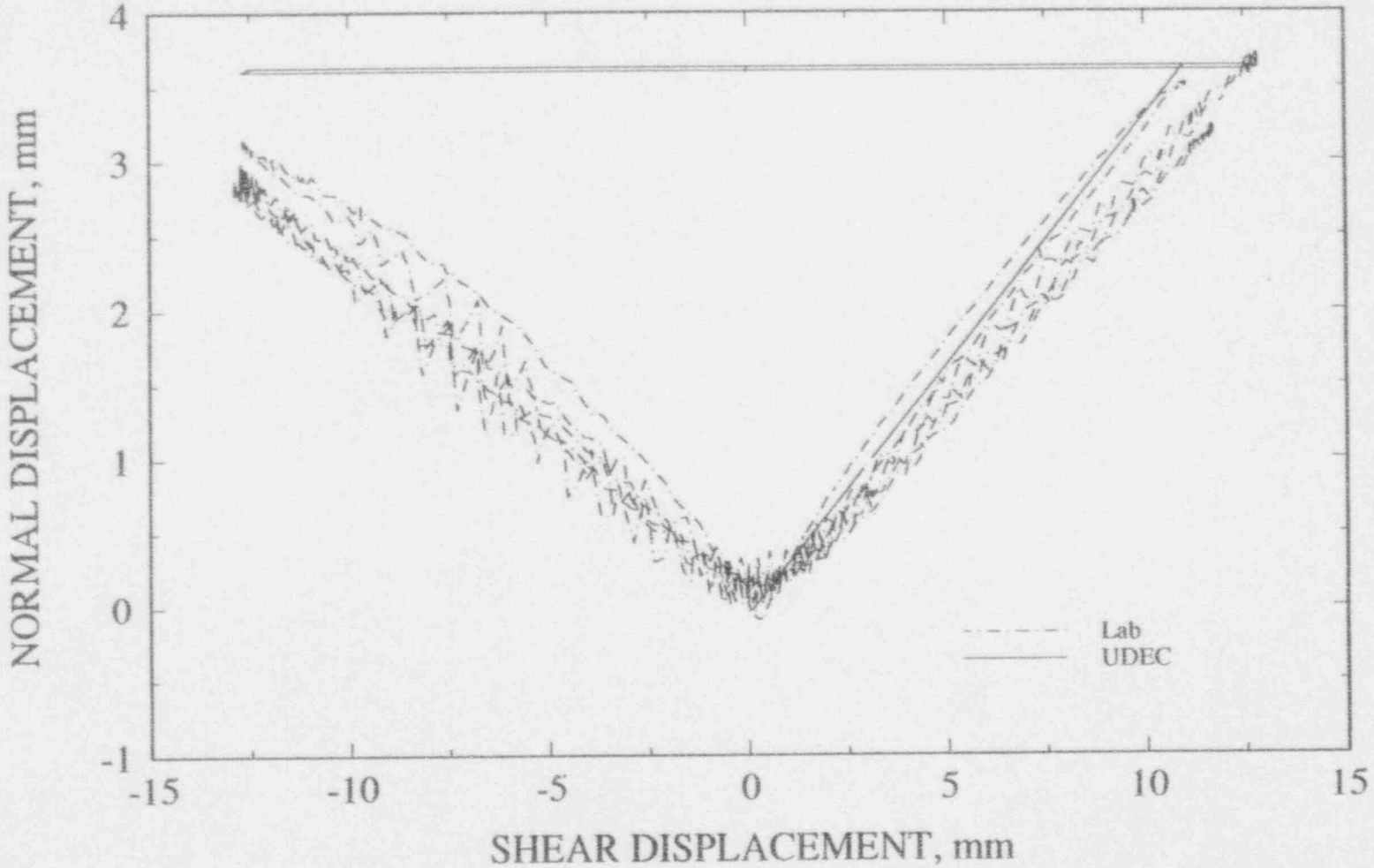

Figure 5-39. Laboratory results and UDEC prediction using Mohr-Coulomb joint model of joint dilation subjected to a harmonic load

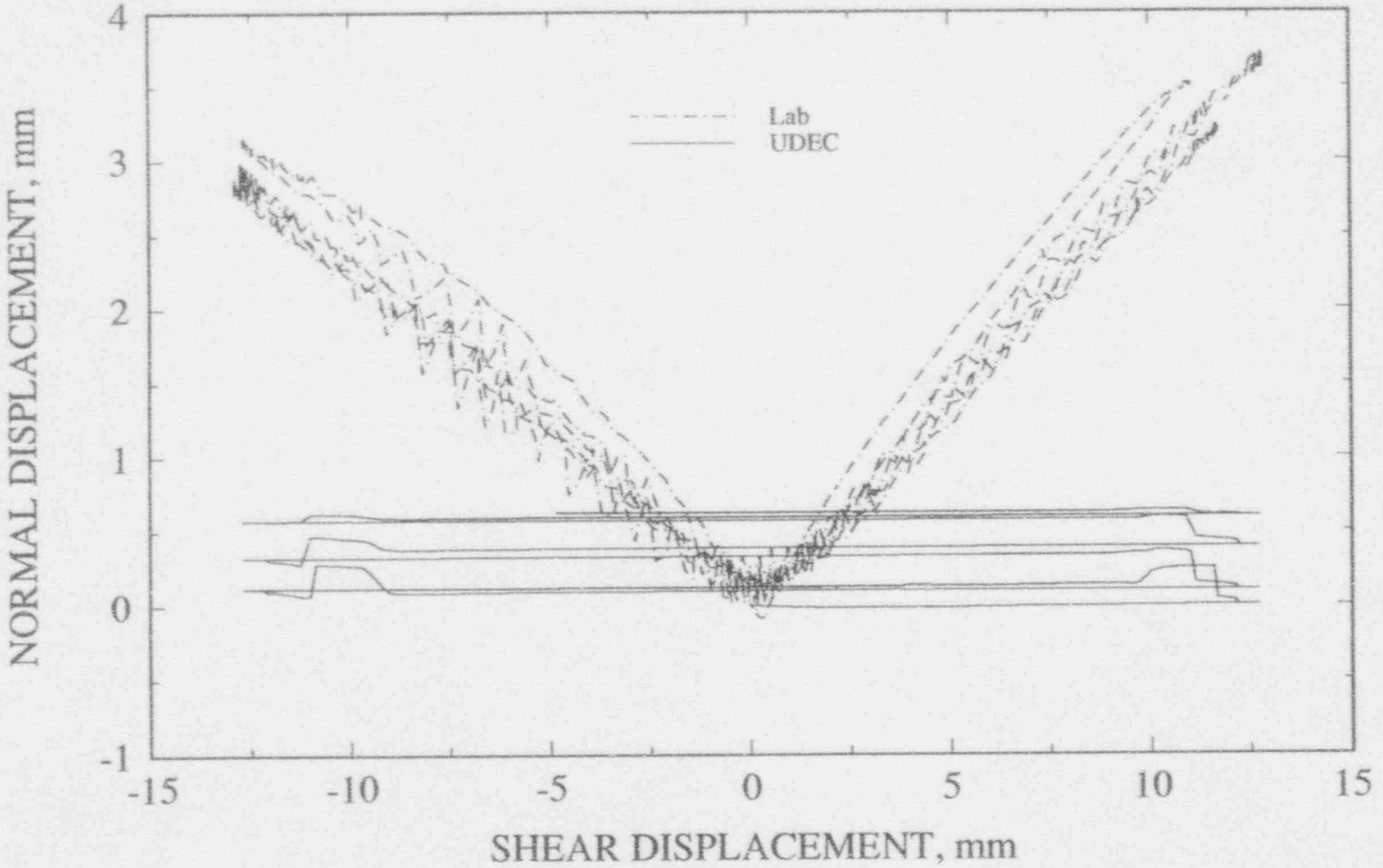

Figure 5-40. Laboratory results and UDEC prediction using Barton-Bandis joint model of joint dilation subjected to a harmonic load

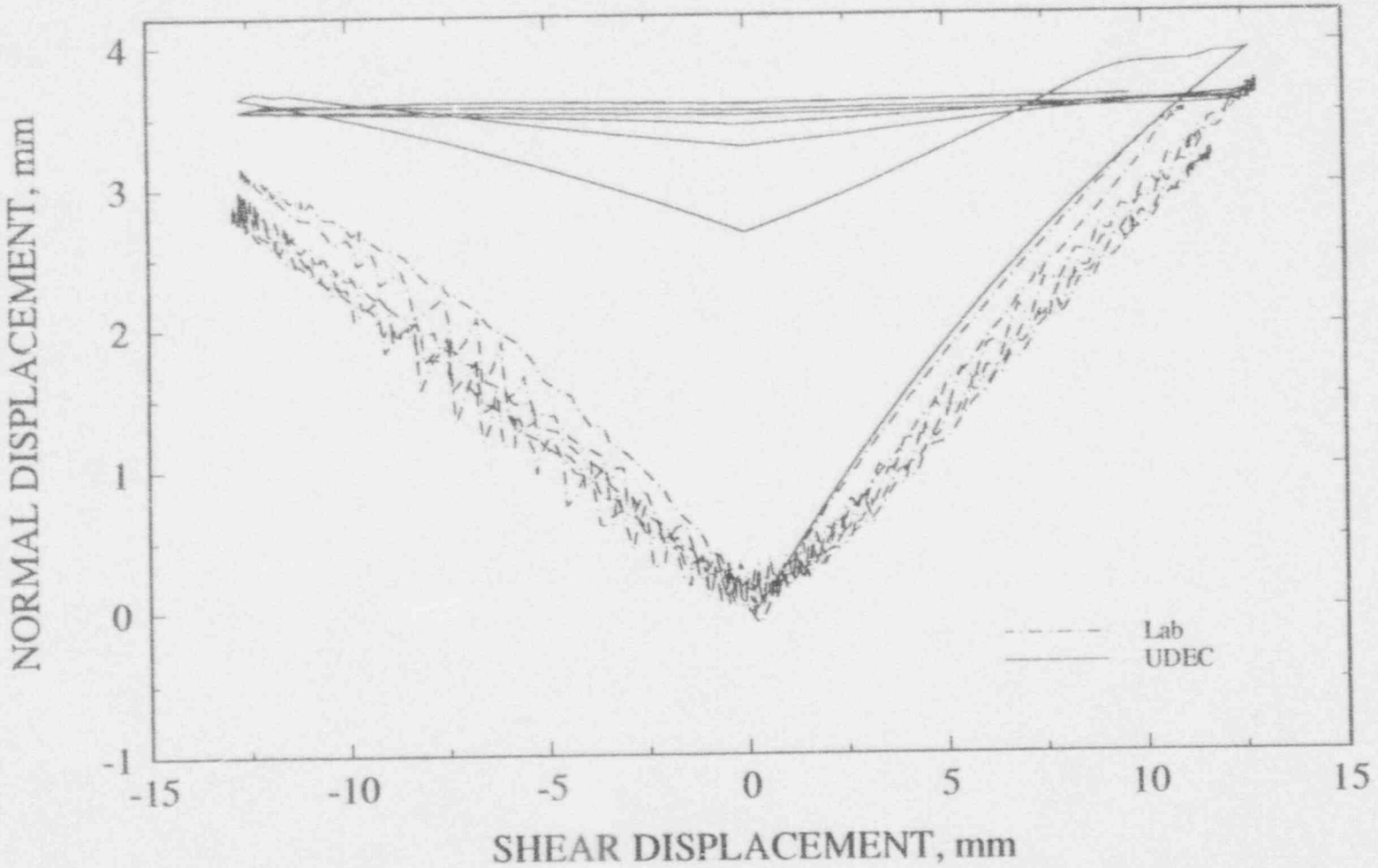

Figure 5-41. Laboratory results and UDEC prediction using Continuously-Yielding joint model of joint dilation subjected to a harmonic load

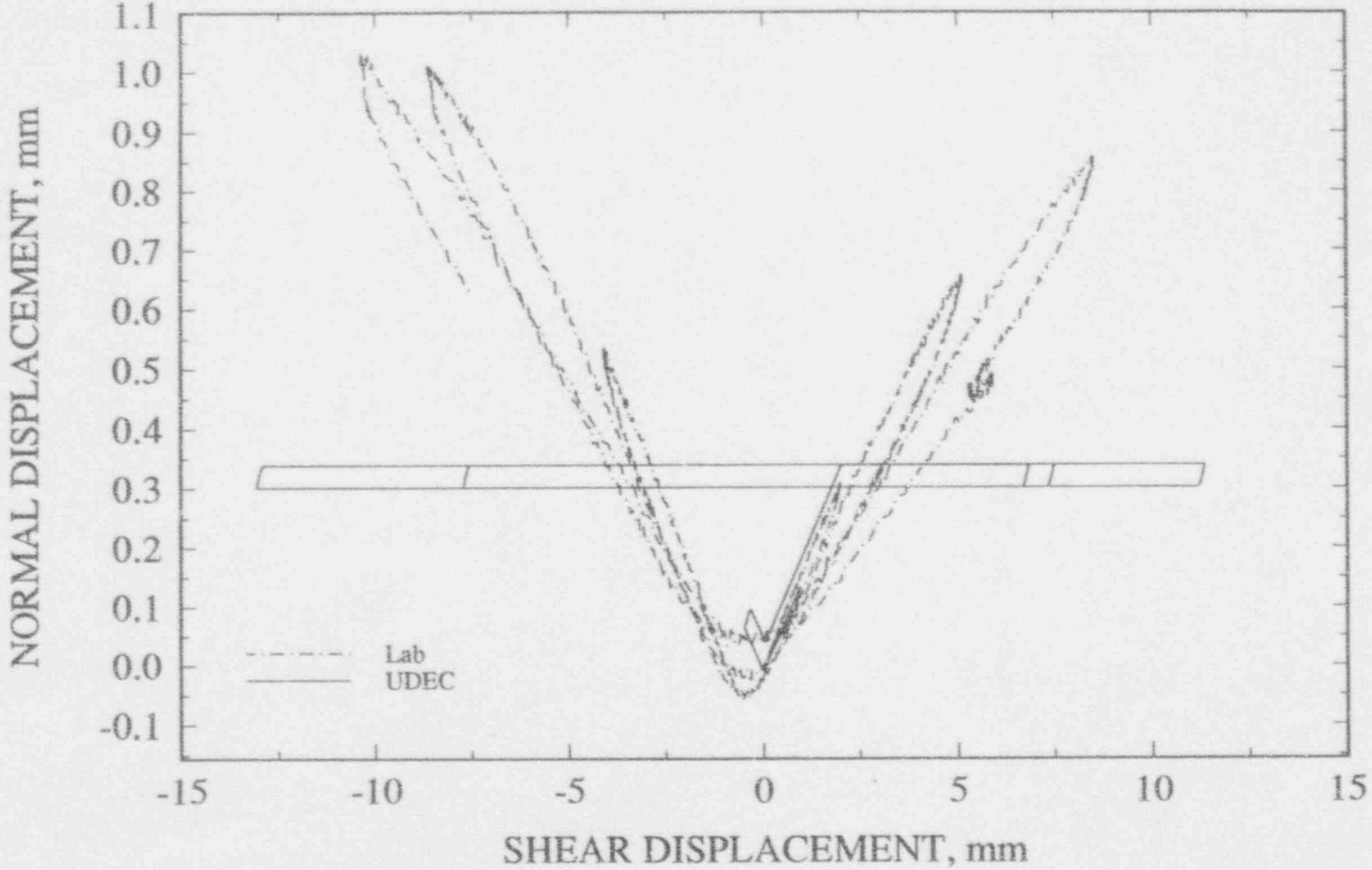

Figure 5-42. Laboratory results and UDEC prediction using Mohr-Coulomb joint model of joint dilation subjected to an earthquake load

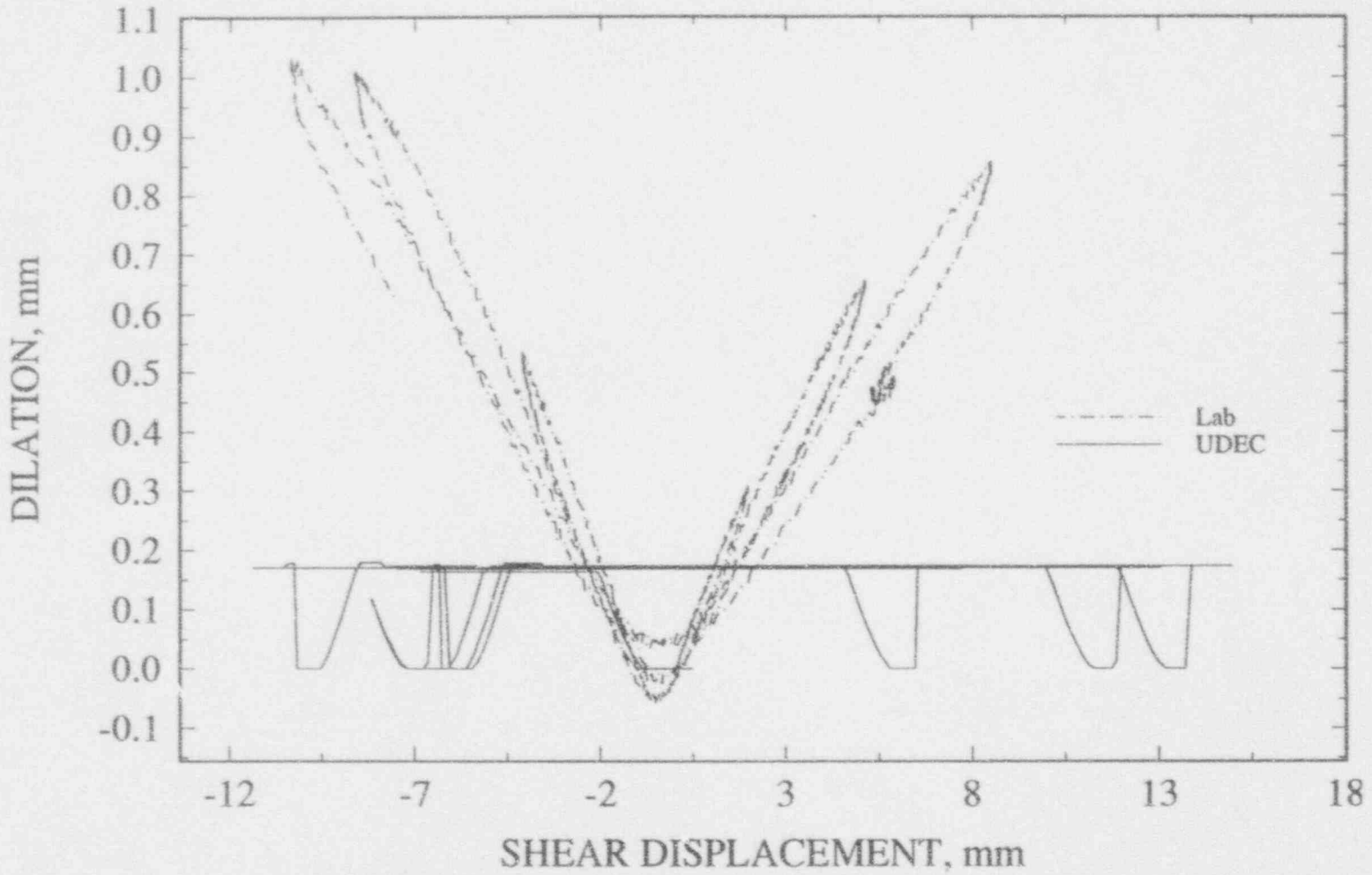

Figure 5-43. Laboratory results and UDEC prediction using Barton-Bandis joint model of joint dilation subjected to an earthquake load

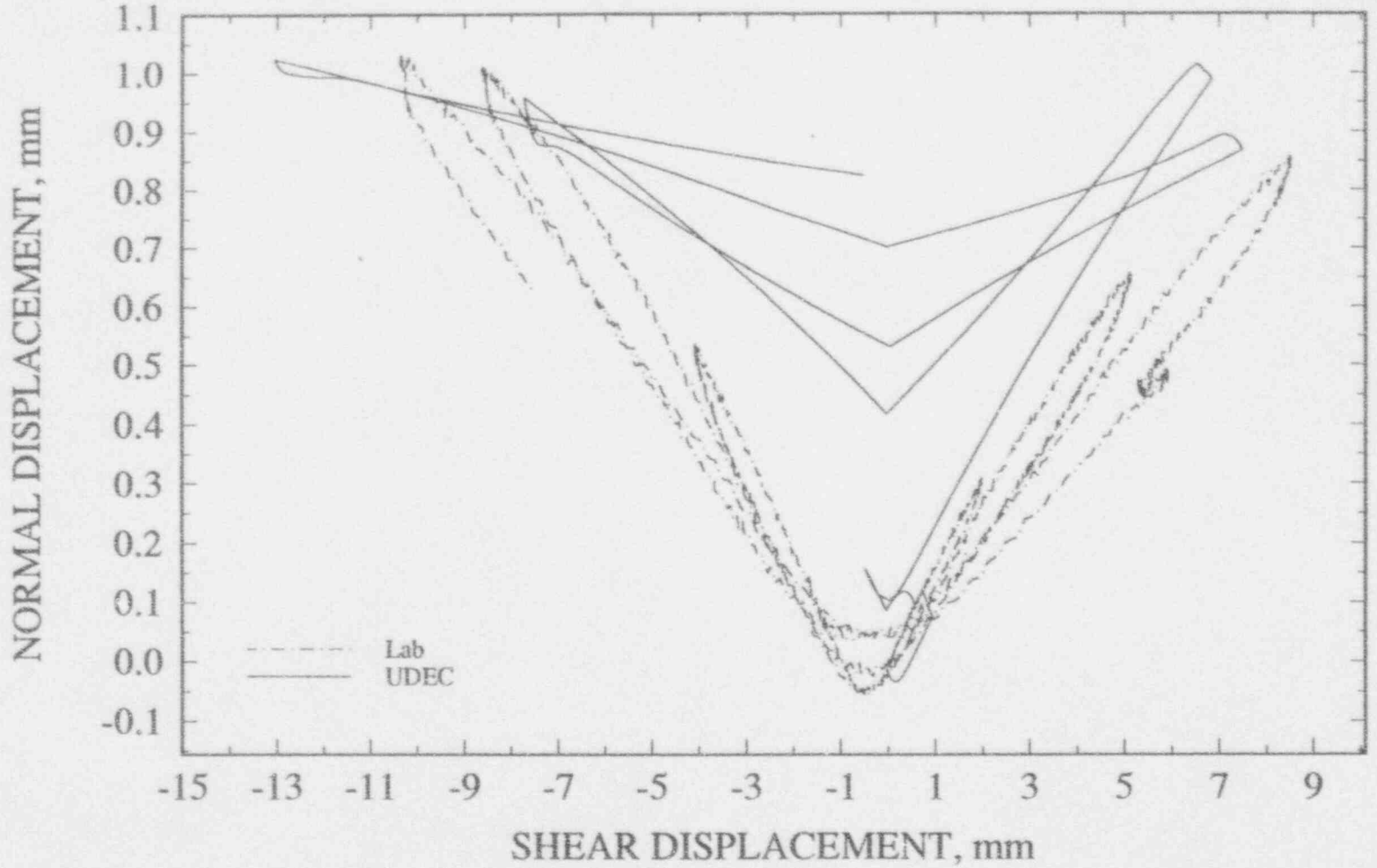

Figure 5-44. Laboratory results and UDEC prediction using Continuously-Yielding joint model of joint dilation subjected to an earthquake load

6 SUMMARY AND CONCLUSIONS

The activity reported herein is the second phase of the qualification study for the assessment of rock joint models and the associated computer codes. In the first phase of the qualification study, a few commercially available computer codes were selected and evaluated using four well-established benchmark problems involving a rock joint that have closed-form solutions or suitable approximations to closed-form solutions. These commercially available codes included the distinct element codes UDEC and 3DEC, the discrete element code DECICE, and the finite element codes HONDO II and SPECTROM–331. The first phase of study was intended to confirm that a code can reproduce the rock joint response of these benchmark problems. Codes with an acceptable performance would be candidates for the second phase of the qualification study in which the dynamic response of well-designed and executed laboratory experiments on single-joint rock specimens would be analyzed. This first-phase study showed that only the UDEC and 3DEC (which is, in general, a 3D version of UDEC) were able to reproduce the response of all four benchmark problems. The UDEC code was selected for the second phase study. The objective of the second phase of qualification study is to determine whether the existing rock joint models and the associated computer codes can simulate the laboratory experimental behavior of single-joint rock specimens when subjected to cyclic pseudostatic and dynamic loads. To accomplish this goal, two major activities were included in this study: assessment of Mohr-Coulomb, Barton-Bandis, and Continuously-Yielding rock joint models in their preliminary forms, and UDEC modeling of cyclic pseudostatic, harmonic, and earthquake tests in the laboratory using the three rock joint models implemented in the code.

Two important, distinct features for a joint during shear test in the laboratory have been identified; one is that the shear strength upon reverse shearing is smaller than that during forward shearing, and the other is that the joint dilation resulting from forward shearing recovers during reverse shearing. These two features of joint behavior are independent of the environmental conditions under which the joint is tested. It should be emphasized that both forward and reverse joint shearing are important phenomena of a rock joint. Reverse shearing can result from an earthquake, thermal load, or both – all of which are expected to be experienced during the life of an HLW repository. Another important finding from the laboratory experiments is that no noticeable effect of the input frequency (shearing velocity) on the peak joint shear strength and the joint shear strength for the reverse shearing is observed within the range of variation of the test input velocity or frequency. It is possible, therefore, to ignore the effect of shearing velocity variations, for the range of velocities expected during an earthquake, in evaluating joint behavior.

Careful examination of the Mohr-Coulomb, Barton-Bandis, and Continuously-Yielding rock joint models has revealed that all three models have adopted essentially the same principle in determining the joint shear strength during reverse shearing. This principle asserts the same joint behaviors under both forward and reverse shearing conditions. With this principle, the same shear strength criterion is applicable to both conditions. The Mohr-Coulomb joint model is the simplest of the three evaluated in this report. This model further assumes that no joint wear will occur under either forward or reverse shearing condition. Consequently, the shear strengths based on this model are the same for shearing in both directions. For the other two models, however, joint wear is explicitly considered in the shear strength criteria, and the joint friction behavior is considered to be governed by two frictional properties; one is the fundamental friction property or the residual friction property, and the other one is the friction property representing joint roughness. The fundamental or residual friction properties for these two models are similar, in concept, to the friction property in the Mohr-Coulomb joint model although the methodologies used to calculate these properties may be different. For a detailed discussion on the methodologies, refer to the

report by Hsiung et al. (1993b). These residual friction properties essentially represent the rock joint surfaces without roughness, a condition that no additional wear to the joint can take place. In the Barton-Bandis model, this friction property is referred to as the residual friction angle, ϕ_r, and for the Continuously-Yielding model, it is the basic friction angle, ϕ. The roughness property is governed by the *JRC* value in the Barton-Bandis model while it is governed by the difference between the initial friction angle, ϕ_{mo}, and the basic friction angle, ϕ, in the Continuously-Yielding joint model. The extent of wear for both joint models is controlled by the amount of the joint shear displacement. To preserve the necessary continuity in joint wear during the course of changing shear direction, both the Barton-Bandis and Continuously-Yielding joint models assert that the remaining friction property at the end of the forward shearing process should be the control of the joint response in the reverse shearing process. The shear strength at the end of the forward shearing is considered to be the peak shear strength at the beginning of the reverse shearing. The implementation of these three models in the UDEC code closely follow this principle. None of these models and their implemented versions in the UDEC code can satisfactorily simulate the joint shear experimental behavior during reverse shearing in which the shear strength is different from that at the end of the forward shearing. As observed from the laboratory cyclic pseudostatic and dynamic (harmonic and earthquake) test results, this difference could be large depending upon a particular joint profile.

The Barton-Bandis and Continuously-Yielding joint models link joint dilation with shearing directly through the roughness properties. Since a joint continues to wear during the process of shearing, the dilation angle used to calculate joint dilation continues to decrease. The constant decreasing in dilation angle implies, therefore, that the joint will eventually stop dilating when it is completely worn. The Mohr-Coulomb joint model calculates dilation based on a constant dilation angle. Dilation starts when shear strength is reached and stops when a critical shear displacement is reached. All three models assume an increasing nature of joint dilation; that is, the amount of dilation will never decrease no matter along which direction the joint is being sheared. This assumption is not consistent with the joint dilation behavior found in the laboratory. Laboratory results showed that the joint tends to recover from the dilation resulting from forward shearing during reverse shearing with a certain amount of hysteresis between the dilation and dilation recovery curves. The dilation recovery can be complete. Although it is not the original intent of the joint dilation models, it is possible in the numerical implementation to assume that the dilation angle is direction-dependent by changing its sign when the direction of shear is reversed. This change makes the simulation of dilation recovery possible. It has been verified numerically by simulating the rock joint response using only the constitutive equations. However, the extent of dilation recovery using either the Barton-Bandis, the Continuously-Yielding joint model, or their implemented versions in the UDEC code, is not nearly sufficient to account for what was observed in the laboratory. The joint dilation in the Barton-Bandis and Mohr-Coulomb joint models have not been implemented properly in the UDEC code. A dilation versus shear displacement curve, predicted by the Barton-Bandis model, reaches a constant value after a small shear displacement. This constant value is significantly smaller than the peak dilation observed in laboratory experiments. The Mohr-Coulomb joint model, on the other hand, predicts the complete recovery of joint dilation irrespective of whether or not the critical shear displacement is reached if the sign can be changed due to change in shear direction. This model, as implemented in the UDEC code, however, predicts complete recovery only when the critical shear displacement is not reached. If the critical shear displacement is exceeded during forward shearing, the amount of dilation realized previously remains constant during the remaining period of forward shearing and the entire period of reverse shearing. This behavior indicates a probable coding error in UDEC.

In conclusion, none of the three rock joint models and their implemented versions in the UDEC code evaluated in this report simulate satisfactorily the joint shear and dilation behaviors as observed from the laboratory cyclic pseudostatic and dynamic test results that appear to show different mechanisms between forward and reverse shearing. Although the prediction of joint dilation from the Mohr-Coulomb model, when dilation angle is considered shear direction dependent, does reflect the dilation recovery nature of joint behavior for reverse shearing, it does not reflect the nature of joint degradation. It should be emphasized that both joint forward and reverse shearing are important phenomena of a rock joint. Reverse shearing can result from an earthquake, thermal load, or both – all of which are expected to be experienced during the life of a HLW repository. As discussed earlier, two important distinct features were considered to be unique with reverse shearing; one is that the shear strength is smaller than that at the end of forward shearing, and the other is that the joint dilation resulting from forward shearing recovers during reverse shearing. Using the three rock joint models that do not consider these two features of the joint behavior in an underground structural design and performance analysis could result in (i) an overestimation of the stability of emplacement drifts and emplacement boreholes, and (ii) prediction of an incorrect pattern of near-field flow (including preferential pathways for water and gas). The work for modifying an existing joint model or developing a new joint model which can simulate these two distinct features of rock joint response under cyclic loading is currently undertaken under Repository Design, Construction, and Operations (RDCO) element Task 2.3.

7 REFERENCES

Barton, N.R., and S.C. Bandis. 1982. Effects of block size on the shear behavior of jointed rock. *23rd U.S. Symposium on Rock Mechanics*. Berkeley, CA.

Barton, N.R., S.C. Bandis, and K. Bakhtar. 1985. Strength, deformation and conductivity coupling of rock joints. *International Journal of Rock Mechanics and Mining Sciences & Geomechanics Abstracts* 22(3): 121-140.

Brady, B.H.G., S.M. Hsiung, and A.H. Chowdhury. 1990. *Qualification Studies on the Distinct Element Code UDEC Against Some Benchmark Analytical Problems*. CNWRA 90-004. San Antonio, TX: Center for Nuclear Waste Regulatory Analyses.

Brandshaug, T., B. Dasgupta, B.H.G. Brady, S.M. Hsiung, and A.H. Chowdhury. 1990. *Qualification Studies on the Finite Element Code HONDO II Against Some Benchmark Analytical Problems*. CNWRA 90-006. San Antonio, TX: Center for Nuclear Waste Regulatory Analyses.

Cundall, P.A., and J.V. Lemos. 1988. Numerical simulation of fault instabilities with the continuously-yielding joint model. *Proceedings of the 2nd International Symposium on Rockbursts and Seismicity in Mines*. Minneapolis, MN: University of Minnesota.

Hsiung, S.M., and A.H. Chowdhury. 1991. *Report on Research Activities for Calendar Year 1990*. NUREG/CR-5817. W.C. Patrick, ed. San Antonio, TX: Center for Nuclear Waste Regulatory Analyses.

Hsiung, S.M., and A.H. Chowdhury. 1993. *NRC High-Level Radioactive Waste Research at CNWRA. Calendar Year 1992*. NUREG/CR-587. Vol. 2. W.C. Patrick, ed. Washington, DC: U.S. Nuclear Regulatory Commission.

Hsiung, S.M., M.P. Ahola, and A.H. Chowdhury. 1993a. *NRC High-Level Radioactive Waste Research at CNWRA, January-June 1992*. NUREG/CR-5817. W.C. Patrick, ed. Washington, DC: U.S. Nuclear Regulatory Commission: 3(1).

Hsiung, S.M., D.D. Kana, M.P. Ahola, A.H. Chowdhury, and A. Ghosh. 1993b. *Laboratory Characterization of Rock Joints*. CNWRA 93-013. San Antonio, TX: Center for Nuclear Waste Regulatory Analyses.

Huang, X., B.C. Haimson, M.E. Plesha, and X. Qiu. 1993. An investigation of the mechanics of rock joints—part I. Laboratory investigation. *International Journal of Rock Mechanics and Mining Sciences & Geomechanics Abstracts* 30(3): 257-269.

ITASCA Consulting Group, Inc. 1992. *UDEC Universal Distinct Element Code Version 1.8 Volume I: User's Manual*. Minneapolis, MN: ITASCA Consulting Group, Inc.

Jing, L., E. Nordlund, and O. Stephansson. 1992. An experimental study on the anisotropy and stress-dependency of the strength and deformability of rock joints. *International Journal of Rock Mechanics and Mining Sciences & Geomechanics Abstracts* 29(G): 535-542.

Kana, D.D., B.H.G. Brady, B.W. Vanzant, and P.K. Nair. 1991. *Critical Assessment of Seismic and Geomechanics Literature Related to a High-Level Nuclear Waste Underground Repository.* NUREG/CR-5440. Washington, DC: U.S. Nuclear Regulatory Commission.

Nuclear Waste Technical Review Board. 1992. *Fifth Report to the U.S. Congress and the U.S. Secretary of Energy.* Washington, DC: U.S. Government Printing Office.

Sharp, J.C. 1970. *Fluid Flow Through Fissured Media.* Ph.D. Thesis. London, United Kingdom: University of London.

Wibowo, J.T., B. Amadei, S. Sture, and A.B. Robertson. 1992. Shear response of a rock joint under different boundary conditions: An experimental study. *Conference of Fractured and Jointed Rock Masses.* Preprints. June 3-5, 1992. Lake Tahoe, CA.

APPENDIX A
UDEC INPUT FILES

Datafile names and brief descriptions

MC7.dat: Test No. 7, Mohr-Coulomb Model
MC8.dat: Test No. 8, Mohr-Coulomb Model
MC9.dat: Test No. 9, Mohr-Coulomb Model
MC10.dat: Test No. 10, Mohr-Coulomb Model
MC11.dat: Test No. 11, Mohr-Coulomb Model
MC14.dat: Test No. 14, Mohr-Coulomb Model
MC24.dat: Test No. 24, Mohr-Coulomb Model

BB7.dat: Test No. 7, Barton-Bandis Model
BB8.dat: Test No. 8, Barton-Bandis Model
BB9.dat: Test No. 9, Barton-Bandis Model
BB10.dat: Test No. 10, Barton-Bandis Model
BB11.dat: Test No. 11, Barton-Bandis Model
BB14.dat: Test No. 14, Barton-Bandis Model
BB24.dat: Test No. 24, Barton-Bandis Model

CY7.dat: Test No. 7, Continuously-Yielding Model
CY8.dat: Test No. 8, Continuously-Yielding Model
CY9.dat: Test No. 9, Continuously-Yielding Model
CY10.dat: Test No. 10, Continuously-Yielding Model
CY11.dat: Test No. 11, Continuously-Yielding Model
CY14.dat: Test No. 14, Continuously-Yielding Model
CY24.dat: Test No. 24, Continuously-Yielding Model

Harmonic.vel: Harmonic Velocity Input

Earth.vel: Earthquake Velocity Input